Effects of Accelerated Aging on SiO_2-treated Wood Samples

by
Callisto Ariadne Beuthe

Under the supervision of
Dr. Reza Foruzanmehr

Co-supervisor
Dr. Marzieh Riahinezhad

Thesis submitted to the University of Ottawa in partial fulfillment of the requirements for the degree of
Master of Applied Science in Civil Engineering

uOttawa

Department of Civil Engineering
Faculty of Engineering
University of Ottawa

Abstract

Wood is a viscoelastic composite material that has been historically prominent in the construction of buildings and continues to see widespread use. When used for exterior applications, wood is exposed to dynamic environmental conditions and can degrade if left untreated. Previous research by Lemaire-Paul *et al.* (2022) has proven that vacuum impregnation of the wood cell structure with a silica (SiO_2) nanoparticle colloid under a vacuum pressure of -90 kPa can enhance the viscoelastic properties, increase the density, and reduce the water uptake of white spruce wood. However, the behaviour of SiO_2-treated wood under different environmental conditions over time has yet to be fully explored. This research aims to examine the durability and performance of SiO_2-treated spruce wood samples subjected to accelerated aging conditions under high temperature and humidity as well as freeze-thaw cycling. Spruce wood samples were treated with 40% SiO_2 nanoparticle colloid under a vacuum pressure of -90 kPa. One set was placed in a hydrolytic aging chamber at 90°C and 80% RH. Another set was placed in a freeze-thaw cycling chamber that cycled from 25°C to -18°C and back at a rate of 6 cycles per day. The samples were removed at regular intervals and thermogravimetric analysis, dynamic mechanical analysis, tensiometry, X-Ray diffraction, and scanning electron microscopy were performed.

When compared to the results obtained from a set of non-treated samples, it was found that the SiO_2-treated samples exhibited lower water uptake values that stabilized over time, as well as a lower rate of decrease in peak cellulose degradation temperatures under hydrolytic aging and a slight increase in peak cellulose degradation temperature over time under freeze-thaw aging. The effects of both aging conditions on the viscoelastic properties of the samples were also found to be insignificant. Both types of samples under both types of aging also exhibited an increase in crystallinity over time. These results indicate that the durability and properties of wood can be improved through nano-SiO_2 impregnation as the material remains relatively stable when subjected to high temperature and humidity conditions as well as freeze-thaw cycling over time.

Keywords: Spruce Wood, Wood Fibers, Accelerated Aging, Hydrolytic Aging, Freeze-Thaw Aging, Silica Nanoparticles, Vacuum Impregnation, Viscoelastic Properties, Water Uptake, Thermal Degradation, Scanning Electron Microscopy, X-Ray Diffraction.

Acknowledgements

I would like to express my sincere gratitude to my supervisors Dr. Reza Foruzanmehr and Dr. Marzieh Riahinezhad for their input, help, and guidance in both my experimental endeavours and the preparation of this manuscript. The completion of this thesis would not have been possible without their unwavering support, patience, and motivation throughout this process.

I would also like to extend my thanks also go to Peter Collins, Kenneth Trischuk, and Itzel Lopez-Carreon of the National Research Council of Canada for their suggestions, support, and technical assistance with the Sigma 701 and Q600 SDT. I would also like to thank Elnaz Esmizadeh for performing ATR-FTIR measurements that were instrumental to my understanding of the effects of the treatment process.

Finally, I would like to thank my family and friends for their love and encouragement during this process. This thesis is dedicated to my parents; thank you for believing in me, for your continued support over the years, and for setting me on the path to my degree in civil engineering.

Table of Contents

List of Figures

List of Tables

List of Abbreviations

ASE	Anti-Swelling Efficiency
ATR	Attenuated Total Reflectance
BCE	Before Common Era
CA	Contact Angle
DMA	Dynamic Mechanical Analysis
DTG	Differential Thermogravimetry
EMC	Equilibrium Moisture Content
FSP	Fiber Saturation Point
FTIR	Fourier Transform Infrared
HRH	Heating Relative Humidity
LOI	Limiting Oxygen Index
MFA	Microfibril Angle
MOE	Modulus of Elasticity
MOR	Modulus of Rupture
NC	Nanocomposite
NS	Nanosilica
NSt	Nanosilica-styrene
NT	Non-Treated
RH	Relative Humidity
SEM	Scanning Electron Microscopy
TGA	Thermogravimetric Analysis
Tanδ	Damping/Loss Tangent
UV	Ultraviolet
WA	Water Absorption
XRD	X-Ray Diffraction
pH	Potential of Hydrogen

Chapter 1

1.0 Introduction

1.1 Background

Wood is known as the oldest composite construction material. It has been used to build structures for over 10,000 years. Evidence of wood buildings such as longhouses dating back to 5500 BCE have been found across Europe (Last, 2014). Currently, the oldest known wooden structure is a Neolithic well found in the Czech Republic that was radiocarbon and tree-ring dated to 5259-5255 BCE (Rybníček *et al.*, 2020). In modern times, wood remains an attractive option in the construction industry. Not only is it a renewable material, but also acts as a carbon sink and effectively offsets carbon emissions in the construction industry (Churkina *et al.*, 2020).

The physical structure of wood contains a natural polymer of cellulose fibres embedded in a matrix of lignin and hemicellulose. Wood that is used for exterior applications such as cladding, siding, and fencing is exposed to dynamic environmental conditions and degrades if left untreated. Wood is a hydrophilic material due to the presence of hydroxyl groups in its molecular structure (Wang & Piao, 2010). The presence of these hydroxyl groups facilitates the formation of hydrogen bonds with water and other polar solvents. The hydrophilic nature and porous vascular system of wood cause the material to become susceptible to hydrolysis. This reaction breaks glycosidic bonds in the backbone of the cellulose and results in the deterioration of the wood cellulose structure (Bobleter, 1994).

Traditional methods of wood treatment to reduce deterioration from water uptake include the application of external coatings, sprays, and varnishes to improve the durability and long-term performance of the material (Lebow, 2010). However, these treatment methods tend to be impermanent due to the low interfacial compatibility between hydrophilic wood and hydrophobic preservatives such as oil creosote and shellac (Li *et al.*, 2007). During prolonged exposure to rain or snowfall, water can infiltrate gaps between the wood and the preservative coating, saturating unfilled voids in the wood cell wall. This weakens the wood structure and wears away at the surface coating.

Research has proven that impregnation of the wood vascular structure with nanoparticle colloids can enhance the durability and properties of wood (Bak & Németh, 2018; Clausen *et al.*, 2011; Ghorbani *et al.*, 2017). This process most commonly involves the use of a vacuum chamber to remove entrapped air within the wood cell structure and facilitate the infiltration of a colloid into the vascular system of the wood. This process allows the colloid to agglomerate and obstruct the lumens, increases the density of the material, and

decreases the permeability of the wood. The use of nanoparticle impregnation to enhance the performance characteristics of wood is an active area of research that can potentially lead to new methods for the long-term preservation of wood. Some of the most promising nanoparticle colloids proposed for wood treatment incorporate silica (SiO_2) nanoparticles. Nanosilica colloids are readily available at a low cost and have been proven to significantly enhance the physical and mechanical properties of wood (Ghorbani *et al.*, 2017, Chang *et al.*, 2015, Giudice & Pereyra, 2009). Research conducted by Lemaire-Paul *et al.* (2022) determined that the vacuum impregnation of silica nanoparticles can decrease the water uptake capacity, increase the density, and improve the viscoelastic properties of white spruce wood. It was found that impregnation under a vacuum pressure of -90 kPa was the optimal treatment condition for enhancing the properties of spruce wood. However, this study also identified a crucial drawback in the treatment process. Upon the pressurization and subsequent infiltration of the SiO_2 colloid in the vascular system of the wood samples, the material is subjected to both alkaline attack and hydrolysis. When the wood cellulose structure comes into contact with the liquid phase of the colloid, the presence of OH (hydroxyl) ions within the colloid perpetuates a hydrolysis reaction. This reaction is exacerbated by the alkalinity of the SiO_2 colloid (pH = 9.1). Alkaline cations can break glycosidic bonds in the atomic structure of the wood, further accelerating the decomposition process and reducing the durability of the material (Bobleter, 1994; Di Blasi *et al.*, 2009).

1.2 Research Significance and Objectives

Although research has proven that SiO_2 nanoparticle impregnation is an effective method of improving wood properties, the durability and performance of SiO_2-treated wood when subjected to different environmental conditions have yet to be fully addressed in the literature. Additionally, the mitigation of the combined effects of hydrolysis and alkaline attack during the vacuum impregnation process has not been adequately examined. This thesis builds on the results obtained by Lemaire-Paul *et al.* (2022) in order to determine the behaviour and properties of SiO_2-treated spruce wood after being subjected to both accelerated aging under high temperature and humidity as well as freeze-thaw cycling. The effects of these accelerated aging conditions on the spruce wood samples were determined using various characterization methods to measure the properties of both SiO_2-treated and non-treated samples before and after aging. This study also introduces a potential method of reducing the negative impact of the impregnation process on the durability of SiO_2-treated wood.

1.3 Research Methodology

The research outlined in this thesis was conducted at the University of Ottawa in collaboration with the National Research Council of Canada. White spruce (*Picea glauca*) samples were vacuum-treated with a nano-SiO_2 colloid at the University of Ottawa. Two types of accelerated aging (hydrolytic aging and freeze-thaw cycling) were performed at the National Research Council of Canada, and a series of characterization tests was performed to determine the effects of both aging conditions on the samples. Dynamic mechanical analysis (DMA) and tensiometry were used to examine changes in the viscoelastic properties and water uptake of the samples. Additionally, changes in the peak cellulose degradation temperature and crystallinity of the samples were used as degradation indicators. These values were determined using thermogravimetric analysis (TGA) and powder X-Ray diffraction (XRD). Finally, ATR-FTIR spectroscopy and scanning electron microscopy (SEM) were performed to determine the impregnation depth and behaviour of the colloid on the surface of the samples. This thesis elaborates on the experimental procedure, analytical results, and conclusions obtained as a result of this study.

1.4 Thesis Organization

This thesis is presented in an article-based format and is divided into 6 chapters that can be outlined as follows:

- Chapter 1 provides a general introduction to the research topic and defines the significance, objectives, and methodology of the research.
- Chapter 2 presents a comprehensive literature review of the theory and concepts behind the study. This section includes a review of the behaviour, properties, and degradation methods of wood. It also provides a summary of previous research conducted on the effects of nanoparticle treatment on wood properties.
- Chapter 3 contains the first article, which describes the experimental procedure and results of the characterization tests performed on spruce wood samples subjected to accelerated aging under high temperature and high humidity conditions.
- Chapter 4 contains the second article, which describes the experimental procedure and results of the characterization tests performed on spruce wood samples subjected to accelerated aging through freeze-thaw cycling.
- Chapter 5 summarizes and discusses the results obtained in Chapters 3 and 4, highlights key findings, and provides recommendations for future work.

1.5 References

Bak, M., & Németh, R. (2018). Effect of different nanoparticle treatments on the decay resistance of Wood. *BioResources*, *13*(4). https://doi.org/10.15376/biores.13.4.7886-7899

Bobleter, O. (1994). Hydrothermal degradation of polymers derived from plants. *Progress in Polymer Science*, *19*(5), 797–841. https://doi.org/10.1016/0079-6700(94)90033-7

Chang, H., Tu, K., Wang, X., & Liu, J. (2015). Fabrication of mechanically durable superhydrophobic wood surfaces using polydimethylsiloxane and silica nanoparticles. *RSC Advances*, *5*(39), 30647–30653. https://doi.org/10.1039/c5ra03070f

Churkina, G., Organschi, A., Reyer, C. P. O., Ruff, A., Vinke, K., Liu, Z., Reck, B. K., Graedel, T. E., & Schellnhuber, H. J. (2020). Buildings as a global carbon sink. *Nature Sustainability*, 3(4), 269–276. https://doi.org/10.1038/s41893-019-0462-4

Clausen, C. A., Kartal, S. N., Arango, R. A., & Green, F. (2011). The role of particle size of particulate nano-zinc oxide wood preservatives on termite mortality and leach resistance. *Nanoscale Research Letters*, *6*(1). https://doi.org/10.1186/1556-276x-6-427

Di Blasi, C., Galgano, A., & Branca, C. (2009). Influences of the chemical state of alkaline compounds and the nature of alkali metal on wood pyrolysis. *Industrial & Engineering Chemistry Research*, *48*(7), 3359–3369. https://doi.org/10.1021/ie801468y

Ghorbani, M., Biparva, P., & Hosseinzadeh, S. (2017). Effect of colloidal silica nanoparticles extracted from agricultural waste on physical, mechanical and antifungal properties of wood polymer composite. *European Journal of Wood and Wood Products*, *76*(2), 749–757. https://doi.org/10.1007/s00107-017-1157-z

Giudice, C. A., & Pereyra, A. M. (2009). Silica nanoparticles in high silica/alkali molar ratio solutions as fire-retardant impregnants for Woods. *Fire and Materials*. https://doi.org/10.1002/fam.1018

Last, J. (2014). Longhouse Lifestyles in the Central European Neolithic. In Fowler, C., Harding, J., and Hofmann, D. (Eds.), *The Oxford Handbook of Neolithic Europe* (pp 273-290). Oxford University Press. https://doi.org/10.1093/oxfordhb/9780199545841.001.0001

Lebow, S. T. (2010). Chapter 15: Wood preservation. In R. J. Ross (Ed.), *Wood handbook: wood as an engineering material* (Centennial Edition, pp. 15.1–15.28). U.S. Dept. of Agriculture, Forest Service, Forest Products Laboratory. https://www.fpl.fs.usda.gov/documnts/fplgtr/fplgtr190/chapter_15.pdf

Lemaire-Paul, M., Beuthe, C. A., Riahinezhad, M., & Foruzanmehr, M. (2022). The impact of vacuum pressure on the effectiveness of SiO_2 impregnation of Spruce Wood. *Wood Science and Technology*, *57*(1), 147–171. https://doi.org/10.1007/s00226-022-01448-0

Li, X., Tabil, L. G., & Panigrahi, S. (2007). Chemical treatments of natural fiber for use in natural fiber-reinforced composites: A Review. *Journal of Polymers and the Environment*, *15*(1), 25–33. https://doi.org/10.1007/s10924-006-0042-3

Rybníček, M., Kočár, P., Muigg, B., Peška, J., Sedláček, R., Tegel, W., & Kolář, T. (2020). World's oldest dendrochronologically dated archaeological wood construction. *Journal of Archaeological Science*, 115, 105082. https://doi.org/10.1016/j.jas.2020.105082

Wang, C., & Piao, C. (2011). From Hydrophilicity to Hydrophobicity: A Critical Review—Part II: Hydrophobic Conversion. *Wood and Fiber Science*, 43(1), 41–56. https://wfs.swst.org/index.php/wfs/article/view/672

Chapter 2

2.0 Literature Review

2.1 Morphology of Wood

2.1.1 General

Wood is both anisotropic and orthotropic. This means it exhibits different behaviour and strength characteristics depending on the direction of the grain (Meier, 2015). Wood is normally described in terms of three principal planes: tangential (T), radial (R), and longitudinal (L). The term *axial* may also be used to refer to the longitudinal plane (Meier, 2015). The three planes are illustrated in Figure 1 below.

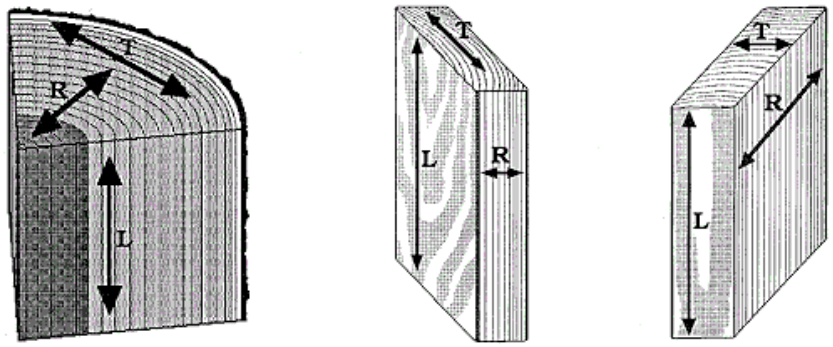

Figure 1. The three principal places of wood (Wengert & Meyer, 1993)

Construction lumber is typically derived from tree trunks. The macroscopic structure of a tree trunk is shown in Figure 2. Trees grow outward from the pith, which is formed during the first year of growth (Ek *et al.*, 2009), before the formation of heartwood (Walker *et al.*, 1993). The heartwood layer consists of dead cells that contain chemicals known as extractives that protect the growing tree from fungal growth and insect damage (Walker *et al.*, 1993). The sapwood layer is the active or "living" part of a tree trunk. The conduction of water and sap takes place in the sapwood layer (Wiedenhoeft, 2010). Nutrients such as carbon, starch, and lipids are also stored in this layer (Wiedenhoeft, 2010).

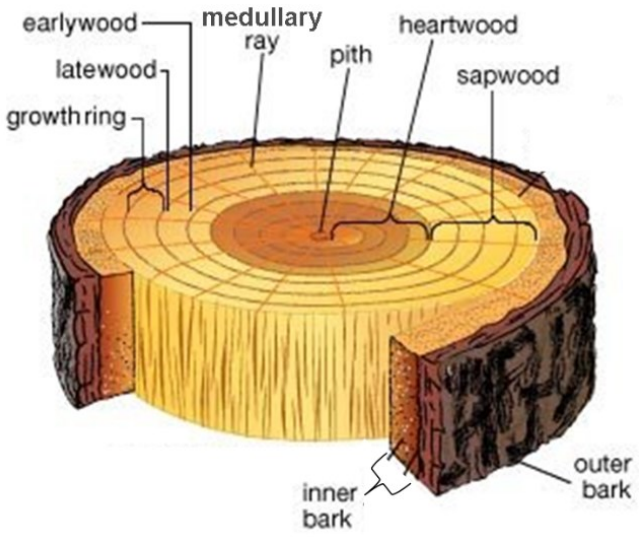

Figure 2. Morphology of the wood macroscopic structure (Wood Stairs, 2017)

New layers of sapwood are formed over time by a thin layer of dividing cells known as cambium located just underneath the inner bark layer (Walker *et al.*, 1993). While the tree continues to form new sapwood layers and grow outwards, the innermost sapwood layers begin to form embolisms due to a lack of oxygen. As the cells in this layer die off and a new heartwood layer is formed, starch deposits begin to hydrolyze into sugars that eventually result in the formation of extractives that persist in the heartwood even after the cells have died (Ek *et al.*, 2009).

The inner bark layer is composed of a combination of phloem tissues and a tissue complex called the periderm. The phloem tissues are responsible for the conduction of sugars produced by photosynthesis (Wiedenhoeft, 2010). The outer bark layer is composed of a hard layer of dead tissues (Ek *et al.*, 2009) that protect the tree from parasites, moisture loss, fire, and damage (Ek *et al.*, 2009; Walker *et al.*, 1993). As the tree ages, the periderm in the inner bark layer is continually pushed into the outer bark, where it dies off and forms new outer bark layers (Ek *et al.*, 2009).

2.1.2 Wood Cellular Structure

Wood used for construction can be classified into two categories: hardwood and softwood. Hardwood originates from angiosperm trees whereas softwood originates from gymnosperm trees (Barker & Owen, 1999). Spruce wood species such as the Norway spruce (*Picea abies*) and white spruce (*Picea glauca*) as are classified as softwoods (Barker & Owen, 1999). As the common nomenclature suggests, the majority of hardwoods are harder than softwoods with the exception of a few categorical outliers. For instance, balsa

and cottonwood are both classified as hardwood, yet are relatively soft. Conversely, softwoods such as the southern pine and yew are comparatively harder than some hardwoods (Williams, 1953; Meier, 2015).

The wood cell systems of both softwoods and hardwoods are arranged in an axial-radial structure, with the wood cells extending parallel to the longitudinal direction (Ek *et al.*, 2009). However, softwoods have a simpler cellular structure when compared to hardwoods. The cellular structure of softwoods is composed entirely of two distinct cell types: tracheids and parenchyma, as shown in Figure 3. Tracheids make up over 90% of the softwood cellular structure, and form the wood cell support and water conduction system (Wiedenhoeft, 2010; Ek *et al.*, 2009). Although all softwoods contain axial tracheids, a select few also exhibit ray tracheids. Ray tracheids are not found in hardwoods and are responsible for the transport of liquids in the radial direction. These cells are most commonly found in species of softwood that also contain resin canals, such as spruce, pine, larch, and Douglas-fir (Wiedenhoeft, 2010). Tracheid cell walls feature an abundance of bordered pits, which facilitate the transport of liquids throughout the tracheid system (Ek *et al.*, 2009; Walker *et al.*, 1993). The remaining ~10% of the softwood cellular structure is composed of longitudinal and ray parenchyma cells. Parenchyma cells are responsible for the storage of nutrients essential to the growth of the tree such as starch and lipids (Wiedenhoeft, 2010).

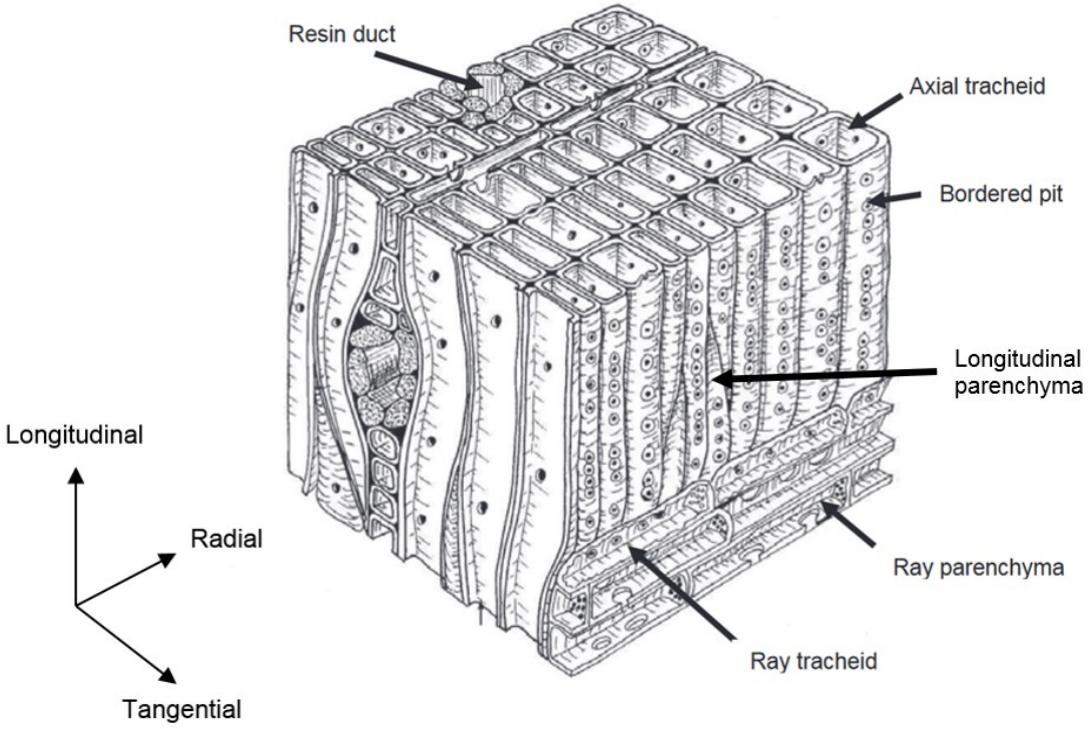

Figure 3. Cellular structure of a typical softwood (edited from Thomassen, 1977 via Pedersen, 2015)

Hardwoods have a more complex cellular structure than softwoods, as shown in Figure 4. The cellular structure of hardwoods is composed of four main cell types: fibres, vessels, tracheids, and parenchyma (Ek *et al.*, 2009). Fibres form the thickest part of the hardwood cell structure and are a major contributing factor to the density and strength of the material (Wiedenhoeft, 2010). Vessels are arranged in a stacked formation and act as the main water conduction system of the cell structure. The first time water attempts to pass through a vessel, a hydrolysis process is perpetuated by the non-cellulosic components of the vessel (Walker *et al.*, 1993), forming a porous section known as a perforation plate at the connection point of two vessels. The formation of this plate is a unique evolutionary trait exhibited only by angiosperm trees (Liu *et al.*, 2020) that facilitates the conduction of water through the wood cell structure (Wiedenhoeft, 2010).

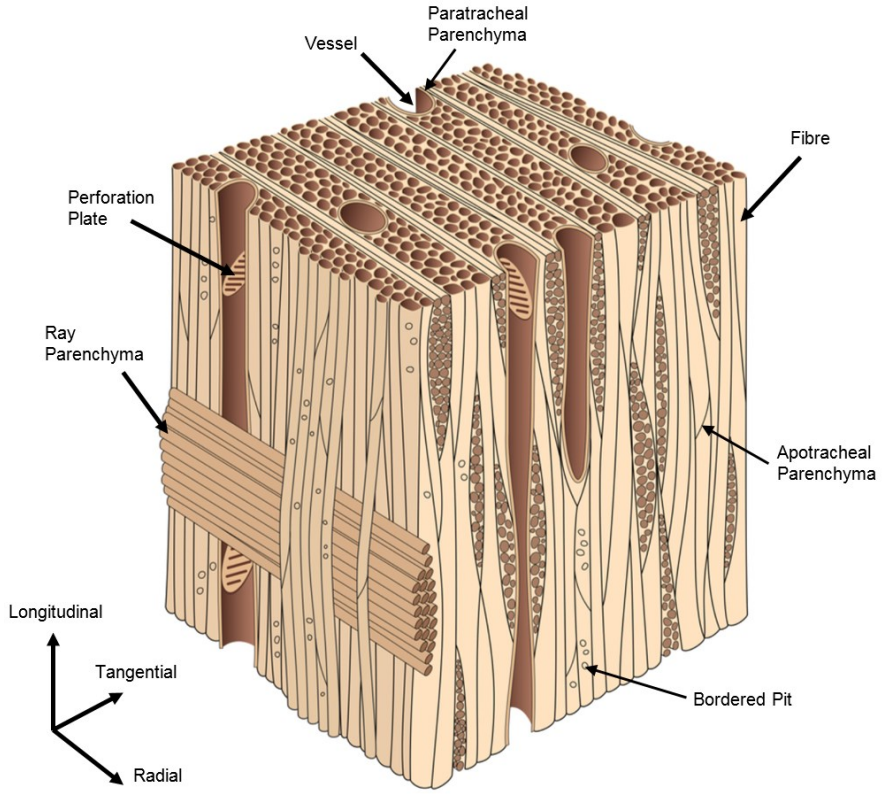

Figure 4. Cellular structure of a typical hardwood (edited from Duffield Timber, 2021)

The same wood cell wall structure is found in all wood species (Rowell, 2013). As shown in Figure 5, the structure contains five layers: the middle lamella, the primary wall, and three additional cell wall layers (S_1, S_2, S_3) that form the secondary wall.

The middle lamella is largely composed of a lignin matrix and contains the highest lignin content of all the layers as well as some pectin and cellulose (Walker *et al.*, 1993; Ek *et al.*, 2009). The primary wall is an

extremely thin layer composed exclusively of unstructured cellulose microfibrils linked by the hemicellulose xyloglucan (Walker *et al.*, 1993; Ek *et al.*, 2009). Microfibrils are cellulose molecules that have aggregated to form long threadlike macromolecules during the natural cellulose synthesis process (Brett, 2000; Wiedenhoeft, 2010). The secondary wall contains three layers of structured cellulose microfibrils with a high variation in both chemical composition and orientation angle. The orientation angle of cellulose is commonly referred to as the microfibril angle (MFA) (Ek *et al.*, 2009). Layer S_2 is the thickest and most important layer of the secondary wall (Rowell, 2013). The orientation of the microfibrils in the S_2 layer is the primary cause of the anisotropic behaviour of wood (Walker *et al.*, 1993). Cave (1968) and Cave & Walker (1994) discovered that a high MFA in the S_2 layer can negatively affect the bending strength and stiffness of wood.

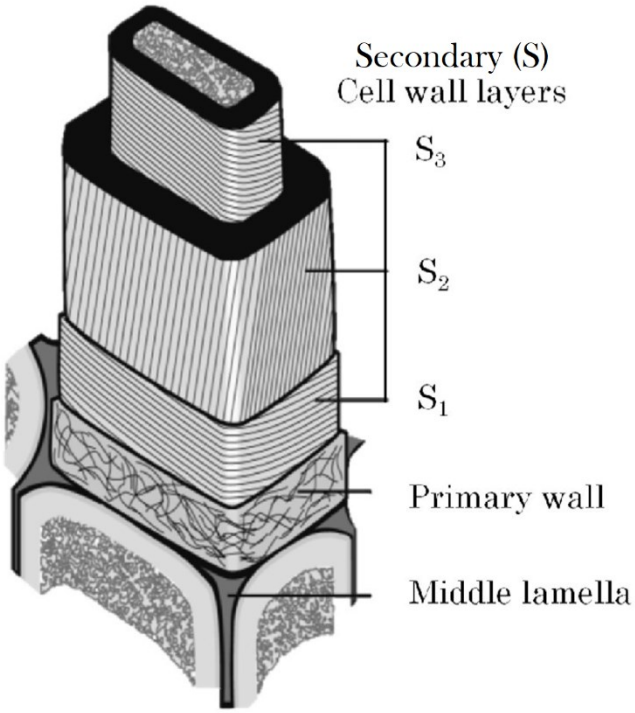

Figure 5. Typical wood cell wall structure (modified from Rowell, 2013 via Purba, 2019)

2.1.3 Chemical Composition

Wood cell walls are heterogeneous and are composed of cellulose microfibrils, hemicellulose, lignin, pectin, and extractives (Rowell, 2013). The exact chemical composition of wood cell walls varies greatly depending on the species in question (Sjöström & Westermark, 1999; Inari *et al.*, 2006). Based on data summarized by Sjöström (1993), the average chemical composition of *Picea glauca* is 39.5% cellulose, 27.5% lignin, 27.6% hemicellulose, and 2.1% extractives.

2.1.3.1 Cellulose

Cellulose is a polymer organized in a simple structure of up to 15,000 β-glucopyranoside residues linked by 1→4 β-glycosidic bonds (Ek *et al.*, 2009). Each individual cellulose chain rotates 180° with respect to its neighbours (Walker *et al.*, 1993). Strong hydrogen bonds between the C_6 and C_2 hydroxyl as well as the C_5 oxygen and C_3 hydroxyl reinforce the material and increase the tensile strength of wood (Ek *et al.*, 2009; Walker *et al.*, 1993). These bonds are represented by the dotted lines in Figure 6.

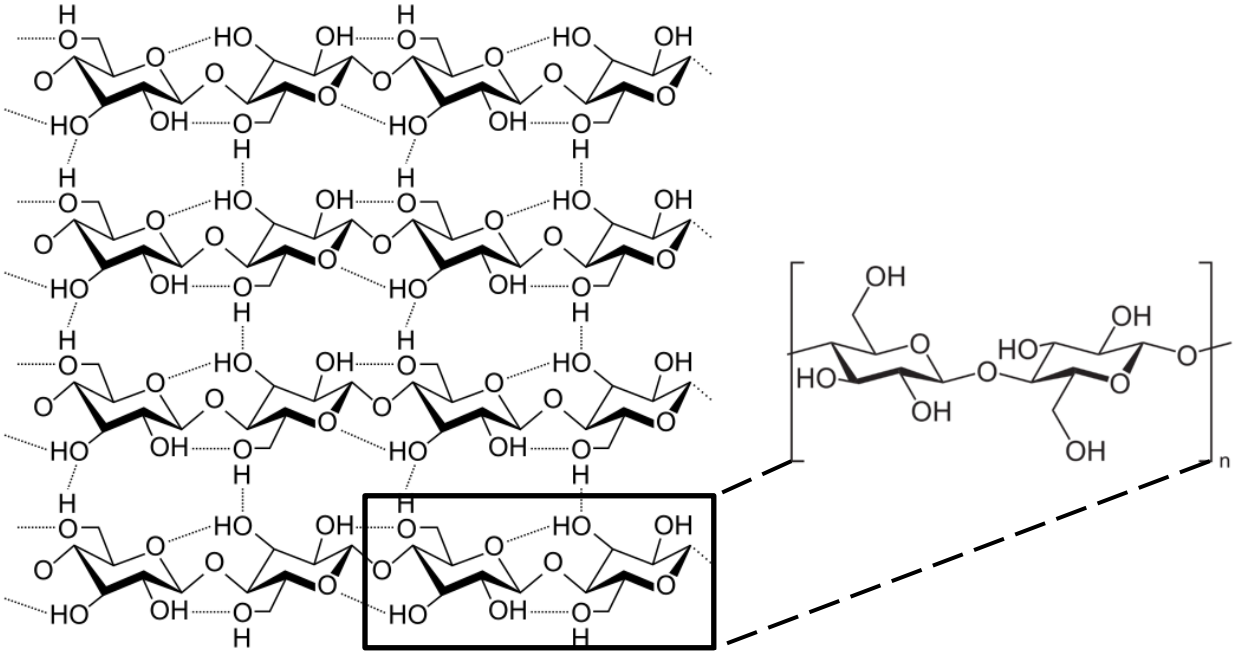

Figure 6. Full cellulose strand structure (left) and a single cellulose chain structure (right) (modified from Laghi, 2019 and NEUROtiker, 2007)

2.1.3.2 Hemicellulose

Hemicelluloses are classified as heteropolymers, meaning they are derived at least two different monomers (Nath, 2018). There are five principal hemicelluloses found in wood, as outlined in Table 1. The structures of these hemicelluloses are primarily composed of pentose (L-arabinose, D-xylose) and hexose (D-glucose, D-mannose, D-galactose) sugars. Hemicellulose chains follow the same 1→4 β-glycosidic bond organization as cellulose microfibrils, as demonstrated by the xyloglucan chain in Figure 7. The role of hemicellulose in the chemical structure of wood is uncertain. Ek *et al.* (2009) theorized that hemicelluloses may influence the moisture equilibrium of the tree. Walker *et al.* (1993) suggests that hemicelluloses may simply exist to bond with cellulose microfibrils and lignin in order to aid in the transfer of shear stress.

Table 1. Principal hemicelluloses found in wood (Sjöström, 1981 via Walker *et al.*, 1993)

Hemicellulose	Occurrence	Percentage in wood (%)
Galactoglucomannan	Softwood	5-8
Glucomannan	Softwood	10-15
Arabinoglucuronoxylan	Softwood	7-10
Arabinogalactan[+]	Larch	5-35
Glucoronoxylan	Hardwood	15-30
Glucomannan	Hardwood	2-5

[+]normally only 1-5% in softwoods, larch is an exception.

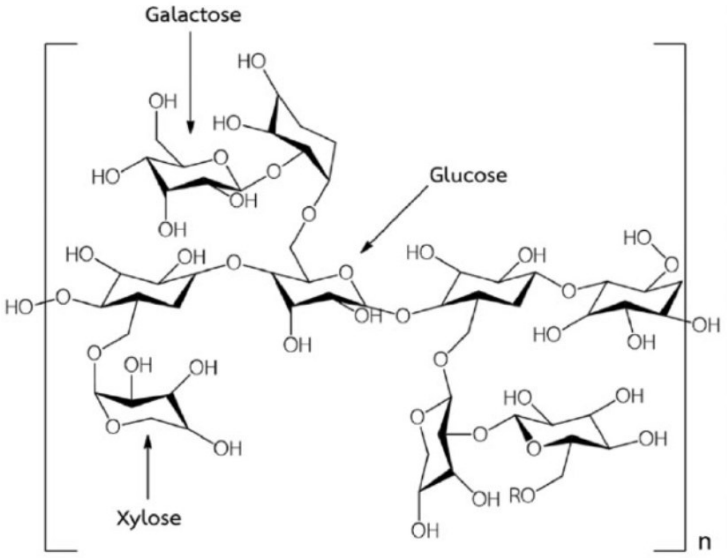

Figure 7. Chemical structure of xyloglucan (Songtipya *et al.*, 2021)

2.1.3.3 Lignin

Lignin is an alkyl-aromatic polymer. Aromatic materials can also be classified as hydrophobic due to the cyclic structure of their molecules. The lignin structure is composed of three types of phenylpropane-derivative monomer units called monolignols: *p*-coumaryl alcohol, coniferyl alcohol, and sinapyl alcohol. These monolignols are connected by C–C and C–O–C bonds (Walker *et al.*, 1993), as shown in Figure 8. The presence of lignin in the wood cell walls serves multiple important functions. Lignin acts as a glue between the cellulose and hemicellulose, protecting the weaker microfibril layers from buckling (Walker *et al.*, 1993) while also enhancing the compressive strength of wood. It also helps mitigate the swelling of wood cell walls due to its hydrophobic properties, and protects against biological degradation due to its high level of compaction.

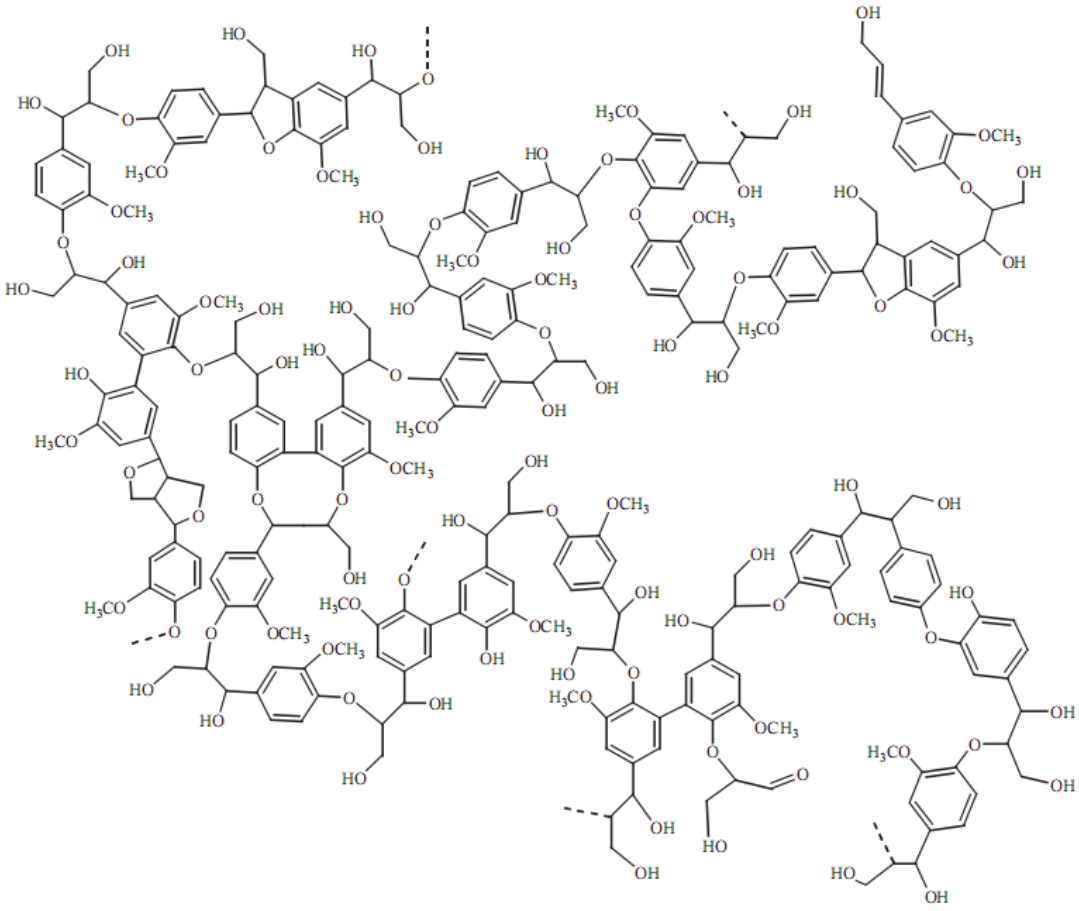

Figure 8. An example of a potential softwood lignin structure (Ek *et al.*, 2009)

2.2 Behaviour, Properties, and Degradation Mechanisms of Wood

2.2.1 Wood Strength

Due to the status of wood as both an orthotropic and an anisotropic material, the compressive strength and tensile strength of wood are entirely dependant on the orientation of the wood grain. Wood is stronger in both tension and compression when a load is applied parallel to the grain (longitudinally). When a load is applied perpendicular to the grain (radially/tangentially), the compressive strength of wood reduces by 80-90%, and the tensile strength may reduce by up to 97% (Harte, 2009). Due to the longitudinal orientation of the cell walls, the wood fibres are easily crushed or pulled apart when a load is applied in either the radial or tangential directions.

The density and porosity of wood can have a significant effect on the mechanical properties of wood. Wood density is highly sensitive to changes to humidity and moisture content (Ek *et al.*, 2009) since it is governed by the thickness and behaviour of the wood fibres (Wiedenhoeft, 2010). When subjected to temperatures

below the fibre saturation point of wood, bound water within the wood will evaporate and the wood will undergo shrinkage (Reeb, 2009). Wood shrinkage may result in an increase in density and a decrease in porosity, and consequently an increase in mechanical properties (Izekor *et al.*, 2010). However, high-temperature shrinkage may also induce the formation of microcracks within the wood cell structure, resulting in the reduction of wood strength (Yamamoto *et al.*, 2013).

2.2.2 Modulus of Rupture and Elasticity

The modulus of rupture (MOR) and modulus of elasticity (MOE) are two of the most commonly tested mechanical properties of wood. Both properties are determined by performing a three-point bending test on a wood sample cut to ASTM standards. The MOR measures the flexural or bending strength of wood and is used to determine the maximum load a wood sample can withstand before rupture (Meier, 2015). It is commonly expressed in megapascals (MPa). The MOE is also known as Young's modulus. It is used to determine the maximum elastic deflection a wood sample can withstand (Meier, 2015). The maximum deflection is calculated by taking the ratio of the maximum stress (load) applied to an object over the strain (deformation) experienced by the object at that point. This value is commonly expressed in gigapascals (GPa).

2.2.3 Viscoelastic Properties

Wood is a naturally viscoelastic composite. This signifies that it exhibits both time-dependent viscous behaviour as well as elastic behaviour when subjected to a constant load (Ozyhar *et al.*, 2013; Huč *et al.*, 2018). A fully elastic material does not dissipate energy and will quickly return to its original state after the applied load is removed. By contrast, a viscoelastic material is able to both store and dissipate energy (Ameli *et al.*, 2022). Since wood is a viscoelastic material, it will be subjected to a time-dependant degradation mechanism known as creep when subjected to continuous stress below its yield strength (Connor, 2020). This process is elaborated upon in Section 2.2.10. Figure 9 demonstrates the difference between the strain accumulated over time for an elastic and a viscoelastic material under the influence of a constant load.

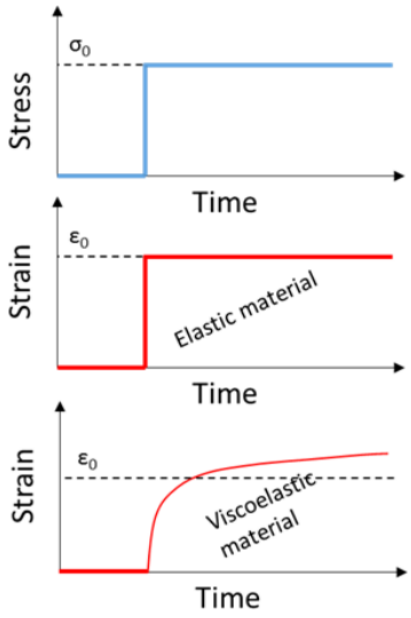

Figure 9. Comparison of strain/time curves of elastic and viscoelastic materials under a constant stress (Naemi *et al.*, 2016)

Viscoelastic behaviour can be described by three variables: the storage modulus, loss modulus, and the loss tangent (also known as the $tan\delta$). Experimentally, these values are found by conducting dynamic mechanical analysis. In this test, an oscillatory load is applied to a sample in cycles over different periods of time, and the reaction of the sample is measured at different temperatures and frequencies (PerkinElmer, 2013). The storage modulus of a viscoelastic material, E', is a representation of the amount of energy needed to be stored in the elastic portion of a material in order to distort it. For a viscoelastic construction material like wood, a high storage modulus signifies that the material will be more resistant to deformation. The loss modulus, E'', represents the ability of the viscous portion of a material to dissipate stored energy as heat during one loading cycle (Schaller, 2020). The two variables can be expressed as follows (Fuss, 2015):

$$E' = \frac{\sigma_0}{\varepsilon_0} cos\delta$$

$$E'' = \frac{\sigma_0}{\varepsilon_0} sin\delta$$

where σ_0 is the peak amplitude of the stress, ε_0 is the peak amplitude of the strain, and δ is the phase angle between the two.

The loss tangent ($tan\delta$) represents the damping coefficient of the material as a function of time, temperature, or frequency (Ebnesajjad, 2014), and is expressed as the tangent of the phase angle, or the ratio of the loss modulus over the storage modulus (Fuss, 2015):

$$tan\delta = \frac{E''}{E'}$$

2.2.4 Dimensional Stability

Wood is a hydrophilic material, as demonstrated by the hydroxyl groups found in all three of its primary chemical components (Hartley & Hamza, 2016). Wood is also hygroscopic, meaning it will naturally absorb water molecules from the surrounding environment until its equilibrium moisture content (EMC) has been reached (Hartley & Hamza, 2016; El-Dabaa & Abdelmohsen, 2023). The EMC value of wood is not constant and will fluctuate depending on the temperature and relative humidity of the surrounding environment (Camuffo, 2004). The hydrophilic/hygroscopic nature of wood makes it highly susceptible to deformation and degradation due to the formation of microcracks during the process of swelling and shrinkage (Reinprecht, 2016; Yamamoto *et al.*, 2013).

Wood is only able to shrink and swell below its fiber saturation point (FSP), which is the point where the wood cell walls are saturated and the cell cavities are empty (Glass & Zelinka, 2010). The FSP of most wood species is typically 30% (Simpson, 2001). During shrinkage, adsorbed water within the wood cell walls is removed, causing the cell wall components to form strong hydrogen bonds with each other instead. Due to the presence of these bonds, the wood will adsorb water at a slower rate during swelling, forming the basis of a hysteresis loop as shown in Figure 10 (Walker *et al.*, 1993). The term *dimensional stability* refers to the level of swelling and shrinkage wood will experience when subjected to changes in temperature and humidity (Sargent, 2019). Due to the anisotropic nature of wood, the total or *volumetric* shrinkage of a wood sample is found by taking the sum of the shrinkage experienced in both the tangential and radial directions, with the longitudinal shrinkage usually being considered negligeable (Meier, 2015). The dimensional stability of a wood sample is dependant not only on the wood moisture content level, but also the wood species and the testing method employed (Sargent, 2019).

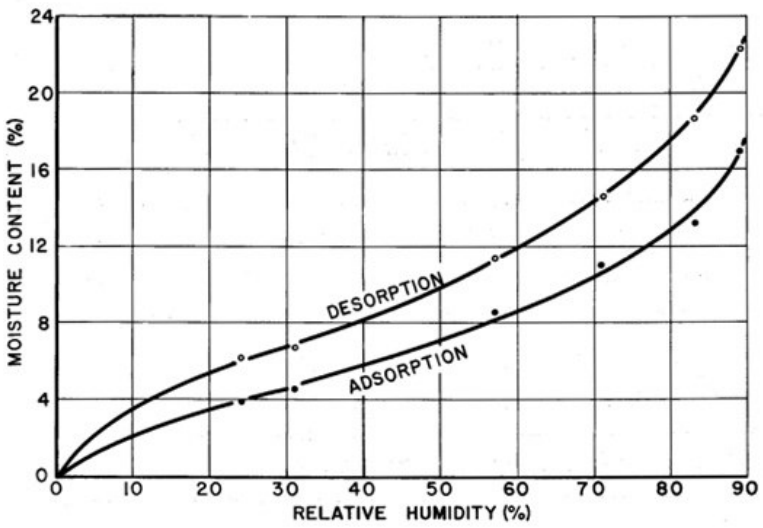

Figure 10. Typical wood hysteresis loop (Shniewind, 1956)

2.2.5 Crystallinity

The *crystallinity* of a material defines the level of order within its crystalline structure (University of Cambridge, 2023). Wood is considered a semi-crystalline polymer (Benedetti *et al.*, 2019), and its components can be semi-crystalline (cellulose) or amorphous (lignin and hemicellulose) (Tarmian & Mastouri, 2019). A semi-crystalline material such as cellulose contains both crystalline and amorphous regions as shown in Figure 11. The crystalline region of a material contains ordered, repeating atomic structures whereas the amorphous region is unstructured and irregular (LibreTexts, 2023).

High temperature and high humidity conditions can cause a significant increase in the crystallinity of wood due to the degradation of the amorphous region of cellulose, as shown in studies performed by Tarmian & Mastouri (2019), Toba *et al.* (2013), and Bhuiyan *et al.* (2000). An increase in crystallinity may result in significant changes in wood properties such as an increase in MOE, a decrease in flexibility (Andersson *et al.*, 2003), an increase in storage modulus, a decrease in loss modulus (Reiniati *et al.*, 2014), and a decrease in EMC (Tarmian & Mastouri, 2019).

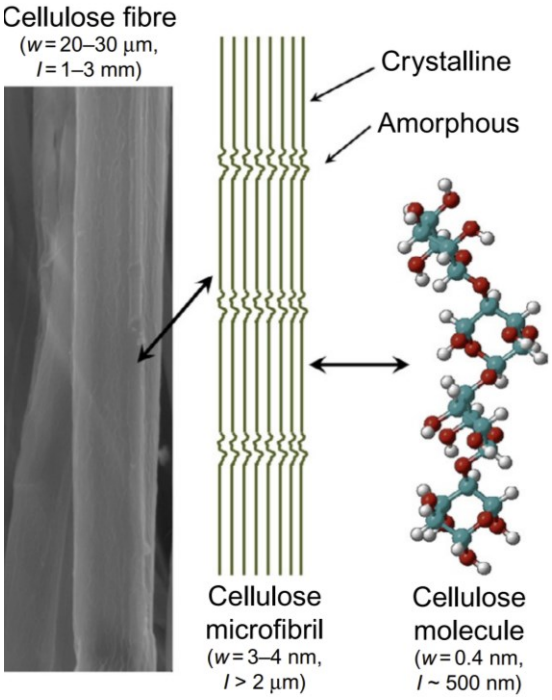

Figure 11. The crystalline structure of cellulose (modified from Popsecu, 2017)

2.2.6 Hydrolytic Degradation

Hydrolysis is a chemical reaction that occurs when a material containing hydroxyl groups comes into prolonged contact with water or other polar solvents. This reaction causes glycosidic bonds within the material to break, weakening the integrity of the molecular structure of the wood (Bobleter, 1994). A hydrolysis reaction can be triggered upon exposure to acids, alkali, or water. Acid hydrolysis occurs when glycosidic bonds are broken to form a conjugated acid upon exposure to H+ ions (Bobleter, 1994). During alkaline hydrolysis, OH^- ions in the reactant cause a reaction known as "peel-off" when glucose groups detach from the ends of cellulose chains in the amorphous region of cellulose (Van Loon & Glaus, 1997; Haas *et al.*, 1967). These ends are commonly referred to as "reducing ends" and eventually transform into metasaccharine acids after separating, as shown in Figure 12. Hydrothermal cleavage is the third type of hydrolysis and occurs when water forms hydrogen bonds with hydroxyl groups in the cellulose structure, creating two glucose molecules and breaking pre-existing glycosidic bonds in the process (Bobleter, 1994). Therefore, the effects of hydrolysis are exacerbated under high-temperature, high-humidity conditions.

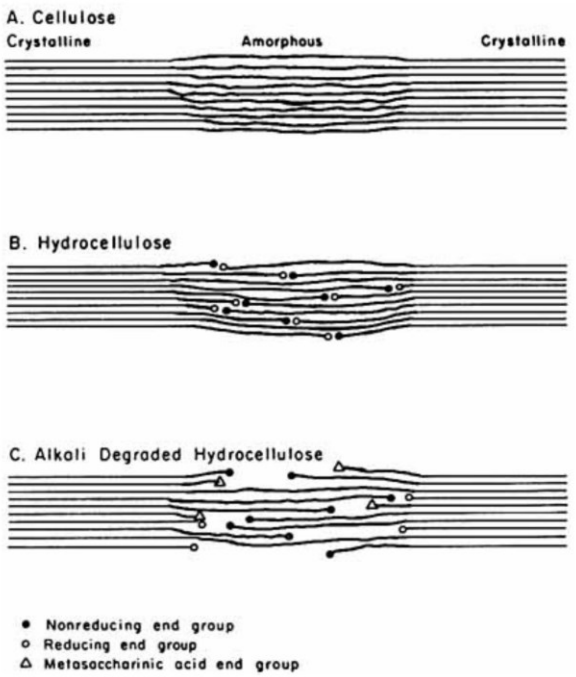

Figure 12. Alkaline degradation of the amorphous region of cellulose (Haas *et al.*, 1967)

2.2.7 Freeze-thaw Degradation

Kübler (1962), Shmulsky & Shvets (2006), and Campean *et al.* (2008) describe a degradation mechanism of wood that only occurs at freezing temperatures and leads to the weaking of the wood cell walls. As the temperature begins to drop below 0°C, free water within the lumens of the wood freezes and applies pressure on the surrounding cell walls, breaking bonds between bound water molecules and the wood. This process effectively compacts the wood cell walls and causes the unfrozen bound water within to be squeezed out and into the lumens, facilitated by a difference between the vapour pressure in air and in the bound water. Once it reaches the lumens, the bound water crystallizes and will evaporate with the remainder of the free water through capillary movement until the wood begins to thaw. This process leads to the formation of microcracks in the wood (Campean *et al.*, 2008).

2.2.8 Thermal Degradation and Flammability

Wood will undergo a thermal degradation process when exposed to temperatures greater than 100°C (Dietenberger & Hasburgh, 2016). The chemical composition and crystallinity of wood can have an effect on the thermal degradation process of wood (Poletto *et al.*, 2012). The thermal degradation process may be accelerated in wood with a high extractive content and high hemicellulose and lignin reactivity, leading to

the degradation of cellulose at lower than standard temperatures (Poletto *et al.*, 2012). At a temperature range of 300-600°C, wood will undergo *pyrolysis*, a process in which biomass is converted to char in the absence of oxygen (Poletto *et al.*, 2012). The formation of char during wood pyrolysis can contribute to a reduction in the rate of pyrolysis progression. If a thick enough layer of char is formed, it can create an insulating effect, reducing the degradation rate and the rate of char production by approximately 0.2 mm/min (Dietenberger & Hasburgh, 2016).

The decomposition of wood between 100-450°C was detailed by Dietenberger and Hasburgh (2016). This process is summarized in Table 2. It is worth noting that Sehlstedt-Persson (2005) determined that pine wood experienced a weight loss of only 0.7% after drying for 450 hours at 103°C, and experienced a maximum weight loss of less than 0.5% after drying at 103°C for ~65 hours or less. Therefore, even though the typical drying temperature of wood is slightly above the 100°C threshold described by Dietenberger and Hasburgh (2016), it can be concluded that wood will not undergo significant thermal deterioration when dried at 103°C for a typical 24-hour period.

Table 2. The decomposition process of wood between 100-450°C (Dietenberger & Hasburgh, 2016)

Temperature	Behaviour
100-200°C	- Wood dehydrates, releasing noncombustible gases and liquids. - Auto-hydrolysis and auto-oxidation become more pronounced. - Natural extractives decompose between 150-200°C (only at a slow heating rate).
130°C	- Volatile organic compounds are detected for the first time. - Carbohydrate polymers are reduced to a carbon char.
200-300°C	- Wood components begin to undergo pyrolysis. - Significant amounts of CO and high-boiling-point tar are released. - Hemicellulose is pyrolyzed. Lignin is pyrolyzed between 225-450°C. - Degree of cellulose polymerization decreases, free radicals appear, and carbonyl, carboxyl, and hydroperoxide groups are formed.
300-350°C	- Significant, highly endothermic depolymerization of cellulose. - Aliphatic side chains break off from aromatic rings in lignin.
370-400°C	- C–C groups in lignin split (exothermic reaction).
≥450°C	- Volatile emissions end. - Char degrades further, oxidizes into CO_2, CO, H_2O.

2.2.9 Biological Degradation

At high moisture content levels, wood becomes vulnerable to fungal growth and decay if left untreated. Wood-rotting fungi will flourish if the moisture content in wood is above 35%. Between 25% and 30% moisture content, fungal spores have more difficulty germinating in wood. If the material has a moisture content of 20% or less, it is considered immune to fungal decay (Baker, 1969). Traditional techniques used to combat fungal infestation commonly include the application of preservative coatings and damp-proof membranes on the surface of the wood (Teng *et al.*, 2018; Garratt's Damp & Timber, 2019).

Wood with a high moisture content also becomes more susceptible to damage caused by wood-eating insects such as termites. Termites require a high moisture content level to survive as their exoskeletons are unsclerotized, meaning that the cuticle or "skin" of their bodies is exposed and cannot retain water (Zukowski & Su, 2020). McManamy *et al.* (2008) found that a wood moisture content of at least 30% was the ideal condition for long-term termite survival. Additionally, they determined that termites were unable to survive longer than a maximum of 12.5 days at a wood moisture content of 24% or less, as their water intake at this level was not enough to compensate for cuticular water loss. In warmer climates, wood-eating insects pose a severe threat to the structural integrity of wood-frame buildings. Yearly fumigation is typically necessary in these regions to reduce the risk of insect damage.

2.2.10 Creep

Creep is a mechanical failure mode defined as the increase in permanent deformation a material can experience over time when subjected to a constant stress below its yield strength (Connor, 2020). The propensity of a material to exhibit creep behaviour is referred to as *creep compliance*. Therefore, if a material is stated to display *high creep compliance*, it will be more susceptible to creep. Since wood is a naturally viscoelastic composite, its vulnerability to creep remains a primary element of concern when used as a structural element in building construction. Due to the orthotropic nature of the material, the creep compliance of wood is slightly higher in the tangential direction than in the radial direction (Ozyhar *et al.*, 2013). The level of creep compliance of wood can be heavily influenced by environmental conditions such as temperature and humidity (Holzer *et al.*, 1989). Bach (1966) deduced from tensile tests that the creep compliance of wood is proportional to the square of the moisture content when it is between 4%-12%.

2.3 Accelerated Aging of Wood

Accelerated aging is a procedure used to evaluate the durability and serviceability of a material over time (Gillespie, 1984). Experimental results are obtained by subjecting a material to environmental conditions elevated beyond those found in real life. Therefore, this procedure can often be used to predict the long-term performance of a material (Frigione & Rodríguez-Prieto, 2021). Accelerated aging can be performed by placing a material under any combination of stressors such as temperature and humidity outside of their normal range to accelerate aging and hence degradation. For example, ASTM D1037-12: *Standard Test Methods for Evaluating Properties of Wood-Base Fiber and Particle Panel Materials* describes one of the more commonly used techniques for wood. For this procedure, dry and water-soaked wood samples are subjected to six cycles of accelerated aging including immersion in water, exposure to steam and water vapour, freezing, and heating. This is followed by conditioning the wood at a set temperature of 20°C and 65% RH for at least 48 hours before testing.

2.3.1 Accelerated Aging of Non-treated Wood

Extensive research has been performed on the behaviour of non-treated wood when subjected to different environmental aging conditions over time. Spruce wood has been the subject of many studies that have incorporated accelerated aging. Karami *et al.* (2020) examined the effects of aging spruce wood (*Picea abies*) samples at 130°C and RH values ranging from 0-25% for 3-7 days. The results of this study showed a significant reduction in Equilibrium Moisture Content (EMC) and a significant lightening of the wood. This short aging time was not enough to significantly affect the mechanical properties of the wood, with a <1% change in density and <3% change in damping reported, where damping (tanδ) is defined as the ratio of the loss modulus over the storage modulus.

Froidevaux and Navi (2013) performed a similar study on spruce wood sampled subjected to accelerated aging at various temperatures and RH levels. Samples aged at 140°C and 10% RH for up to 12 days exhibited a significant reduction in radial failure stress but experienced little to no change in their radial Young's modulus. They also found that samples aged at 120°C and 25% RH experienced a loss in radial strength that was 3% higher than samples aged at 120°C and 0% RH, proving that the RH level has a significant effect on the mechanical performance of wood.

The effect of humidity on spruce wood was studied further by Endo *et al.* (2016), who subjected Sitka spruce wood to accelerated aging in an autoclave at 120°C and RH values ranging from 0-100% for up to 7 days. It was found that an increase in moisture content significantly increased the weight loss of the samples. At a heating relative humidity (HRH) of 92%, the spruce wood samples experienced a 7.9% weight loss after 7

days. The samples also demonstrated a reduction in equilibrium moisture content (EMC), but this change was reversible through sample moistening treatment. This reduction in EMC also had an effect on the vibrational properties of wood samples. At an HRH level of 92%, the specific dynamic Young's modulus (E'/ρ) of the samples was reduced significantly while the damping (tanδ) experienced a significant increase.

Additionally, in a study performed by García Esteban *et al.* (2005), it was found that the hygroscopic response of wood will decrease after being subjected to accelerated aging. In their study, wood samples were subjected to five 3-day aging cycles at 50°C and 90% RH followed by desiccation to anhydrous weight. García Esteban *et al.* (2005) found that the wood moisture content and sample length stabilized between the fourth and fifth cycles. The hygroscopic behaviour of the samples was tested by placing them in thermostatic baths under increasing air humidity values. A loss of hygroscopic response was detected at all degrees of humidity for the aged samples when compared to unaged samples. This behaviour was attributed to a gradual decrease in the concentration of hydroxyl groups caused by the fixation of water within the wood cell walls when subjected to accelerated aging.

Freeze-thaw aging is another type of accelerated aging that has been examined at length by Szmutku *et al.* (2013). In their study, spruce wood (*Picea abies*) samples were subjected to a freezing cycle at -25°C for 12 hours, followed by a thaw cycle at 10°C for 12 hours. This freeze-thaw cycling process was repeated for 1 week. Changes to the wood properties after freeze-thaw cycling include a 10% reduction in oven-dry density, a 17% reduction in bending strength, a 29% reduction in modulus of elasticity, and a compressive strength reduction of 30%. They also determined that cyclical freeze-thawing is more detrimental to wood properties than continuous freezing followed by a short thawing period.

Similar findings were also examined by Campean *et al.* (2008), who subjected spruce wood samples to a 20-hour freezing cycle at -30°C, followed by a slow thawing cycle that peaked at 70°C before cooling to 30°C. When comparing the moisture content (MC) of the frozen samples before and after freezing, it was found that there was a 6-10% MC reduction. The samples also exhibited a 6% reduction in bending strength and a 13% reduction in modulus of elasticity. This reduction in moisture content demonstrated by both studies can be related to the removal of bound water from within the lumens as described by Campean *et al.* (2008).

2.3.2 Accelerated Aging of Nanoparticle-treated Wood

Comparatively little research has been performed to examine the effects of accelerated aging on wood samples that have been treated with nanoparticle solutions or colloids. Harandi *et al.* (2016) examined the antifungal effects of impregnating poplar wood with a 5% polyvinyl butyral solution containing either 1% or 2% TiO_2 and ZnO nanoparticles. The samples were exposed to fungal spores and subjected to accelerated

aging at 60°C and 75% RH for 20 days, followed by ultraviolet (UV) radiation at a wavelength of 365 nm for 120 hours. This study determined that samples treated with 2% TiO_2 and ZnO nanoparticles were highly resistant to fungal growth in both dark and light conditions, with an average mass loss of 4.5% and 0.97% respectively.

Machová *et al.* (2019) studied the effects of impregnating oak wood samples with iron nanoparticles (INP). Samples were impregnated with a concentration of 4 g INP/L of demineralized water and subjected to UV radiation with an intensity of 0.35 W m-2 and a wavelength of 340 nm for a set number of 120-minute cycles. They determined that increased exposure to UV radiation had a significant effect on the colour of the INP-treated samples. INP-treated samples would continuously become lighter when compared to NT samples subjected to the same aging conditions. NT samples would also darken significantly at the beginning of the aging process, whereas the INP-treated samples did not.

2.4 Nanotechnological Wood Additives

Treatments are routinely applied to protect wood against various forms of degradation, as well as improve its performance characteristics when used as a construction material. Common examples include the use of copper azoles and borates as preservatives for use in outdoor applications such as decks and fences (Groenier & Lebow, 2006). Waxes, oils, and varnishes are typically used to laminate and protect exposed wood in indoor applications (Woodshop Direct, 2018). These treatment methods are not ideal for use in the construction industry. Since oil and wax treatment leave a considerable number of voids in the wood cell walls unfilled, prolonged exposure to water through rain or snowfall will result in the continuous expulsion of oil and wax from the wood cell wall through a process called preferential wetting (Voulgaridis & Banks, 1983; Borgin, 1968).

Over the past decade, the use of vacuum-aided nanoparticle impregnation has also been explored to reinforce wood for use in the construction industry and has become an active area of research. The vacuum impregnation process facilitates the infiltration of a nanoparticle solution or colloid into the wood vascular system. This obstructs the vascular system of the wood and can result in an improvement in mechanical properties, hydrophobicity, decay resistance, and insect mortality (Li *et al.*, 2007; Bak & Németh, 2018; Clausen *et al.*, 2011). The following section highlights recent studies that have investigated the use of various nanoparticle colloids and solutions to modify and enhance the properties of wood.

2.4.1 Mechanical Properties

Xu *et al.* (2020) studied the effects of nanosilica sol impregnation on the mechanical properties of wood. At a weight percent gain of 30.3%, the modulus of elasticity, bending strength, and average hardness of a treated sample increased by 52.3%, 28.6%, and 86.3% respectively when compared to an untreated sample. This represents a significant improvement in the mechanical properties of Chinese Fir. These improvements were attributed to the natural strengthening of the cell walls, and the reinforcement of the overall wood structure through the filling of voids by the silica sol.

Bak *et al.* (2019) impregnated beech and scots pine samples with hydrophobic silica nanoparticles in two different forms in order to examine changes in the dimensional stability of the wood. Experiments utilized hydrophobized silica (SiO_2) nanoparticles that were suspended either in ethanol (C_2H_6O), or in a tetrahydrofuran solution bonded through the inclusion of polydimethylsiloxane (PDMS). Changes in the dimensional stability of the wood samples were determined by measuring the retention, equilibrium moisture content (EMC), anti-swelling efficiency (ASE), and water uptake of the samples. In all cases, the SiO_2-PDMS composite was superior, resulting in the lowest EMC and water uptake as well as a slightly higher ASE. One disadvantage to this treatment was the obvious color change in the wood after becoming a composite, which may be an undesirable side effect when it is used in decorative applications.

Nur Izreen Farah *et al.* (2021) recently conducted a similar study on the dimensional stability of sesenduk wood using a LmwPF resin reinforced by silicon dioxide nanoparticles. The results of this study indicated that a significant enhancement in ASE and water absorption (WA) can be expected. Whereas untreated wood demonstrated no ASE and a WA rate of 69.42%, treated sesenduk wood samples featured an ASE of 54.1% and WA rate of 31.45%. Similar reductions have been corroborated by Ghorbani *et al.* (2017), who reported an ASE value of 58.87%, and a WA value of approximately 27% for poplar wood impregnated with a mixture of nanosilica and styrene monomer. By comparison, the control sample featured no ASE and a WA of 190%. Consequently, the implementation of nanotechnology significantly improved the dimensional stability of the material.

2.4.2 Flammability

Giudice and Pereyra (2009) conducted a study on the flammability of pine wood panels impregnated with silica nanoparticles added to silica/alkali colloidal solutions. After the ignition of a sample, the silicate system built up inside the lignin “remain[ed] intact at very high temperatures”, while simultaneously acting as an insulator by separating the lignocellulose from the cell walls, effectively slowing the burning process.

Garskaite *et al.* (2019) studied the impact of sodium silicate (Na_2SiO_3) and titanium dioxide (TiO_2) nanoparticle impregnation in scots pine wood samples. Four different types of solutions were tested: An aqueous Na_2SiO_3 solution at 10% and 20%, and two mixtures of 10% and 20% Na_2SiO_3 with 0.5 g of suspended TiO_2 (Na_2SiO_3-$nTiO_2$). The flammability of the samples was determined using an oxygen index instrument to detect the limiting oxygen index (LOI) upon combustion of each sample. The LOI signifies the minimum concentration of oxygen needed to be present in the air for a material to reach combustion (Iron Boar Labs Ltd., 2019). The test results yielded increases in the LOI values for all types of solutions when compared with the LOI of untreated wood (26.5%), but the largest increase was observed in the 20% Na_2SiO_3-$nTiO_2$, which demonstrated an LOI of 40.5%, indicating a significant delay in ignition. These findings further reinforced the potential for the use of nanoparticle impregnation to enhance the flame-retardant properties of wood.

2.4.3 Resistance to Biological Attack

Ghorbani *et al.* (2018) studied the effects of nanosilica (NS), nanocomposite (NC), nanosilica-styrene (NSt), and styrene (St) impregnation on the resistance of poplar wood against white-rot fungi. Untreated poplar wood samples experienced a mass loss of 29% when exposed to white-rot fungi, while those impregnated with any type of nanoparticles only experienced an average mass loss of 1.85%. The introduction of nanoparticles was found to actively block micropores in the wood cell wall. Closing these micropores helps block access to the cell wall interior and prevents the infiltration of spores. The presence of nanoparticles also aids in the displacement of moisture from the cell wall, which further discourages the formation of fungi. In particular, the NS-treated samples showed the highest resistance to decay.

Research has yet to be conducted on the termite-resistant properties of wood treated with silica nanoparticles. However, Debnath *et al.* (2011) and Rouhani *et al.* (2013) examined the insecticidal effects of nanosilica treatment on rice grain and cowpeas, respectively. For the rice grain samples laced with silica nanoparticles with a size range of 15-30 nm, Debnath *et al.* (2011) found that after only 2 days, an insect mortality rate of 90% or higher was achievable at a concentration of 2 g nanoparticle/kg of rice. Rouhani *et al.* (2013) observed similar results in cowpea samples treated with silica nanoparticles with a size range of 20-60 nm. After 7 days, insect mortality rates of 93% and 96% were observed in cowpeas treated with concentrations of 2 g/kg and 2.5 g/kg, respectively. Consequently, the results indicate that wood treated with silica nanoparticles may also experience a higher rate of insect mortality, although additional studies are required to prove this hypothesis.

2.4.4 Hydrophobicity

The impregnation of a nanosilica sol to improve the hydrophobicity of wood samples was also studied by both Wang *et al.* (2013) and Xu *et al.* (2020). Chinese Fir samples impregnated with nanosilica sol were found to have contact angles (CA) of up to 150°, which classified the samples as superhydrophobic. The analysis performed by Xu *et al.* (2020) also yielded a significant increase in CA values in comparison to the untreated sample. This data was further corroborated by Chang *et al.* (2015), who found a CA of 152° upon impregnation of a hydrophobic silica (SiO_2) and polydimethylsiloxane (PDMS) solution in Chinese Fir samples.

Additionally, Bak *et al.* (2023) impregnated Scots pine sapwood and European beech with a fluorinated silica nanoparticle suspension. This suspension was prepared in order to change the hydrophilic nanoparticles into a hydrophobic material by stirring silica nanoparticles in a 1% fluoroalkyl silane solution. After treatment, it was found that on average, the CA values of both species of wood approached the superhydrophobic 150° CA classification. It was also found that this treatment method significantly reduced the water uptake of the wood samples by blocking the cell wall surfaces, pits, and micropores to the point that water was excluded entirely from the cell lumens.

2.5 Knowledge Gap

The past decade has seen an increasing interest in the use of nanotechnology to reliably enhance the performance of wood. Research has proven that nanoparticle impregnation can be employed to significantly improve the physical and mechanical properties of wood. Many studies have also been performed to determine the effects that changes and fluctuations in environmental conditions such as temperature and humidity can have on non-treated wood. However, there are very few studies that focus on investigating the potential effects that accelerated aging can have on samples treated by nanoparticle impregnation. The current study seeks to address this knowledge gap by investigating the effects of two types of accelerated aging (hydrolytic aging and freeze-thaw cycling) on white spruce wood samples impregnated with a nano-SiO_2 colloid.

2.6 References

Ameli, F., Moghadam, S., & Shahmarvand, S. (2022). Polymer flooding. In Chemical Methods (pp. 33–94). *Elsevier*. https://doi.org/10.1016/B978-0-12-821931-7.00003-1

Andersson, S., Serimaa, R., Paakkari, T., Saranpää, P., & Pesonen, E. (2003). Crystallinity of wood and the size of cellulose crystallites in Norway spruce (picea abies). *Journal of Wood Science*, 49(6), 531–537. https://doi.org/10.1007/s10086-003-0518-x

Bach, L. (1966). *Nonlinear mechanical behavior of wood in longitudinal tension* (thesis), University Microfilms Inc, Ann Arbor.

Bak, M., & Németh, R. (2018). Effect of Different Nanoparticle Treatments on the Decay Resistance of Wood. *BioResources*, 13(4), 7886–7899. https://doi.org/10.15376/biores.13.4.7886-7899

Bak, M., Molnár, F., & Németh, R. (2019). Improvement of dimensional stability of wood by silica nanoparticles. *Wood Material Science & Engineering*, 14(1), 48–58. https://doi.org/10.1080/17480272.2018.1528568

Bak, M., Takács, D., Rákosa, R., Németh, Z. I., & Németh, R. (2023). One-Step Process for the Fabrication of Hydrophobic and Dimensional Stable Wood Using Functionalized Silica Nanoparticles. *Forests*, 14(3), 651. https://doi.org/10.3390/f14030651

Baker, M. C. (1969). Decay of wood. *Canadian Building Digest; No. CBD-111*. https://doi.org/10.4224/40000811

Barker, B., & Owen, N. L. (1999). Identifying Softwoods and Hardwoods by Infrared Spectroscopy. *Journal of Chemical Education*, 76(12), 1706. https://doi.org/10.1021/ed076p1706

Benedetti, L., Brulé, B., Decreamer, N., Evans, K. E., & Ghita, O. (2019). Shrinkage behaviour of semi-crystalline polymers in laser sintering: PEKK and PA12. *Materials & Design*, 181, 107906. https://doi.org/10.1016/j.matdes.2019.107906

Bobleter, O. (1994). Hydrothermal degradation of polymers derived from plants. *Progress in Polymer Science*, *19*(5), 797–841. https://doi.org/10.1016/0079-6700(94)90033-7

Borgin, K. (1968). The protection of wood against dimensional instability. *Forestry in South Africa*, 9, 81–94.

Brett, C. T. (2000). Cellulose microfibrils in plants: Biosynthesis, deposition, and integration into the cell wall. In *International Review of Cytology* (Vol. 199, pp. 161–199). Elsevier. https://doi.org/10.1016/S0074-7696(00)99004-1

Campean, M., Ispas, M., & Porojan, M. (2008). Considerations on Drying Frozen Spruce Wood and Effects upon Its Properties. *Drying Technology*, 26(5), 596–601. https://doi.org/10.1080/07373930801946411

Camuffo D. (2004). Thermodynamics for cultural heritage. *Proceedings of the International School of Physics "Enrico Fermi"*, 154(Physics Methods in Archaeometry), 37–98. https://doi.org/10.3254/978-1-61499-010-9-37

Cave, I. D. (1968). The anisotropic elasticity of the plant cell wall. *Wood Science and Technology*, 2(4), 268–278. https://doi.org/10.1007/BF00350273

Cave, I. D., & Walker, J. C. (1994). Stiffness of wood in fast-grown plantation softwoods: the influence of microfibril angle. *Forest Products Journal*, 44, 43-48.

Chang, H., Tu, K., Wang, X., & Liu, J. (2015). Fabrication of mechanically durable superhydrophobic wood surfaces using polydimethylsiloxane and silica nanoparticles. *RSC Advances*, 5(39), 30647–30653. https://doi.org/10.1039/C5RA03070F

Clausen, C. A., Kartal, S. N., Arango, R. A., & Green, F. (2011). The role of particle size of particulate nano-zinc oxide wood preservatives on termite mortality and leach resistance. *Nanoscale Research Letters*, 6(1), 427. https://doi.org/10.1186/1556-276X-6-427

Connor, N. (2020, November 16). *Stages of Creep – Primary – Secondary – Tertiary – Definition*. Material Properties. https://material-properties.org/stages-of-creep-primary-secondary-tertiary-definition/

Debnath, N., Das, S., Seth, D., Chandra, R., Bhattacharya, S. Ch., & Goswami, A. (2011). Entomotoxic effect of silica nanoparticles against Sitophilus oryzae (L.). *Journal of Pest Science*, 84(1), 99–105. https://doi.org/10.1007/s10340-010-0332-3

Dietenberger, M. A., & Hasburgh, L. E. (2016). Wood Products: Thermal Degradation and Fire. In *Reference Module in Materials Science and Materials Engineering*. Elsevier. https://doi.org/10.1016/B978-0-12-803581-8.03338-5

Duffield Timber. (2021). *The cellular structure of a hardwood. Hardwood vs. Softwood: What Are The Differences?* Retrieved July 9, 2023, from https://duffieldtimber.com/the-workbench/categories/timber-trends/hardwood-vs-softwood-what-are-the-differences.

Ebnesajjad, S. (2014). Surface and Material Characterization Techniques. In *Surface Treatment of Materials for Adhesive Bonding* (pp. 39–75). Elsevier. https://doi.org/10.1016/B978-0-323-26435-8.00004-6

Ek, M., Gellerstedt, G., & Henriksson, G. (Eds.). (2009). *Wood Chemistry and Wood Biotechnology*. Walter de Gruyter. https://doi.org/10.1515/9783110213409

El-Dabaa, R., & Abdelmohsen, S. (2023). Hygroscopy and adaptive architectural façades: An overview. *Wood Science and Technology*, 57(3), 557–582. https://doi.org/10.1007/s00226-023-01464-8

Endo, K., Obataya, E., Zeniya, N., & Matsuo, M. (2016). Effects of heating humidity on the physical properties of hydrothermally treated spruce wood. *Wood Science and Technology*, 50(6), 1161–1179. https://doi.org/10.1007/s00226-016-0822-4

Frigione, M., & Rodríguez-Prieto, A. (2021). Can Accelerated Aging Procedures Predict the Long Term Behavior of Polymers Exposed to Different Environments? *Polymers*, 13(16), 2688. https://doi.org/10.3390/polym13162688

Froidevaux, J., & Navi, P. (2013). Aging law of spruce wood. *Wood Material Science and Engineering*, 8(1), 46–52. https://doi.org/10.1080/17480272.2012.725427

Fuss, F. K. (2015). The Loss Tangent of Visco-Elastic Models. In L. Dai & R. N. Jazar (Eds.), Nonlinear Approaches in Engineering Applications (pp. 137–157). *Springer International Publishing*. https://doi.org/10.1007/978-3-319-09462-5_6

García Esteban, L., Gril, J., De Palacios De Palacios, P., & Guindeo Casasús, A. (2005). Reduction of wood hygroscopicity and associated dimensional response by repeated humidity cycles. *Annals of Forest Science*, 62(3), 275–284. https://doi.org/10.1051/forest:2005020

Garratt's Damp & Timber. (2019). *Preventing timber decay and rot*. Retrieved July 9, 2023, from https://garrattsdamp.com/blog/preventing-timber-decay-rot.

Garskaite, E., Karlsson, O., Stankeviciute, Z., Kareiva, A., Jones, D., & Sandberg, D. (2019). Surface hardness and flammability of Na 2 SiO 3 and nano-TiO 2 reinforced wood composites. *RSC Advances*, 9(48), 27973–27986. https://doi.org/10.1039/C9RA05200C

Ghorbani, M., Biparva, P., & Hosseinzadeh, S. (2018). Effect of colloidal silica nanoparticles extracted from agricultural waste on physical, mechanical and antifungal properties of wood polymer composite. *European Journal of Wood and Wood Products*, 76(2), 749–757. https://doi.org/10.1007/s00107-017-1157-z

Gillespie, R.H. (1984). Accelerated aging of wood-based panel products: a review and commentary. *Proceedings of a workshop on the durability of structural panels, Pensacola, Florida, October 5-7, 1982*. U.S. Dept. of Agriculture, Forest Service, Forest Products Laboratory. https://www.fpl.fs.usda.gov/documnts/pdf1984/gille84a.pdf

Giudice, C. A., & Pereyra, A. M. (2009). Silica nanoparticles in high silica/alkali molar ratio solutions as fire-retardant impregnants for woods. *Fire and Materials*, 34, 177–187. https://doi.org/10.1002/fam.1018

Glass S. V., & Zelinka, S. L. (2010). Chapter 4: Moisture Relations and Physical Properties of Wood. In R. J. Ross (Ed.), *Wood handbook: wood as an engineering material* (Centennial Edition, pp. 4.1–4.19). U.S. Dept. of Agriculture, Forest Service, Forest Products Laboratory. https://www.fpl.fs.usda.gov/documnts/fplgtr/fplgtr190/chapter_04.pdf

Groenier, J. & Lebow, S. (2006). *Preservative-treated wood and alternative products in the Forest Service.* U.S. Dept. of Agriculture, Forest Service, Technology & Development Program. https://www.fs.usda.gov/research/treesearch/25451

Haas, D. W., Hrutfiord, B. F., & Sarkanen, K. V. (1967). Kinetic study on the alkaline degradation of cotton hydrocellulose. Journal of Applied Polymer Science, 11(4), 587–600. https://doi.org/10.1002/app.1967.070110408

Harandi, D., Ahmadi, H., & Mohammadi Achachluei, M. (2016). Comparison of TiO2 and ZnO nanoparticles for the improvement of consolidated wood with polyvinyl butyral against white rot. *International Biodeterioration & Biodegradation*, 108, 142–148. https://doi.org/10.1016/j.ibiod.2015.12.017

Harte, A. (2009). Introduction to timber as an engineering material. *ICE manual of construction materials*, 2, 707-715. Retrieved from https://www.universityofgalway.ie/media/timberengineeringresearchgroup/Harte---2009---Introduction-to-timber-as-an-engineering-material.pdf.

Hartley, I., & Hamza, M. F. (2016). Wood: Moisture Content, Hygroscopicity, and Sorption. In *Reference Module in Materials Science and Materials Engineering*. Elsevier. https://doi.org/10.1016/B978-0-12-803581-8.02219-0

Holzer, S. M., Loferski, J. R., & Dillard, D. A. (1989). A Review Of Creep In Wood: Concepts Relevant To Develop Long-Term Behavior Predictions For Wood Structures. *Wood and Fiber Science*, 21(4). https://wfs.swst.org/index.php/wfs/article/view/1389

Huč, S., Hozjan, T., & Svensson, S. (2018). Rheological behavior of wood in stress relaxation under compression. *Wood Science and Technology*, 52(3), 793–808. https://doi.org/10.1007/s00226-018-0993-2

Inari, G. N., Petrissans, M., Lambert, J., Ehrhardt, J. J., & Gérardin, P. (2006). XPS characterization of wood chemical composition after heat-treatment: XPS characterization of wood. *Surface and Interface Analysis*, 38(10), 1336–1342. https://doi.org/10.1002/sia.2455

Izekor, D.N., Fuwape, J.A., & Oluyege, A.O. (2010). Effects of density on variations in the mechanical properties of plantation grown Tectona grandis wood. *Archives of Applied Science Research*, 2, 113-120. https://www.scholarsresearchlibrary.com/articles/effects-of-density-on-variations-in-the-mechanical-properties-of-plantation-grown-tectona-grandis-wood.pdf

Karami, E., Bardet, S., Matsuo, M., Bremaud, I., Gaff, M., & Gril, J. (2020). Effects of mild hygrothermal treatment on the physical and vibrational properties of spruce wood. *Composite Structures*, 253, 112736. https://doi.org/10.1016/j.compstruct.2020.112736

Kübler, H. (1962). Shrinkage and swelling of wood by coldness. *Holz als Roh-und Werkstoff*, 20(9), 364–368.

Laghi, L. (2019). *Cellulose strand*. Wikimedia Commons. Retrieved July 9, 2023, from https://commons.wikimedia.org/wiki/File:Cellulose_strand.svg.

LibreTexts. (2023). *12.1: Crystalline and amorphous solids*. Chemistry LibreTexts. https://chem.libretexts.org/Bookshelves/General_Chemistry/Book%3A_General_Chemistry%3A_Principles_Patterns_and_Applications_(Averill)/12%3A_Solids/12.01%3A_Crystalline_and_Amorphous_Solids

Li, X., Tabil, L. G., & Panigrahi, S. (2007). Chemical Treatments of Natural Fiber for Use in Natural Fiber-Reinforced Composites: A Review. *Journal of Polymers and the Environment*, 15(1), 25–33. https://doi.org/10.1007/s10924-006-0042-3

Liu, P.-L., Zhang, X., Mao, J.-F., Hong, Y.-M., Zhang, R.-G., E, Y., Nie, S., Jia, K., Jiang, C.-K., He, J., Shen, W., He, Q., Zheng, W., Abbas, S., Jewaria, P. K., Tian, X., Liu, C., Jiang, X., Yin, Y., … Lin, J. (2020). The Tetracentron genome provides insight into the early evolution of eudicots and the

formation of vessel elements. *Genome Biology*, 21(1), 291. https://doi.org/10.1186/s13059-020-02198-7

Machová, D., Baar, J., Paschová, Z., Pařil, P., Křenková, J., & Kúdela, J. (2019). Color changes and accelerated ageing in oak wood treated with ammonia gas and iron nanoparticles. *European Journal of Wood and Wood Products*, 77(4), 705–716. https://doi.org/10.1007/s00107-019-01406-x

Nath, S. (2018). *Statistical mechanics of biopolymers* (thesis), Banaras Hindu University, Varanasi. http://hdl.handle.net/10603/283566

Iron Boar Labs Ltd. (2019). *Limiting Oxygen Index (LOI)*. MakeItFrom.com: Material Properties Database. Retrieved June 14, 2021, from https://www.makeitfrom.com/glossary/Limiting-Oxygen-Index-LOI/.

McManamy, K., Koehler, P.G., Branscome, D.D., & Pereira, R.M. (2008). Wood Moisture Content Affects the Survival of Eastern Subterranean Termites (Isoptera: Rhinotermitidae), Under Saturated Relative Humidity Conditions. *Sociobiology*, 52, 145-156. Retrieved from https://www.researchgate.net/publication/224497282_Wood_Moisture_Content_Affects_the_Survival_of_Eastern_Subterranean_Termites_Isoptera_Rhinotermitidae_Under_Saturated_Relative_Humidity_Conditions.

Meier, E. (2015). Wood!: Identifying and using hundreds of woods worldwide. The Wood Database.

Naemi, R., Behforootan, S., Chatzistergos, P., & Chockalingam, N. (2016). Viscoelasticity in Foot-Ground Interaction. In M. F. El-Amin (Ed.), *Viscoelastic and Viscoplastic Materials*. InTech. https://doi.org/10.5772/64170

NEUROtiker. (2007). *Cellulose Sessel*. Wikimedia Commons. Retrieved July 9, 2023, from https://commons.wikimedia.org/wiki/File:Cellulose_Sessel.svg.

Nur Izreen Farah, A., Zaidon, A., Anwar, U., Rabiatol Adawiah, M., & Lee, S. (2021). Improved Performance of Wood Polymer Nanocomposite Impregnated with Metal Oxide Nanoparticle-reinforced Phenol Formaldehyde Resin. *Journal of Tropical Forest Science*, 33(1), 77–87. https://doi.org/10.26525/jtfs2021.33.1.77

Ozyhar, T., Hering, S., & Niemz, P. (2013). Viscoelastic characterization of wood: Time dependence of the orthotropic compliance in tension and compression. *Journal of Rheology*, 57(2), 699–717. https://doi.org/10.1122/1.4790170

Pedersen, N.B. (2015). Microscopic and spectroscopic characterisation of waterlogged archaeological softwood from anoxic environments (thesis). Department of Geosciences and Natural Resource Management, Frederiksberg.

PerkinElmer. (2013). *Dynamic Mechanical Analysis (DMA) A Beginner's Guide*. Waltham, MA. Retrieved from https://www.perkinelmer.com/CMSResources/Images/44-74546GDE_IntroductionToDMA.pdf.

Poletto, M., Zattera, A. J., & Santana, R. M. C. (2012). Thermal decomposition of wood: Kinetics and degradation mechanisms. *Bioresource Technology*, 126, 7–12. https://doi.org/10.1016/j.biortech.2012.08.133

Popsecu, C.-M. (2017). *Wood as bio-based building material*. In D. Jones & C. Brischke (Eds.), Performance of Bio-based Building Materials (pp. 21–96). Woodhead Publishing. https://doi.org/10.1016/B978-0-08-100982-6.00002-1

Purba, C. Y. C. (2019). Characterization and valorization of secondary quality hardwood as structural material. https://doi.org/10.13140/RG.2.2.25329.22885

Reeb, J. E. (2009). *Wood and Moisture Relationships, EM8600*. Oregon State University Extension Service. https://catalog.extension.oregonstate.edu/sites/catalog/files/project/pdf/em8600.pdf

Reinprecht, L. (2016). Wood Deterioration, Protection and Maintenance (1st ed.). *Wiley*. https://doi.org/10.1002/9781119106500

Rouhani, M., Samih, M. A., & Kalantari, S. (2013). Insecticidal effect of silica and silver nanoparticles on the cowpea seed beetle, Callosobruchus maculatus F. (Col.: Bruchidae). *Journal of Entomological Research*, 4(4), 297–305. https://www.researchgate.net/publication/304533974_Insecticidal_effect_of_silica_and_silver_nanoparticles_on_the_cowpea_seed_beetle_Callosobruchus_maculatus_FCol_Bruchidae

Rowell, R. M. (2013). *Handbook of wood chemistry and wood composites* (2nd ed). Taylor & Francis.

Sargent, R. (2019). Evaluating dimensional stability in solid wood: A review of current practice. *Journal of Wood Science*, 65(1), 36. https://doi.org/10.1186/s10086-019-1817-1

Schaller, C. (2020). *4.8: Storage and loss modulus*. Chemistry LibreTexts. https://chem.libretexts.org/Bookshelves/Organic_Chemistry/Polymer_Chemistry_(Schaller)/04%3A_Polymer_Properties/4.08%3A_Storage_and_Loss_Modulus

Schniewind, A. P. (1956). Some aspects of wood moisture relations. *Western Dry Kiln Clubs. Meeting 8, Oregon State University*. https://ir.library.oregonstate.edu/concern/conference_proceedings_or_journals/4j03d074h

Sehlstedt-Persson, M. (2005). *Properties of solid wood: Responses to drying and heat treatment* (thesis). Luleå tekniska universitet, Luleå. http://ltu.diva-portal.org/smash/record.jsf?pid=diva2:991608

Shmulsky, R., & Shvets, V. (2006). The effect of subzero temperatures on FSP of cottonwood. Forest Products Journal, 56(2), 74–77.

Simpson, W. T. (2001). Wood: Dimensional Change from Moisture. In *Encyclopedia of Materials: Science and Technology* (pp. 9627–9629). Elsevier. https://doi.org/10.1016/B0-08-043152-6/01743-5

Sjöström, E. (1993). *Wood chemistry: Fundamentals and applications* (2nd ed). Academic Press.

Sjöström, E., & Westermark, U. (1999). Chemical Composition of Wood and Pulps: Basic Constituents and Their Distribution. In E. Sjöström & R. Alén (Eds.), *Analytical Methods in Wood Chemistry,*

Pulping, and Papermaking (pp. 1–19). Springer Berlin Heidelberg. https://doi.org/10.1007/978-3-662-03898-7_1

Songtipya, L., Songtipya, P., Prodpran, T., Kalkornsurapranee, E., & Johns, J. (2021). Fabrication of water-soluble loose-fill foam from tamarind (Tamarindus indica L.) seed polysaccharide by mechanical frothing and freeze-drying process. *Journal of Cellular Plastics*, 57(5), 643–658. https://doi.org/10.1177/0021955X20948560

Szmutku, M. B., Popa, V., & Câmpean, M. (2013). Experimental study regarding the freezing and thawing dynamics of spruce wood. *Pro Ligno*, 9(1). http://www.proligno.ro/en/articles/2013/201301.htm

Tarmian, A., & Mastouri, A. (2019). Changes in moisture exclusion efficiency and crystallinity of thermally modified wood with aging. *iForest - Biogeosciences and Forestry*, 12(1), 92–97. https://doi.org/10.3832/ifor2723-011

Teng, T.-J., Mat Arip, M. N., Sudesh, K., Nemoikina, A., Jalaludin, Z., Ng, E.-P., & Lee, H.-L. (2018). Conventional technology and nanotechnology in Wood Preservation: A Review. *BioResources*, 13(4). https://doi.org/10.15376/biores.13.4.teng

University of Cambridge. (2023). *Crystallinity*. Dissemination of IT for the Promotion of Materials Science (DoITPoMS). https://www.doitpoms.ac.uk/tlplib/polymerbasics/crystallinity.php

Van Loon, L. R., & Glaus, M. A. (1997). Review of the kinetics of alkaline degradation of cellulose in view of its relevance for safety assessment of radioactive waste repositories. *Journal of Environmental Polymer Degradation*, 5(2), 97–109. https://doi.org/10.1007/BF02763593

Voulgaridis, E. V., & Banks, W. B. (1983). Laboratory Evaluation of the Performance of Water Repellents Applied to Long Wood Specimens. *Holzforschung*, 37(5), 261–266. https://doi.org/10.1515/hfsg.1983.37.5.261

Walker, J. C. F., Butterfield, B. G., Harris, J. M., Langrish, T. A. G., & Uprichard, J. M. (1993). Primary Wood Processing: Principles and practice. *Springer Netherlands*. https://doi.org/10.1007/978-94-015-8110-3

Wang, X., Chai, Y., & Liu, J. (2013). Formation of highly hydrophobic wood surfaces using silica nanoparticles modified with long-chain alkylsilane. *Holzforschung*, 67(6), 667–672. https://doi.org/10.1515/hf-2012-0153

Wengert, E. M., & Meyer, D. (1993, November). *Warp in Drying*. Woodweb. https://www.woodweb.com/knowledge_base/Warp_in_Drying.html

Wiedenhoeft, A. (2010). *Chapter 3: Structure and function of wood*. In R. J. Ross (Ed.), Wood handbook : wood as an engineering material (Centennial Edition, pp. 3.1–3.18). U.S. Dept. of Agriculture, Forest Service, Forest Products Laboratory. https://www.fpl.fs.usda.gov/documnts/fplgtr/fplgtr190/chapter_03.pdf

Williams, S. (1953). Wood Structure. *Scientific American*, 188(1), 64–67. https://doi.org/10.1038/scientificamerican0153-64

Wood Stairs. (2017). *Tree Diagram*. How to Evaluate Wood. Retrieved from https://www.woodstairs.com/how-to-evaluate-wood/.

Woodshop Direct. (2018). *What Are The Best Treatments For Indoor Wood?*. Retrieved July 9, 2023, from https://www.woodshopdirect.co.uk/blog/diy-guides/what-are-the-best-treatments-for-indoor-wood/.

Xu, E., Zhang, Y., & Lin, L. (2020). Improvement of Mechanical, Hydrophobicity and Thermal Properties of Chinese Fir Wood by Impregnation of Nano Silica Sol. *Polymers*, 12(8), 1632. https://doi.org/10.3390/polym12081632

Yamamoto, H., Sakagami, H., Kijidani, Y., & Matsumura, J. (2013). Dependence of Microcrack Behavior in Wood on Moisture Content during Drying. *Advances in Materials Science and Engineering*, 2013, 1–7. https://doi.org/10.1155/2013/802639

Zukowski, J., & Su, N.-Y. (2020). A Comparison of Morphology among Four Termite Species with Different Moisture Requirements. *Insects*, 11(5), 262. https://doi.org/10.3390/insects11050262

Chapter 3

3.0 Effects of hydrolytic aging on the performance of nanosilica (SiO_2)-treated spruce wood

3.1 Abstract

This study aims to examine the effects of hydrolytic aging at 90°C and 80% RH on white spruce wood samples impregnated with a nano-SiO_2 colloid at a gauge pressure of -90 kPa. Scanning electron microscopy, powder X-Ray diffraction, dynamic mechanical analysis, tensiometry, and thermogravimetric analysis were chosen as characterization methods to determine the behaviour of SiO_2-treated samples after subjecting them to accelerated aging for 3 months. Samples were taken out of the hydrolytic chamber and tested alongside a non-treated set at 1-month intervals to determine the effects of the treatment process and the aging conditions on the wood. The results showed that although the treatment process had a detrimental effect on the wood as a result of alkaline attack, the product was able to agglomerate on the surface of the samples and increase the initial crystallinity index, reduce the water uptake, and stabilize the storage modulus as well as the cellulose degradation rate of the samples.

Keywords: Spruce Wood, Wood Treatment, Accelerated Aging, Hydrolytic Aging, Silica Nanoparticles, Vacuum Impregnation, Viscoelastic Properties, Water Uptake, Thermal Degradation, True Density, XRD.

3.2 Introduction

The use of wood in construction has seen an increase over time in response to an increase in demand for construction materials that feature low carbon emissions (Churkina *et al.*, 2020). As of February 2022, 139 mass timber buildings that feature eight or more stories have been built around the world. Fifteen of these structures were built in Canada (Safarik *et al.*, 2022). When considering wood as a construction material, the reduction of water uptake and the potential to increase the hydrophobicity of wood are considered essential avenues of research since wood is a naturally hydrophilic material. If used for outdoor applications, wood may be exposed to high-humidity conditions as well as rain and snow. Under these conditions, water can easily infiltrate the wood cell structure, causing swelling as well as the degradation of the material via cellulose hydrolysis (Bobleter, 1994). This process is perpetuated due to the presence of hydroxyl (−OH) groups throughout the chemical structure of wood. Prolonged exposure to water can significantly weaken

the wood and requires the application of preservatives such as coatings, sprays, and varnishes to protect the structural integrity of wooden structures.

Although wood remains one of the most sustainable building materials, the toxicity of the preservatives used in wood treatment continues to be a cause of concern which in turn, stimulates continued innovation in the industry. Many treatment products such as creosote coal-tar and chromated copper arsenate that can leach toxic chemicals into the surrounding environment have been phased out (Government of Canada, 2021). However, even the most environmentally friendly products contain a fundamental flaw due to their hydrophobic nature. The interfacial incompatibility between the hydrophilic wood and the hydrophobic preservatives allows water to permeate between the wood and the preservative layer, simultaneously wearing away at both the wood and the surface treatment (Li *et al.*, 2007). Over the past decade, the use of nanoparticle vacuum impregnation has been posited by researchers as an alternative treatment method. The interfacial incompatibility can be eliminated using hydrophilic nanoparticles. Other benefits include the ability to increase the mechanical properties of wood, reduce the water uptake, and increase the hydrophobicity of wood (Lemaire-Paul *et al.*, 2022).

High-temperature and high-humidity conditions have been proven to exacerbate the cellulose hydrolysis process. The effects of accelerated aging on non-treated wood, traditionally treated wood, and pure cellulose have previously been studied by Zou *et al.* (1994) and Žlahtič & Humar (2016), among others. Zou *et al.* (1994) found that aging pure cellulose papers at 90°C and 80% RH resulted in a significant decrease in fibre strength due to hydrolysis. Žlahtič & Humar (2016) subjected different species of wood to outdoor weathering as well as accelerated aging conditions of 38°C and 68% RH, including alternating cycles of UV radiation of 0.35 W/m^2 and artificial rain. The wood samples were treated with waxes, oils, and biocides. Žlahtič & Humar (2016) detected a significant mass loss in the aged samples and determined that wax was the most efficient treatment method as the hydrophobicity of the wood was maintained after aging.

The effects of artificial aging on wood samples treated by nanoparticle vacuum impregnation have not been extensively studied yet. For example, the effects of UV radiation on wood samples treated by nanoparticle impregnation have been studied by Clausen (2012) and Machová *et al.* (2019). However, almost no research has been performed on the effects of high-temperature/high-humidity aging on nanoparticle-treated samples. This article aims to build on the results obtained by Lemaire-Paul *et al.* (2022) to determine the effects of hydrolytic aging on spruce wood samples impregnated with a nano-SiO_2 colloid.

3.3 Materials and Methods

3.3.1 Sample Preparation

Picea glauca (white spruce) wood samples were first cut to the nominal sizes required for each characterization method. The samples were cut along the longitudinal axis to expose the tangential-radial plane of the wood cell structure. The samples were then sanded with 150 grit sandpaper to eliminate any surface irregularities. Before beginning the vacuum-induced impregnation process, the samples were oven-dried for 24 hours at 103°C, the conventional drying temperature to obtain accurate moisture content readings (Curling, 2017).

The dry samples were then placed in a Buehler Cast N' Vac 1000 vacuum chamber at -90 kPa[1] for ten minutes. This pressure represents the optimal impregnation pressure determined by Lemaire-Paul *et al.* (2022). While under vacuum, the samples were submerged in a 40% nano-SiO_2 colloid, and the chamber was pressurized to atmospheric pressure and maintained for one hour. This process was intended to facilitate the evacuation of entrapped air and the agglomeration of the colloid within the vascular system of the wood. The colloid used was LUDOX AS-40, purchased from Sigma-Aldrich. This colloid consists of a 40 wt. % suspension of silica in H_2O with a particle size of 20-24 nm, an aqueous density of 1.3 g/cm^3 at 25°C, and a pH of 9.1 (Sigma-Aldrich, 2023a). After one hour, the samples were removed from the colloid and immediately placed in an oven at 50°C for one hour, followed by 103°C for ten minutes. These drying conditions enable the further agglomeration of the colloid within the wood structure (Lemaire-Paul *et al.*, 2022).

Following this preliminary drying cycle, the samples were subjected to washing cycles (i.e., a repeated secondary vacuum cycle using distilled water) in order to mitigate the effects of alkaline attack by the colloid on the wood samples. During this procedure, the samples were once again placed under a -90 kPa vacuum, submerged in distilled water, and subjected to three 10-minute pressurization cycles from -90 kPa to atmospheric pressure while submerged. This vacuum cycling and washing process allowed the distilled water to infiltrate and "flush" the wood cellulose structure and combat the effects of the colloid alkalinity on the wood samples. The samples were oven-dried at 103°C for 24 hours after the washing process was completed. This washing process was introduced after a preliminary 1-month study was performed to examine the detrimental effects of the treatment process on the peak cellulose degradation temperature of the samples. The results of this preliminary study are presented in Appendix A.

[1] All pressures referenced in this document are gauge pressures unless otherwise noted.

3.3.2 Accelerated Aging Conditions

A Blue M CEO958-4 steady-state stability chamber was maintained at 80% RH and a temperature of 90°C. These conditions were chosen since they represent an extreme when compared to the climate of Ontario, which exhibits a maximum temperature of 26.8°C in July and an average yearly RH of 63% (WorldData.info, 2023). A non-treated (NT) set of spruce wood samples was aged and tested alongside the SiO_2-treated samples in order to establish a baseline and determine the effects of the SiO_2 treatment by comparing the results. Samples were removed at 1-month intervals for characterization and any samples subjected to non-destructive tests were returned to the chamber for further aging after each testing period.

3.3.3 Characterization

Samples were dried for 24 hours at 103°C before and after each test was performed in order to ensure that potential variations in the moisture content had little to no effect on the readings. This does not reflect real-world conditions and should be taken into consideration when relating the results of this study to practical applications. Tests performed for this study include dynamic mechanical analysis (DMA), tensiometry, thermogravimetric analysis (TGA), powder X-Ray diffraction (XRD), and scanning electron microscopy (SEM). Statistical analysis was applied to the data obtained from each characterization method.

3.3.3.1 Scanning Electron Microscopy

SEM analysis was performed on NT and SiO_2-treated wood samples using a JEOL JSM-6610 Series Scanning Electron Microscope. Images were taken under low vacuum (LV) conditions at an absolute pressure of 30 Pa and an acceleration voltage of 10 kV.

3.3.3.2 Dynamic Mechanical Analysis

SiO_2-treated and NT spruce wood samples with dimensions of (25 × 10 × 1.8 mm) were subjected to DMA tests using a TA Instruments Q800 DMA. The dimensions of the samples were measured at each testing interval after drying and before performing any tests. A 3-point bending clamp was used to measure the viscoelastic properties including the storage modulus (E'), loss modulus (E''), and damping ($\tan\delta$) of the samples under a temperature ramp of 5-40°C at a rate of 5°C/min and a frequency of 1 Hz.

3.3.3.3 Tensiometry

SiO_2-treated and NT spruce wood samples with dimensions of (7 × 2 × 1 mm) were subjected to tensiometry tests. The samples were weighed, and their dimensions were measured at each testing interval after drying and before performing any tests. An Attension Sigma 701 Force Tensiometer employing the Washburn method for porous materials (Auvinen, 2020) was used to measure the water uptake of the samples. Samples were suspended above distilled water from a standard sample holder clip and brought into contact with the surface of the water, allowing the water to infiltrate the sample through the tangential-radial plane for ten minutes. Mass uptake readings were recorded by the apparatus approximately every 0.2-0.4 seconds. These readings were manually converted to Weight % using:

$$Weight\ \% = 100 \times \frac{M_{test}}{M_{dry}} \quad (1)$$

Where M_{test} is the mass recorded by the apparatus throughout the test (in g), and M_{dry} is the mass of the sample after drying for 24 hours (in g).

This equation differs from the standard equation used to calculate Weight %:

$$Weight\ \% = 100 \times \frac{(M_{wet} - M_{dry})}{M_{dry}} \quad (2)$$

Where M_{wet} is the mass of the sample (in g) after the absorption of water.

Equation (1) could be used instead of Equation (2) since the tensiometer automatically zeroes the balance as soon as a sample comes into contact with the water. This removes the need to subtract the dry mass from the wet mass since only the mass gained through the absorption of water is recorded by the instrument.

To account for the effect slight variations in sample length can have on water uptake readings, the Weight % values were plotted as a function of $\sqrt{t}/L$ as shown in Figure 13 where t is the time elapsed, and L is the length of the sample. In order to facilitate the comparison of the weight uptake of different samples, Weight % readings are taken at $\sqrt{t}/L = 3$.

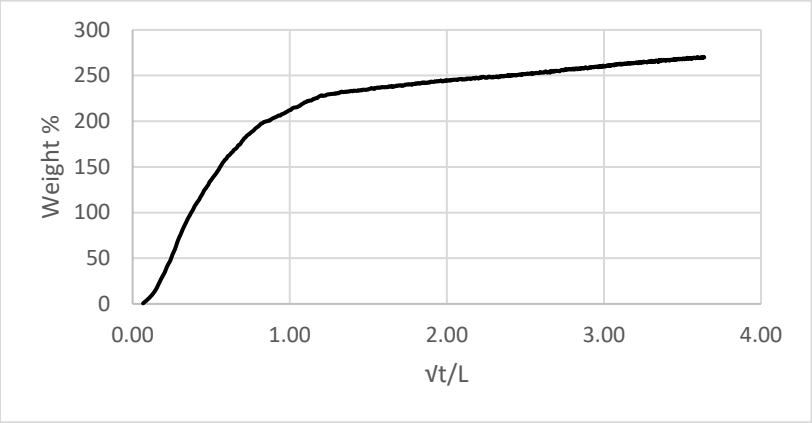

Figure 13. Example of a typical water uptake graph

3.3.3.4 Thermogravimetric Analysis

TGA was performed on SiO_2-treated and NT spruce wood samples with dimensions of (3 × 2 × 1 mm) using both a TA Instruments Q600 SDT. Changes in weight were recorded over time in the form of derivative weight readings, expressed as the first derivative of Weight % with respect to temperature. Samples were heated from 20-500°C at a rate of 10°C/min. Due to the high temperatures employed by this method, these tests could be performed immediately after removing the samples from the chamber and did not first require a 24-hour drying cycle.

3.3.3.5 X-Ray Diffraction

Powder XRD was used to measure the crystallinity index of NT and SiO_2-treated spruce wood samples. These measurements were taken using a Bruker D8 Endeavor with a LinxEye XE-T 1-D silicon strip detector. Both machines used a copper K-alpha beam frequency to generate diffractograms with intensity plotted as a function of 2θ (the exit angle of the beam), as shown in Figure 14. Intensity can vary depending on factors such as the density and the size of the sample tested. Therefore, in cases where a control graph cannot be established, the intensity of different samples cannot be compared to each other. In such cases, a factor known as the crystallinity index is calculated to determine differences in crystallinity between samples.

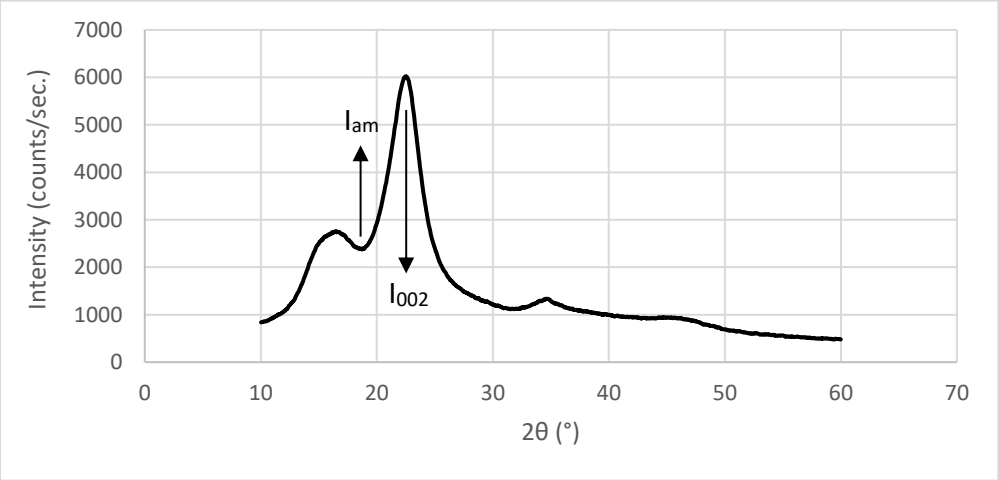

Figure 14. Example of a typical XRD diffractogram

The crystallinity index of each sample was determined using the following equation (Segal *et al.*, 1959):

$$CrI = \left(1 - \left(\frac{I_{am}}{I_{002}}\right)\right) \times 100 \quad (3)$$

Where CrI is the crystallinity index, I_{am} is the intensity of the amorphous valley, and I_{002} is the intensity of the crystalline peak. An example of the points on an XRD diffractogram where these variables can be identified is shown in Figure 14.

3.3.3.6 Statistical Analysis

Two different types of statistical analysis were applied to the results of this study: Welch's T-test and the paired Student's T-test. For both of these analyses, all samples were considered to be independent.

Welch's T-test (Welch, 1947) was applied for both destructive and non-destructive characterization tests to determine the significance of the experimental results when comparing the SiO_2-treated samples to the NT samples at each testing interval. It was also used to compare individual differences in both types of samples at each testing interval exclusively for destructive tests, since the samples tested were not the same throughout the process. This test was chosen to account for the possibility of unequal variances. Welch's T-test is defined using the following equations (StatsDirect Limited, 2016).

The T-score was calculated using:

$$t = \frac{\bar{x}_1 - \bar{x}_2}{\sqrt{\frac{s_1^2}{n_1} + \frac{s_2^2}{n_2}}} \quad (4)$$

where *t* is the T-score, $\bar{x}_1$ and $\bar{x}_2$ are the sample means, s_1 and s_2 are sample standard deviations, and n_1 and n_2 are the sample sizes.

The sample standard deviations were calculated using:

$$s_j^2 = \frac{\sum_{i=1}^{n_j}(x_i - \bar{x}_j)^2}{n_j - 1} \quad (5)$$

where *j* represents either the number 1 or 2 depending on the sample.

The number of degrees of freedom, *df*, was calculated using:

$$df = \frac{\left[\frac{s_1^2}{n_1} + \frac{s_2^2}{n_2}\right]^2}{\frac{\left(\frac{s_1^2}{n_1}\right)^2}{n_1 - 1} + \frac{\left(\frac{s_2^2}{n_2}\right)^2}{n_2 - 2}} \quad (6)$$

The paired Student's T-test was applied to determine the significance of the differences in both NT and SiO_2-treated sample results from one testing interval to the next, but only for non-destructive tests where the samples remained the same throughout the testing period. This test was chosen since it applies exclusively to the same set of samples compared before and after testing (Shier, 2004). The paired Student's T-test is defined using the following equations (Shier, 2004).

The T-score was calculated using:

$$t = \frac{\bar{d}}{SE(\bar{d})} \quad (7)$$

Where *t* is the T-score, $\bar{d}$ is the mean difference, and $SE(\bar{d})$ is the standard error of the mean difference.

The standard error of the mean differences was calculated using:

$$SE(\bar{d}) = \frac{s_d}{\sqrt{n}} \quad (8)$$

Where s_d is the sample standard deviation of the differences and *n* is the number of samples.

The number of degrees of freedom, *df*, was calculated using:

$$df = n - 1 \tag{9}$$

For both types of tests, the corresponding P-value was calculated using the *P Value from T Score Calculator* provided online by Stangroom (2023). A significance level of 0.05, or 95% confidence interval was used. Thus, if the P-value was found to be smaller than 0.05, the result was considered to be significant.

3.4 Results and Discussion

Characterization tests for samples subjected to accelerated aging in the hydrolytic aging chamber were performed at 0 months (control) and after 1 month, 2 months, and 3 months of aging. DMA and tensiometry tests are considered to be non-destructive and the same samples were returned to the chamber after each testing interval. TGA is a destructive test and required the use of a separate set of samples for every testing cycle. XRD and SEM are destructive tests since the samples need to be further cut to size before testing. These two tests were performed on different samples picked from each testing interval after the aging process had been completed.

3.4.1 Scanning Electron Microscopy

SEM was performed on unaged (0 month) NT and SiO_2-treated samples to determine the behaviour of the colloid during the treatment process. The micrographs shown in Figures 15 and 16 demonstrate the differences between the NT and SiO_2-treated samples, as the brighter areas of Figure 16 represent the agglomerated SiO_2 colloid. Although it was initially hypothesized that the SiO_2 colloid would be able to infiltrate and clog the lumens of the wood, these micrographs show that the vacuum treatment process instead perpetuated an acid-base reaction between the colloid (pH = 9.1) and the wood (pH = 4.8) (Geffert *et al.*, 2019), causing the nano-SiO_2 colloid to agglomerate on the surface of the sample along the longitudinal axis as shown in Figures 16a) and 16b). It also agglomerated on the tangential-radial plane of the sample as demonstrated in Figures 16c) and 16d). The colloid formed a hard protective layer over the open lumens, although full coverage was not achieved, and some lumens remained open as seen in Figure 15d). The inability of the wood to enter the lumens was further proven by the results of the ATR-FTIR tests presented in Appendix C.

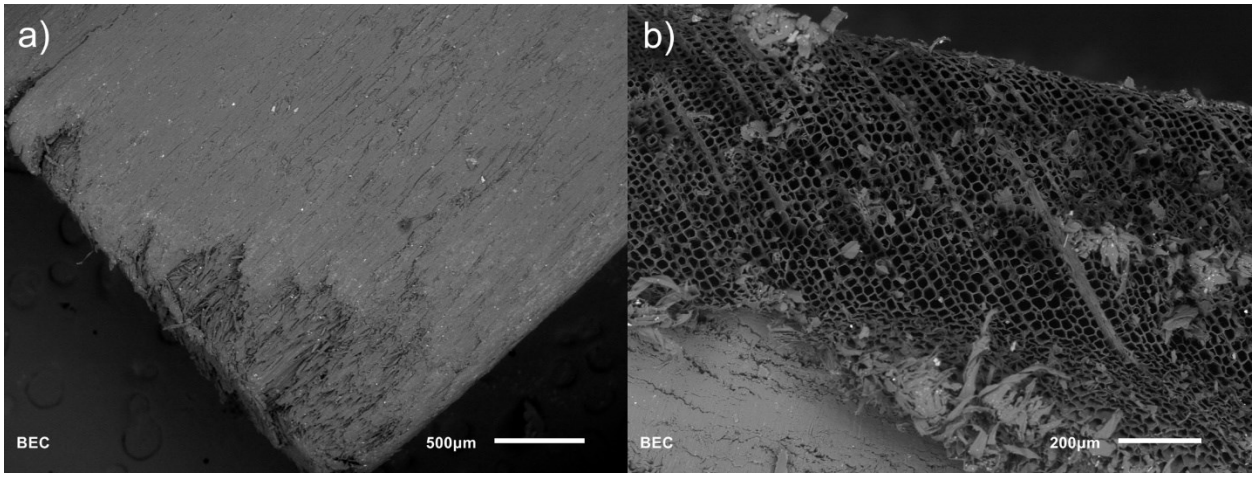

Figure 15. SEM images of the a) longitudinal plane and b) tangential-radial plane of an unaged NT sample

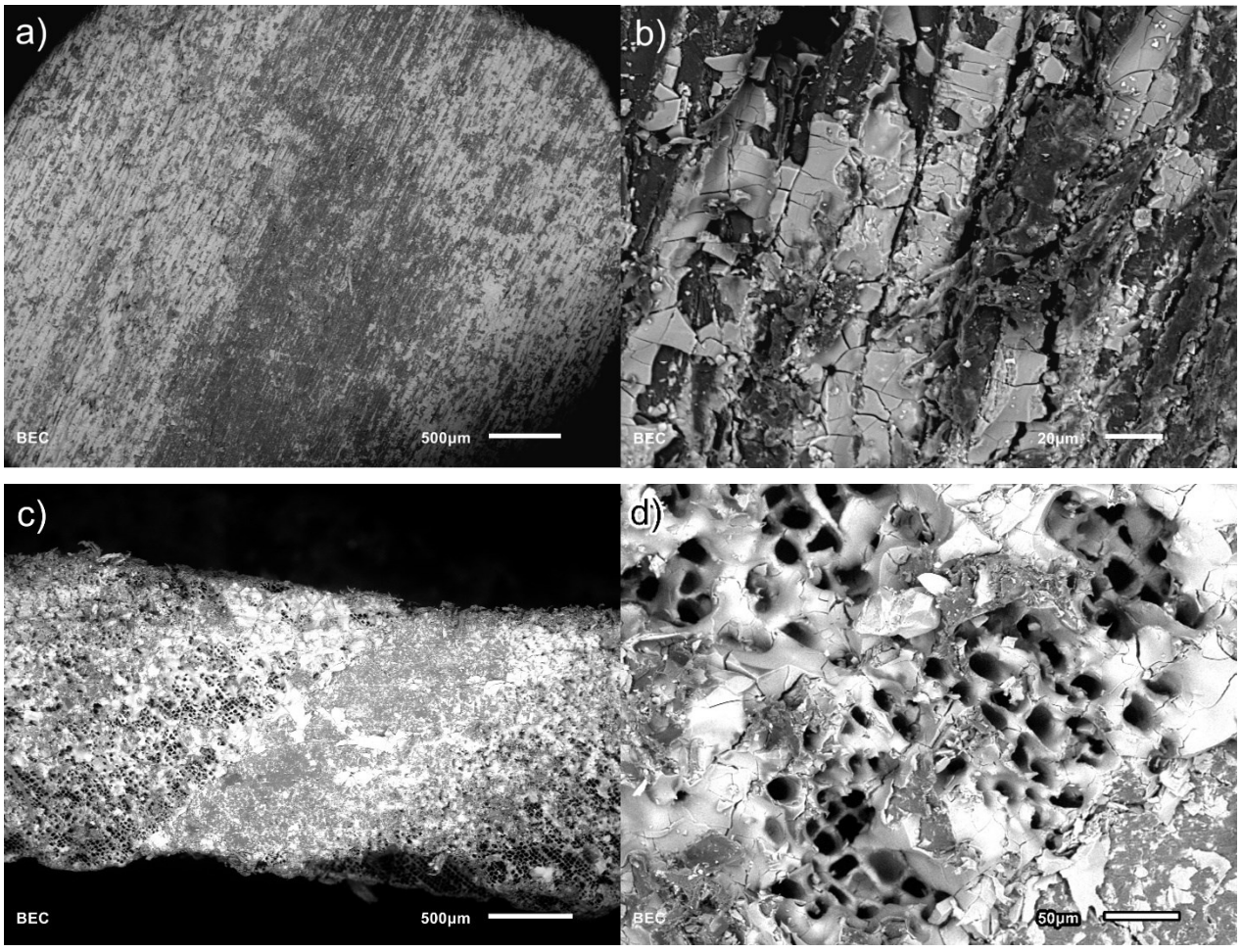

Figure 16. SEM images of the a,b) longitudinal plane and c,d) tangential-radial plane of an unaged SiO_2-treated sample

It is worth noting that additional SEM was performed on samples that had undergone accelerated aging. However, the results of these tests did not show any visible differences when compared to the unaged samples. Therefore, it can be concluded that the degradation of the wood cell structure was not visible at the level of magnification used in the SEM analysis performed for this study.

Unlike SEM, which scatters electrons on the surface of the sample to obtain a backscattered image, transmission electron microscopy allows electrons to pass through the surface of the sample, resulting in a higher resolution image (Gleichmann, 2020). For future experiments, it is recommended that transmission electron microscopy should also be performed on the samples in order to more effectively identify any signs of degradation.

3.4.2 X-Ray Diffraction

Powder XRD was performed on an average of 10 NT and 10 SiO_2-treated samples per aging interval. The results of this analysis are shown in Figure 17. At 0 months, the difference in crystallinity index between the SiO_2-treated samples and the NT samples was found to be statistically significant, as shown in Table 3. This demonstrates that the SiO_2 treatment process increased the crystallinity of the spruce wood samples. Similar behaviour was observed by Mohomane *et al.* (2021), who found that the crystallinity index of wood cellulose fibres increased when treated via spin-coating in a water-nanosilica solution.

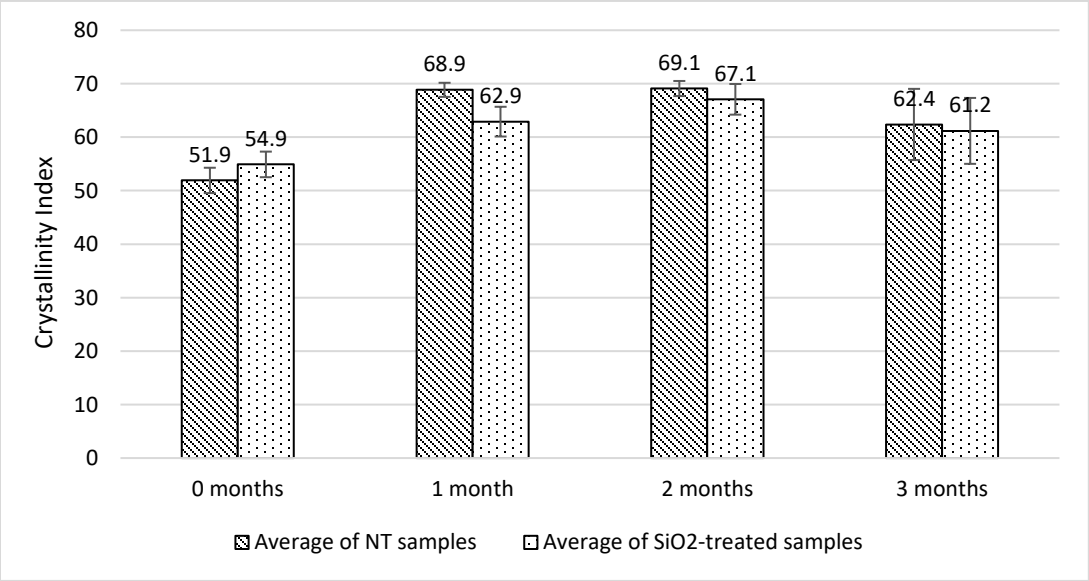

Figure 17. Crystallinity index of NT and SiO_2-treated samples after 3 months of hydrolytic aging

This behaviour was likely caused by the degradation of the amorphous region of cellulose within the SiO_2-treated samples as a result of alkaline hydrolysis and "peel-off" during the vacuum treatment process (Van Loon & Glaus, 1997). The degradation of the amorphous region of the SiO_2-treated samples causes an increase in the crystallinity index since the crystalline region becomes more pronounced. The XRD curves shown in Figure 18 also demonstrate this behaviour, as the amorphous region of a typical SiO_2-treated sample curve is less pronounced than for the NT sample.

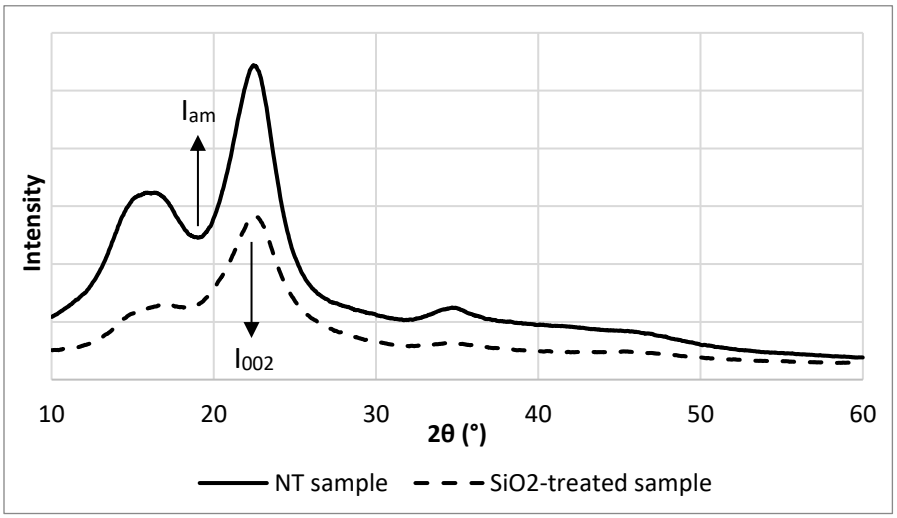

Figure 18. Example of typical XRD curves for NT and SiO_2-treated samples at 0 months

Table 3 shows that the increase in crystallinity demonstrated by both the NT samples and the SiO_2-treated samples at each interval was found to be statistically significant. This reflects studies performed by Tarmian & Mastouri (2016) and Toba *et al.* (2013), who have shown that an increase in crystallinity can be perpetuated by high temperature and high humidity conditions. This cause of this effect was hypothesized by Toba *et al.* (2013) to be due to the formation of hydrogen bonds between noncrystalline cellulose and cellulose at the surface of the crystalline region during repeated wetting/drying. Additionally, Bhuiyan *et al.* (2000) found that an increase in the crystallinity of cellulose will be twice as high under high humidity conditions when compared to oven dry conditions. This increase in crystallinity is caused by the crystallization of the quasicrystalline and amorphous components of cellulose under hydrolytic aging conditions (Bhuiyan *et al.*, 2000). This phenomenon is exhibited by the results shown in Tables 4 and 5: for the NT samples after 1 month of hydrolytic aging, the average intensity of the amorphous peak (I_{am}) showed a statistically insignificant decrease, and the average intensity of the crystalline peak (I_{002}) showed a statistically significant increase.

The greatest increase occurred from 0 months to 1 month of accelerated aging, where the crystallinity index of the NT samples increased by 32.63%, while the SiO_2-treated samples exhibited an increase of 14.56%. At 2 months, the crystallinity index of the NT samples remained stable, but appeared to exhibit an increase for the SiO_2-treated samples. As shown in Tables 4 and 5, the 2-month data shows a significant increase in crystallinity, with similar amorphous and crystalline peak values to those of the NT samples. This outlier behaviour is indicative of an error in the dataset due to inherent variations in wood properties, and additional tests on samples aged for 2 months are required to improve the average before making a conclusive observation on this set. Both the NT and the SiO_2-treated samples also experienced a significant decrease from 2 months to 3 months. This may be related to a delay in the degradation of the crystalline phase of cellulose. The crystalline portion of cellulose contains strong hydrogen bonds and is known to require higher degradation temperatures when subjected to hydrolysis (Yu & Wu, 2010). Therefore, it could be hypothesized that the crystalline portion of cellulose did not degrade until 3 months of hydrolytic degradation had occurred, leading to a lower crystallinity index at 3 months since both the amorphous and crystalline portions of the cellulose would have experienced degradation. Additionally, Tarmian and Mastouri (2019) hypothesized that the removal of extractives could also be responsible for the decrease in crystallinity after aging. However, the large standard deviation found at 3 months should first be eliminated by gathering additional results for this dataset before any hypothesis can be confirmed.

Since the crystallinity index of the SiO_2-treated samples was higher than the NT samples at 0 months but remained lower than the NT samples at subsequent testing intervals, it can be concluded that the SiO_2 treatment process caused an increase in crystallinity directly after treatment but inhibited an increase in crystallinity when exposed to hydrolytic aging conditions over time. Since the colloid formed a protective layer over the ends of the sample lumens, the SiO_2-treated samples were less susceptible to the infiltration of water under high-humidity conditions.

Table 3. Statistical analysis for crystallinity index values of NT and SiO_2-treated samples

Comparison Type	Aging Period	T-score	P-value	Result
NT samples	0 to 1 month	-17.079	<< .05	Significant
	0 to 2 months	-16.867	<< .05	Significant
	0 to 3 months	-4.201	<< .05	Significant
	1 to 2 months	-2.971	<< .05	Significant
	2 to 3 months	2.825	<< .05	Significant
SiO_2-treated samples	0 to 1 month	-5.985	<< .05	Significant
	0 to 2 months	-8.720	<< .05	Significant
	0 to 3 months	-2.644	<< .05	Significant
	1 to 2 months	-3.059	<< .05	Significant
	2 to 3 months	2.472	<< .05	Significant
NT vs SiO_2-treated samples	0 months	-2.279	<< .05	Significant
	1 month	5.773	<< .05	Significant
	2 months	1.800	<< .05	Not Significant
	3 months	0.388	<< .05	Not Significant

Table 4. Average crystalline and amorphous peak values of NT and SiO_2-treated samples

Sample Type	Peak	0 months	1 month	2 months	3 months
NT samples	I_{am}	4690.61	4410.57	4369.66	3909.72
	I_{002}	9428.74	14265.68	14277.59	11173.60
SiO_2-treated samples	I_{am}	1732.35	1504.085	3520.37	1914.60
	I_{002}	3846.015	4059.82	10208.80	5365.87

Table 5. Statistical analysis for crystalline and amorphous peak values of NT and SiO_2-treated samples

		I_{am}			I_{002}		
Comparison Type	**Aging Period**	**T-score**	**P-value**	**Result**	**T-score**	**P-value**	**Result**
NT samples	0 to 1 month	1.531	> .05	Not Sig.	-6.171	<< .05	Significant
	0 to 2 months	1.333	> .05	Not Sig.	-5.648	<< .05	Significant
	0 to 3 months	3.243	<< .05	Significant	-1.473	> .05	Not Sig.
	1 to 2 months	0.180	> .05	Not Sig.	-0.015	> .05	Not Sig.
	2 to 3 months	1.667	> .05	Not Sig.	2.573	<< .05	Significant
SiO_2-treated samples	0 to 1 month	2.070	> .05	Not Sig.	-0.610	> .05	Not Sig.
	0 to 2 months	-10.323	<< .05	Significant	-5.163	<< .05	Significant
	0 to 3 months	-1.015	> .05	Not Sig.	-1.853	> .05	Not Sig.
	1 to 2 months	-11.232	<< .05	Significant	-4.949	<< .05	Significant
	2 to 3 months	7.021	<< .05	Significant	3.347	<< .05	Significant

3.4.3 Tensiometry

Water uptake measurements were performed on 10 SiO_2-treated samples and 10 NT samples at regular intervals throughout the accelerated aging process. Figure 19 shows the average water uptake at each testing interval for both sets of samples. The average water uptake of the SiO_2-treated samples remained consistently lower than the average water uptake of the NT samples. Similar results were described by Lemaire-Paul *et al.* (2022). The water uptake of the SiO_2-treated samples is greatly reduced due to the reduction of open lumens through the agglomeration of the colloid on the tangential-radial ends of the samples during the vacuum-induced impregnation process.

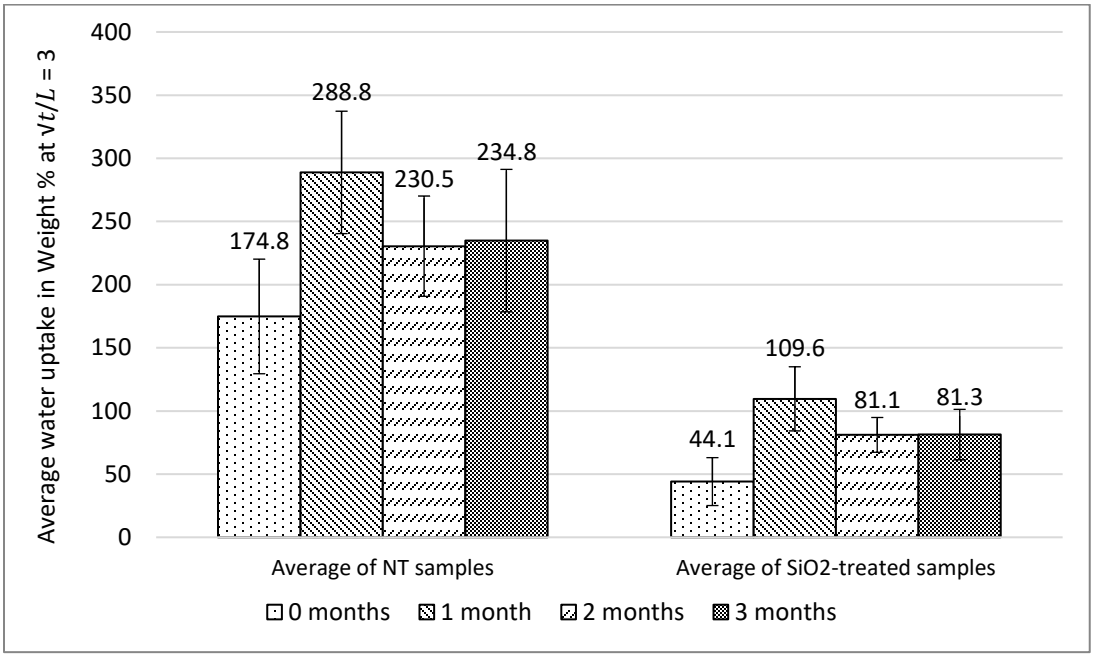

Figure 19. Average water uptake of NT and SiO_2-treated samples at different accelerated aging intervals

Both types of samples exhibited a significant increase after 1 month of aging followed by a significant decrease and stabilization from 2-3 months. It is possible that the combination of high-temperature, high-humidity aging conditions and subsequent drying cycles at 103°C may have had counteracting effects on the spruce wood samples. This hypothesis is based on three assumptions: 1) that the samples were below their fiber saturation point (FSP) throughout the 3-month period, 2) that the samples reached a stable equilibrium moisture content (EMC) shortly after being placed in the aging chamber at each testing interval, and 3) that the drying oven had a significantly lower RH than the aging chamber, leading to a lower EMC during drying (Walker *et al.*, 1993).

Wood is only able to absorb moisture below its FSP, which is equal to a moisture content (MC) of around 30% for most species (Walker *et al.*, 1993; Yona *et al.*, 2021). At 90°C and 80% RH, wood has an EMC of around 10-11% (Simpson & Rosen, 1981; Glass & Zelinka, 2010). When placed in the oven at 103°C, it can be assumed that the EMC of the samples fell below 10%. At each aging cycle, the wood samples were subjected to a hysteresis loop, as the samples underwent shrinkage when being dried at 103°C followed by swelling when placed back in the aging chamber. Shrinkage occurs when wood is dried below its FSP and bound water begins to evaporate (Reeb, 2009). This process exerts mechanical stress on the wood samples and will result in the degradation of the samples through the deformation of the wood (Reinprecht, 2016) and the propagation of microcracks (Yamamoto *et al.*, 2013). Since cellulose is classified as a semi-crystalline polymer, the increase in crystallinity after 1 month of aging (see Section 3.4.2) would have intensified the shrinkage of the wood cell walls (Benedetti *et al.*, 2019). This likely resulted in an increase in microcrack development and consequently an increase in water uptake when tested at 1 month as shown in Figure 19.

The decrease and stabilization of the water uptake values after 2 months of aging may be related to a decrease in hygroscopic response because of the phenomenon of hysteresis. During shrinkage, adsorbed water within the wood cell walls is removed, causing the cell wall components to form strong hydrogen bonds with each other instead. Due to the presence of these bonds, the wood will adsorb water at a slower rate during swelling, forming the basis of a hysteresis loop as shown in Section 2.3.1. García Esteban *et al.* (2005) found that the hygroscopic response of wood will decrease after being subjected to accelerated aging at 50°C and 90% followed by desiccation. In their study, it was determined that the wood moisture content and sample length stabilized between the fourth and fifth cycles, and after measuring the behaviour of the samples in thermostatic baths, a loss of hygroscopic response was detected in the aged samples at all levels of humidity. This behaviour was attributed to a gradual decrease in the concentration of −OH (hydroxyl) groups caused by the fixation of water within the wood cell walls when subjected to accelerated aging (García Esteban *et al.*, 2005).

Table 6 describes the steps involved in performing the water uptake measurements at each testing interval for both the NT and SiO_2-treated samples. Before the water uptake measurements were taken at 2 months, the samples had undergone a total of 5 drying cycles at 103°C. It is likely that the hygroscopicity of both types of samples stabilized between the fourth and fifth drying cycles as described by García Esteban *et al.* (2005). This loss of hygroscopic response resulted in the reduction of water adsorption during the aging and swelling process and a decrease in the EMC of the wood. Since the rate of wood shrinkage is dependent on the change in wood moisture content (Hansen, 1987), the samples likely experienced less shrinkage when dried at 103°C after 2 months of aging. This hypothesis is supported by the observed stabilization of the

crystallinity index of the samples past 2 months shown in Figure 19, indicating that the effect of the crystallinity on the samples did not intensify any further.

Therefore, after 2 months of aging, the rate of crack propagation and hydrolytic degradation decreased due to a reduction in the rate of shrinkage and a loss in hygroscopic response. This led to the reduction and stabilization of water uptake values between 2 months and 3 months of aging for both types of samples.

Table 6. Water uptake measurement procedure

	Testing Interval (number of months aged)			
Procedure Steps	**0 months**	**1 month**	**2 months**	**3 months**
Aging	n/a	✓	✓	✓
24hr drying cycle (103°C)	✓	✓	✓	✓
Water uptake measurement	✓	✓	✓	✓
24hr drying cycle (103°C)	✓	✓	✓	n/a
Cumulative number of drying cycles **before** water uptake measurement	1	3	5	7

Statistical analysis as shown in Table 7 further reinforces the benefits of the SiO_2 treatment process. The difference in water uptake for the NT and SiO_2-treated sets at each interval were all found to be statistically significant. The standard deviation values of the SiO_2-treated samples were also found to be lower than those exhibited by the NT samples. This not only proves that the SiO_2 treatment process had a positive effect on reducing the water uptake of wood, but also that the water uptake remained consistently lower even when subjected to accelerated hydrolytic aging conditions.

Table 7. Statistical analysis of the water uptake readings of hydrolytically aged NT and SiO_2-treated samples

Comparison Type	Aging Period	T-score	P-value	Result
NT samples	0 to 1 month	-7.936	<< .05	Significant
	0 to 2 months	-4.051	<< .05	Significant
	0 to 3 months	-3.391	<< .05	Significant
	1 to 2 months	6.240	<< .05	Significant
	2 to 3 months	0.008	> .05	Not Significant
SiO_2-treated samples	0 to 1 month	-8.528	<< .05	Significant
	0 to 2 months	-2.118	> .05	Not Significant
	0 to 3 months	-5.493	<< .05	Significant
	1 to 2 months	3.113	<< .05	Significant
	2 to 3 months	-0.820	> .05	Not Significant
NT vs SiO_2-treated samples	0 months	7.976	<< .05	Significant
	1 month	9.833	<< .05	Significant
	2 months	10.661	<< .05	Significant
	3 months	6.878	<< .05	Significant

3.4.4 Dynamic Mechanical Analysis

DMA tests were performed on 10 SiO_2-treated samples and 10 NT samples at regular intervals throughout the accelerated aging process in order to study the effect of the aging process on the viscoelastic properties of each sample. A temperature sweep from 5-40°C was performed at a constant frequency (1 Hz) to perform these tests. The average storage modulus, loss modulus, and tanδ (damping) values recorded during DMA tests at a temperature of 25°C (ambient) were used to compare the two sets of samples. Additional values taken at 10°C (below ambient) and 35°C (above ambient) were also analysed, with similar results to the ones shown below for 25°C. The numerical results of this analysis are presented in Appendix B.

Figures 20-22 present the results of the DMA measurements. When comparing the two types of samples, the viscoelastic properties of the SiO_2-treated samples were significantly lower than those of the NT samples. This was likely due to sample degradation that occurred at 0 months caused by alkaline attack during the impregnation process. This does not reflect the results found by Lemaire-Paul *et al.* (2022) who found that the SiO_2 treatment process significantly increased the viscoelastic properties of the samples. This discrepancy is likely due to the difference in the treatment procedure and type of colloid used for this study. Lemaire-Paul *et al.* (2022) used a LUDOX HS-40 colloid with a particle size of 12 nm (Sigma-Aldrich, 2023b) and did not raise the pressure from -90 kPa to atmospheric pressure. Instead, the pressure was maintained at -90 kPa pressure throughout the treatment process. Although the increase to atmospheric

pressure was meant to allow for better infiltration of the nanoparticles, the nanoparticle size of the LUDOX AS-40 colloid used for this study was 20-24 nm. Therefore, it is likely that the nanoparticles were largely unable to infiltrate the lumens of the wood and instead only reacted to form a coating at the surface of the samples. During the retention period at atmospheric pressure, the liquid phase of the colloid, which contained −OH groups, could successfully infiltrate the wood's vascular system due to the increase in pressure from -90 kPa to 101 kPa. This infiltration resulted in an alkaline attack.

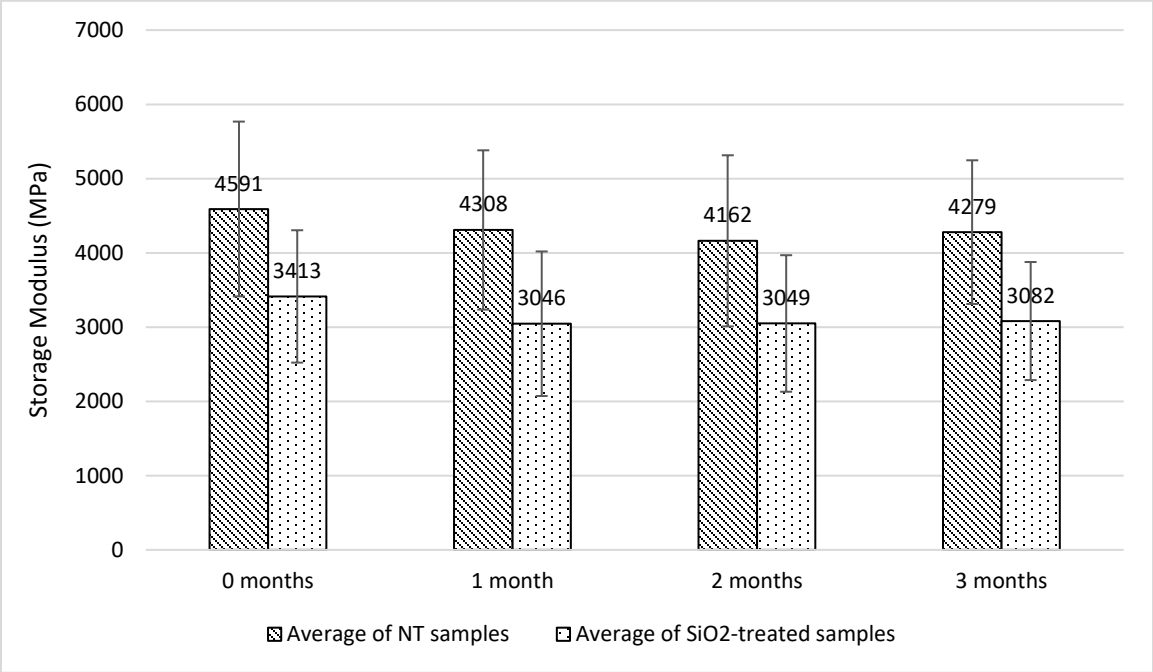

Figure 20. Average storage modulus of hydrolytically aged NT and SiO_2-treated samples at 25°C over time

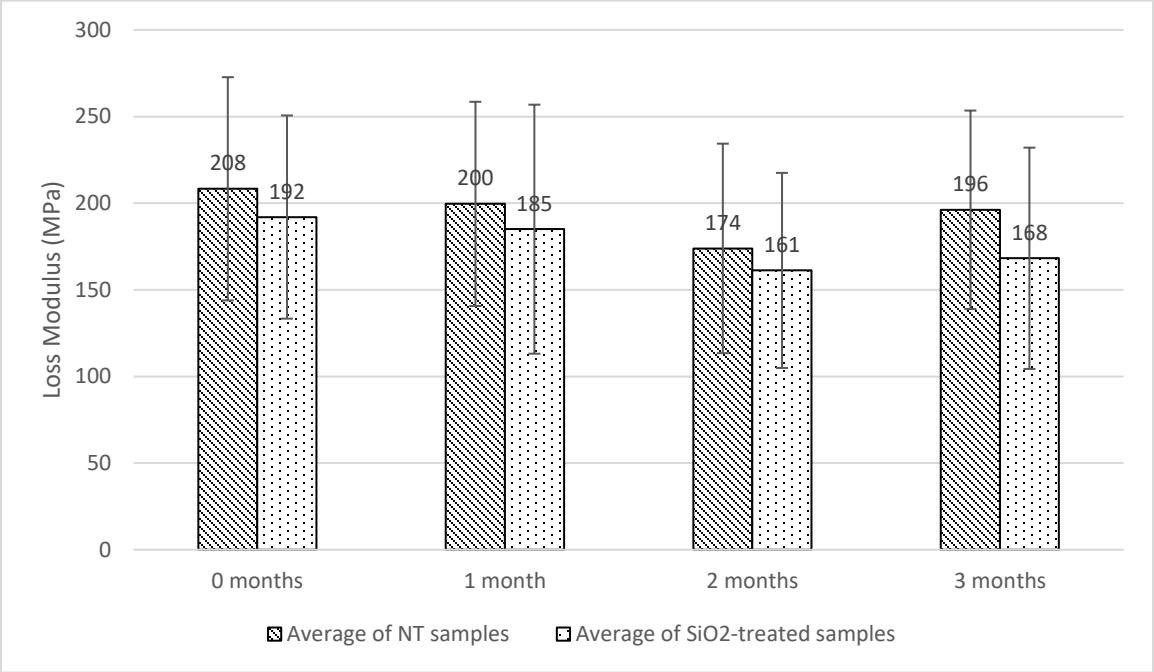

Figure 21. Average loss modulus of hydrolytically aged NT and SiO_2-treated samples at 25°C over time

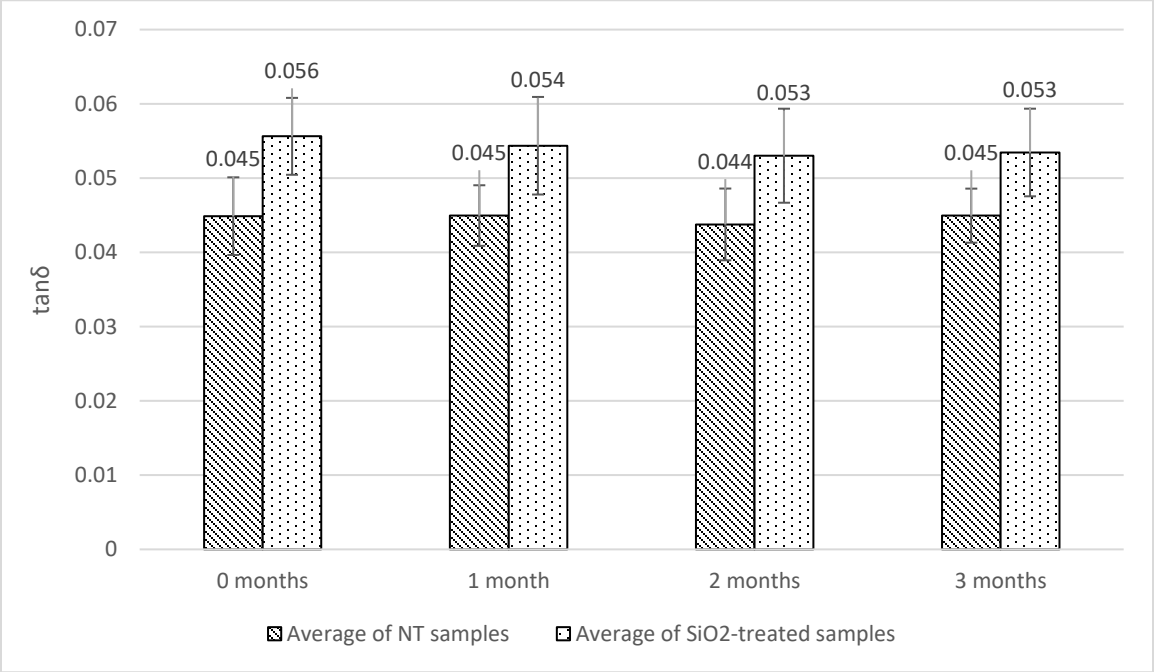

Figure 22. Average tanδ values of hydrolytically aged NT and SiO_2-treated samples at 25°C over time

The changes in storage modulus values from 0 months to 1/2/3 months exhibited by both the NT and the SiO_2-treated samples over time were largely found to be statistically significant as shown in Table 8. The only exception was the change in SiO_2-treated samples from 0-1 month, which was found to be statistically insignificant. This indicates that the aging conditions caused the storage modulus of the NT samples to decrease significantly from the beginning of the aging period whereas they did not have a significant, detrimental effect on the storage modulus of the SiO_2-treated samples until 2 months had passed.

All changes in loss modulus values from 0 months to 1/2/3 months exhibited by the NT over time were found to be statistically significant. Changes in loss modulus values of the SiO_2-treated samples were found to statistically significant from 0-1 month and from 0-2 months, but not from 0-3 months. It is worth noting that this set contained the highest number of eliminated outlier values and therefore this discrepancy could be attributed to experimental error caused by a small sample size. Further testing would be required to obtain a better average and draw a conclusion for the SiO_2-treated samples at 3 months.

Considering the intermediate periods from 1-2 months and 2-3 months, a different trend emerges. All changes in storage and loss modulus values were found to be statistically insignificant for the SiO_2-treated samples. All changes in loss modulus values for the NT samples from 1-2 and 2-3 months were also found to be statistically insignificant. However, the changes in storage modulus values of the NT samples were statistically significant between 1-2 months, but not between 2-3 months. Therefore, the continued hydrolytic aging process did not seem to have a significant effect on the storage modulus of the NT samples past 2 months or the SiO_2-treated samples past 1 month. These results reflect the data shown in Figure 20, where the largest decrease in storage modulus for the NT samples occurred between 0-1 month. Additionally, the storage modulus of the NT samples continued to decrease up to the 2-month testing period, and the storage modulus of SiO_2-treated samples appeared to stabilize after 1 month.

The tanδ values of the samples remained relatively stable as shown in Figure 22. Table 8 suggests that the only significant difference in tanδ occurred for both sample types between 1-2 months, although this amounted to a very small decrease (< 0.001) that can be considered negligible.

Typically, wood samples aged under high-temperature, high-humidity conditions are expected to exhibit a significant decrease in storage modulus, an increase in loss modulus, and an increase in tanδ (Zhan *et al.*, 2018; Zeniya *et al.*, 2018). Additionally, an increase in crystallinity such as the one described in Section 3.4.2 will result in an increase in storage modulus and a decrease in loss modulus (Reiniati *et al.*, 2014). It could be hypothesized that these two phenomena counteracted each other during this study, resulting in the unexpected behaviour exhibited by the viscoelastic properties of both types of samples. It should also be noted that high standard deviation values were exhibited by both types of samples due to the low sample size and sensitivity of the testing method, as shown in Table 10. Therefore, a conclusive reason for the

behaviour exhibited by both the NT and SiO_2-treated samples over time cannot currently be determined, and additional testing with a larger number of samples is required to reach a definitive hypothesis.

However, since these standard deviation values remain consistent for both sample types and testing intervals, the NT and SiO_2-treated samples can also be compared with each other. The differences between the storage modulus and tanδ values of both the NT and SiO_2-treated samples at each aging condition were found to be statistically significant with the exception of a single outlier at 2 months for the storage modulus, as shown in Table 9. This trend was not exhibited by the loss modulus values, where all differences were found to be statistically insignificant for both types of samples. Therefore, it can be concluded that the SiO_2 treatment process was found to have a significant, detrimental effect on the storage modulus but did not affect the loss modulus of the samples.

Since the loss modulus values of the SiO_2-treated samples were comparable to those exhibited by the NT samples and the storage modulus values were significantly lower than those exhibited by the NT samples, the tanδ values of the SiO_2-treated samples were also found to be significantly higher than those exhibited by the NT samples. Consequently, this high damping property could be beneficial if this wood treatment method was incorporated into the construction of earthquake-resistant structural systems (Jayamon *et al.*, 2016).

Table 8. Statistical analysis of the viscoelastic properties of hydrolytically aged NT and SiO_2-treated samples at 25°C

	NT Samples			SiO_2-treated samples		
Comparison Interval	**Statistical analysis of average values at 25°C**			**Statistical analysis of average values at 25°C**		
Storage Modulus	**T- score**	**P-value**	**Result**	**T- score**	**P-value**	**Result**
0 months vs 1 month	-5.020	<< .05	Sig.	-2.416	> .05	Not Sig.
0 months vs 2 months	-4.978	<< .05	Sig.	-3.685	<< .05	Sig.
0 months vs 3 months	-3.678	<< .05	Sig.	-3.508	<< .05	Sig.
1 month vs 2 months	-3.004	<< .05	Sig.	-2.526	> .05	Not Sig.
2 months vs 3 months	-2.636	> .05	Not Sig.	-1.482	> .05	Not Sig.
Loss Modulus	**T- score**	**P-value**	**Result**	**T- score**	**P-value**	**Result**
0 months vs 1 month	-3.778	<< .05	Sig.	-2.724	<< .05	Sig.
0 months vs 2 months	-5.111	<< .05	Sig.	-5.384	<< .05	Sig.
0 months vs 3 months	-4.187	<< .05	Sig.	-2.021	> .05	Not Sig.
1 month vs 2 months	-2.297	> .05	Not Sig.	-2.735	> .05	Not Sig.
2 months vs 3 months	-0.458	> .05	Not Sig.	-0.425	> .05	Not Sig.
Tan delta	**T- score**	**P-value**	**Result**	**T- score**	**P-value**	**Result**
0 months vs 1 month	-0.579	> .05	Not Sig.	-0.814	> .05	Not Sig.
0 months vs 2 months	-0.868	> .05	Not Sig.	-1.675	> .05	Not Sig.
0 months vs 3 months	0.054	> .05	Not Sig.	-1.582	> .05	Not Sig.
1 month vs 2 months	-2.348	<< .05	Sig.	3.225	<< .05	Sig.
2 months vs 3 months	-0.089	> .05	Not Sig.	0.875	> .05	Not Sig.

Table 9. Statistical analysis of the viscoelastic properties of NT samples when compared to SiO_2-treated samples at 25°C (hydrolytically aged)

Comparison Interval	Statistical analysis of average values at 25°C		
Storage Modulus	**T-score**	**P-value**	**Result**
0 months	2.523	<< .05	Significant
1 month	2.337	<< .05	Significant
2 months	2.085	> .05	Not Sig.
3 months	2.493	<< .05	Significant
Loss Modulus	**T-score**	**P-value**	**Result**
0 months	0.592	> .05	Not Sig.
1 month	0.405	> .05	Not Sig.
2 months	0.419	> .05	Not Sig.
3 months	0.827	> .05	Not Sig.
Tan delta	**T-score**	**P-value**	**Result**
0 months	-4.622	<< .05	Significant
1 month	-3.276	<< .05	Significant
2 months	-3.488	<< .05	Significant
3 months	-3.570	<< .05	Significant

Table 10. Average storage modulus, loss modulus, and tanδ values of hydrolytically aged NT and SiO_2-treated samples at 25°C

	NT Samples		SiO_2-treated samples	
Aging Intervals	**Average Storage Modulus at 25°C (MPa)**	**Standard Deviation**	**Average Storage Modulus at 25°C (MPa)**	**Standard Deviation**
0 months	4591.20	1176.64	3413.40	891.23
1 month	4308.44	1072.66	3045.86	973.32
% change	-6.16		-10.77	
0 months	4591.20	1176.64	3413.40	891.23
2 months	4162.13	1152.10	3049.43	919.29
% change	-9.35		-10.66	
0 months	4591.20	1176.64	3413.40	891.23
3 months	4279.25	967.44	3081.80	794.82
% change	-6.79		-9.71	
Aging Intervals	**Average Loss Modulus at 25°C (MPa)**	**Standard Deviation**	**Average Loss Modulus at 25°C (MPa)**	**Standard Deviation**
0 months	208.35	64.42	192.04	58.63
1 month	199.67	58.93	185.09	71.86
% change	-4.17		-3.62	
0 months	208.35	64.42	192.04	58.63
2 months	173.00	60.46	161.28	56.30
% change	-16.97		-16.02	
0 months	208.35	64.42	192.04	58.63
3 months	196.26	57.27	168.23	63.87
% change	-5.80		-12.40	
Aging Intervals	**Average tanδ at 25°C (MPa)**	**Standard Deviation**	**Average tanδ at 25°C (MPa)**	**Standard Deviation**
0 months	0.04487	0.00523	0.05562	0.00518
1 month	0.04495	0.00408	0.05436	0.00657
% change	0.178		-2.265	
0 months	0.04487	0.00523	0.05562	0.00518
2 months	0.04376	0.00483	0.05301	0.00633
% change	-2.473		-4.693	
0 months	0.04487	0.00523	0.05562	0.00518
3 months	0.04494	0.00364	0.05344	0.00590
% change	0.156		-3.92	

3.4.5 Thermogravimetric Analysis

TGA was performed on an average of 2-5 SiO_2-treated samples and 2-5 NT samples at each testing interval during the accelerated aging process. The peak degradation temperature of cellulose (the point at which the maximum mass loss was detected) typically occurred at temperatures between 350–370°C, as shown in Figure 23. The SiO_2-treated samples exhibited consistently lower peak cellulose degradation temperatures than the NT samples. This was likely due to the degradation of cellulose in the treated samples caused by alkaline attack during the vacuum impregnation process.

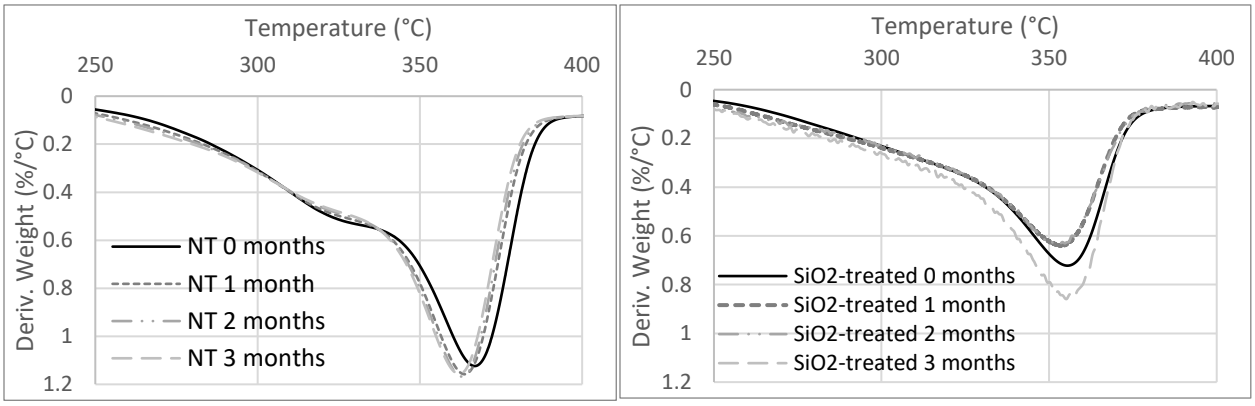

Figure 23. DTG curves of hydrolytically aged NT and SiO_2-treated samples at different aging intervals

A comparison of the peak cellulose degradation temperatures at each time interval is shown in Figure 24. The results indicate that from 0 months to 1 month, the NT samples showed a 0.85% decrease, while the SiO_2-treated samples exhibited a 0.57% decrease. From 0 months to 2 months, the NT samples exhibited a 0.92% decrease while the SiO_2-treated samples demonstrated a 0.47% decrease. Finally, from 0 months to 3 months, the NT samples demonstrated a 1.33% decrease while the SiO_2-treated samples showed a 0.82% decrease. As shown in Table 11, these decreases in average peak cellulose degradation temperature were found to be statistically significant for the NT samples. They were also found to be statistically insignificant for the SiO_2-treated samples, with the exception of the significant 0-1 month difference. Therefore, it can be said that the aging conditions had a significant detrimental effect on the peak cellulose degradation temperature of the NT samples, whereas the SiO_2-treated samples remained largely unaffected.

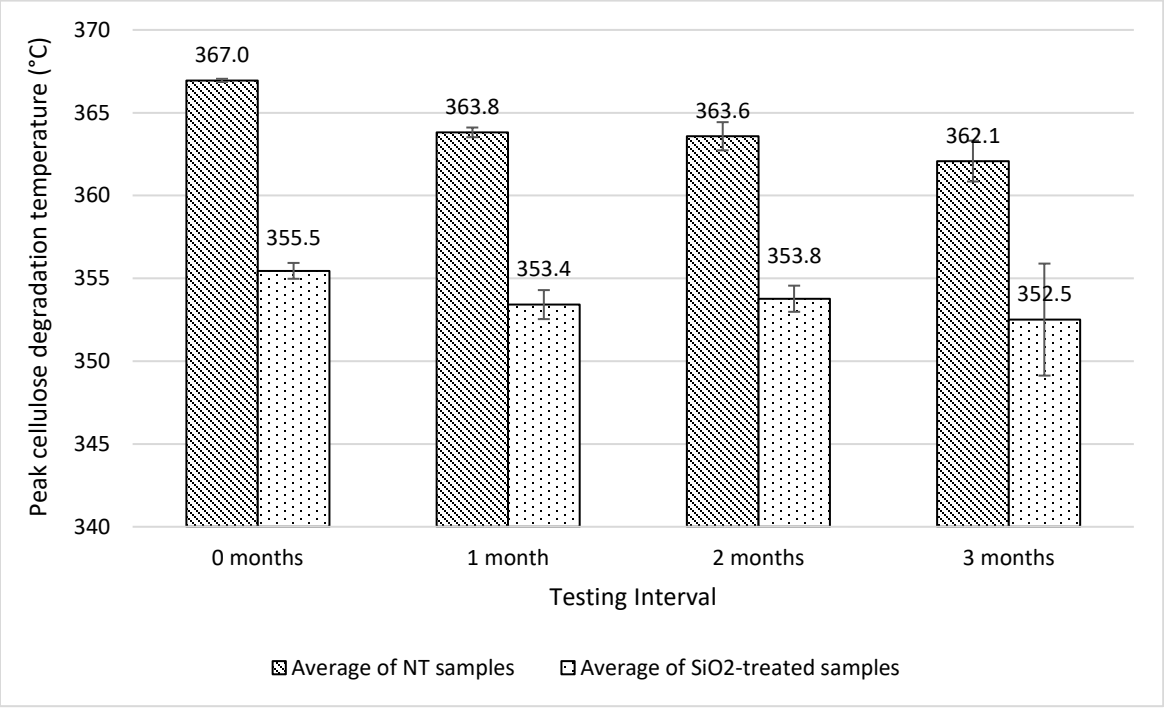

Figure 24. Peak cellulose degradation temperature for NT and SiO_2-treated samples at different accelerated aging intervals

Ultimately, the SiO_2-treated samples exhibited lower peak degradation temperatures throughout the testing process as well as a lower rate of degradation than the NT samples after 1 month of hydrolytic aging. This observed variation is likely caused by different reactions to the effects of prolonged exposure to the accelerated aging conditions. The high level of relative humidity within the chamber facilitated the infiltration of water into both sample types, breaking hydrogen bonds within the samples via hydrolysis and causing the cellulose to degrade. Water likely entered the vascular system of the NT samples but was largely unable to penetrate the vascular system of the treated samples due to obstruction by the SiO_2 colloid, leading to a lower rate of degradation for the SiO_2-treated samples. It is worth noting that differences in peak cellulose degradation rates between 1 month to 2 months and between 2 months to 3 months were found to be statistically insignificant for both sample types, as shown in Table 11. After the initial 1-month aging period, the rate of change in the cellulose degradation rate of both types of samples appeared to stabilize, likely due to the loss of hygroscopic response after 1 month described in Section 3.4.3. Therefore, it can be concluded that the SiO_2 nanoparticle treatment process had a positive effect on reducing the degradation rate of cellulose within spruce wood samples subjected to hydrolytic aging conditions.

Table 11. Statistical analysis for differences in peak cellulose degradation temperature of TGA samples at different accelerated aging intervals

Comparison Type	Aging Period	T-score	P-value	Result
NT samples	0 to 1 month	17.918	<< .05	Significant
	0 to 2 months	10.004	<< .05	Significant
	0 to 3 months	7.810	<< .05	Significant
	1 to 2 months	1.943	> .05	Not Significant
	2 to 3 months	1.306	> .05	Not Significant
SiO_2-treated samples	0 to 1 month	5.101	<< .05	Significant
	0 to 2 months	2.039	> .05	Not Significant
	0 to 3 months	1.724	> .05	Not Significant
	1 to 2 months	-1.017	> .05	Not Significant
	2 to 3 months	0.675	> .05	Not Significant
NT vs SiO_2-treated samples	0 months	44.587	<< .05	Significant
	1 month	23.092	<< .05	Significant
	2 months	10.552	<< .05	Significant
	3 months	5.317	<< .05	Significant

3.5 Conclusions

This research has examined the effects of high-temperature, high-humidity aging on spruce wood impregnated with a nano-SiO_2 colloid under a -90 kPa vacuum. The SEM results proved that the SiO_2 colloid agglomerated and clogged the extremities of the wood samples.

When comparing NT samples to SiO_2-treated samples subjected to accelerated aging in a hydrolytic chamber at 80% RH and 90°C over a period of 3 months, the XRD results demonstrated a statistically significant increase in crystallinity for both the NT and SiO_2-treated samples after 1 month of aging. This behaviour indicates that degradation of the wood samples was triggered by the high-temperature, high-humidity aging conditions (Tarmian & Mastouri, 2019; Toba *et al.*, 2013; Bhuiyan *et al.*, 2000). The crystallinity index values of the SiO_2-treated samples also remained lower than those found for the NT samples with the exception of the 0-month interval. For the SiO_2-treated samples, the increase in crystallinity at 0 months occurred due to the degradation of amorphous cellulose when subjected to alkaline hydrolysis during the treatment process (Van Loon & Glaus, 1997).

The average water uptake values found for the SiO_2-treated samples remained consistently lower than those of the NT samples after 3 months of hydrolytic aging. While the accelerated aging process did have a statistically significant effect on both types of samples, the nano-SiO_2 impregnation process successfully

clogged the lumens and allowed the water uptake of the treated samples to remain lower than the NT samples even when subjected to a high temperature and relative humidity for an extended period. Aging at high-temperature and high-humidity conditions followed by drying cycles at 103°C likely caused the formation of a hysteresis loop. At each aging interval, the samples underwent shrinkage when being dried at 103°C followed by swelling when placed back in the aging chamber. This effect in combination with the increase in crystallinity would also have increased the efficiency of the wood shrinkage (Benedetti *et al.*, 2019) and may have led to the formation of microcracks in the wood structure (Yamamoto *et al.*, 2013), ultimately leading to an increase in water uptake after 1 month of aging. However, after 2 months of aging, the water uptake values of the samples decreased and stabilized. This was likely due to a reduction of the hygroscopic response of the samples caused by a decrease in hydroxyl group concentration within the chemical structure of the wood (García Esteban *et al.*, 2005).

Both the storage and loss modulus values of the NT and SiO_2-treated samples decreased significantly as a result of the aging process, with the storage modulus exhibiting a more pronounced decrease. The storage modulus values of the SiO_2-treated samples were also found to decrease at a slower rate than the NT samples, indicating that the accelerated aging process may have had a more detrimental effect on the storage modulus of the NT samples. The SiO_2-treated samples exhibited high damping values, but the treatment process was also found to have a detrimental effect on the storage modulus of the SiO_2-treated samples due to alkaline hydrolysis. Additionally, TGA results showed that SiO_2-treated samples exhibited lower peak cellulose degradation temperatures as a further result of the degradation caused by alkaline hydrolysis during treatment. However, the agglomeration of the SiO_2 colloid on the extremities of the wood surface caused the treated samples to become less susceptible to cellulose hydrolysis during aging. Therefore, the SiO_2-treated samples also demonstrated a lower cellulose degradation rate over time.

It can be concluded that the nano-SiO_2 vacuum treatment process had a positive effect on the water uptake and rate of cellulose degradation of the treated samples when subjected to accelerated hydrolytic aging. Additionally, the stability of the SiO_2-treated samples indicates they may be able to withstand the effects of high-temperature, high-humidity conditions for a longer period of time without being compromised. The significant effect of the XRD results on multiple aspects of this study offers new insights for future research endeavours. During future experiments, it is recommended that the samples should be subjected to a month-long crystallization process at 80% relative humidity and 90°C to maximize the crystallinity before starting the impregnation process. This step will help to ensure that the crystallinity remains constant throughout the study and can be excluded from other analytical considerations.

3.6 References

Auvinen, H. (2020, July 7). *Powder Wettability - how to measure wettability of powders?*, Biolin Scientific https://www.biolinscientific.com/blog/powder-wettability-how-to-measure-wettability-of-powders

Benedetti, L., Brulé, B., Decreamer, N., Evans, K. E., & Ghita, O. (2019). Shrinkage behaviour of semi-crystalline polymers in laser sintering: PEKK and PA12. *Materials & Design*, 181, 107906. https://doi.org/10.1016/j.matdes.2019.107906

Bhuiyan, Md. T. R., Hirai, N., & Sobue, N. (2000). Changes of crystallinity in wood cellulose by heat treatment under dried and moist conditions. *Journal of Wood Science*, 46(6), 431–436. https://doi.org/10.1007/BF00765800

Bobleter, O. (1994). Hydrothermal degradation of polymers derived from plants. *Progress in Polymer Science*, *19*(5), 797–841. https://doi.org/10.1016/0079-6700(94)90033-7

Churkina, G., Organschi, A., Reyer, C. P. O., Ruff, A., Vinke, K., Liu, Z., Reck, B. K., Graedel, T. E., & Schellnhuber, H. J. (2020). Buildings as a global carbon sink. *Nature Sustainability*, 3(4), 269–276. https://doi.org/10.1038/s41893-019-0462-4

Clausen, C. (2012). Enhancing durability of wood-based composites with nanotechnology. U.S. Department of Agriculture, Forest Service, Forest Products Laboratory. https://doi.org/10.2737/FPL-GTR-218

Curling, S. (2017). Test methods for bio-based building materials. In Jones, D. and Brischke, C. (Eds.), *Performance of bio-based Building Materials* (pp. 385–481). essay, Elsevier Science & Technology. https://doi.org/10.1016/C2015-0-04364-7

García Esteban, L., Gril, J., De Palacios De Palacios, P., & Guindeo Casasús, A. (2005). Reduction of wood hygroscopicity and associated dimensional response by repeated humidity cycles. *Annals of Forest Science*, 62(3), 275–284. https://doi.org/10.1051/forest:2005020

Geffert, A., Geffertova, J., & Dudiak, M. (2019). Direct Method of Measuring the pH Value of Wood. *Forests*, 10(10), 852. https://doi.org/10.3390/f10100852

Glass S. V., & Zelinka, S. L. (2010). Chapter 4: Moisture Relations and Physical Properties of Wood. In R. J. Ross (Ed.), *Wood handbook: wood as an engineering material* (Centennial Edition, pp. 4.1–4.19). U.S. Dept. of Agriculture, Forest Service, Forest Products Laboratory. https://www.fpl.fs.usda.gov/documnts/fplgtr/fplgtr190/chapter_04.pdf.

Gleichmann, N. (2020). *SEM vs TEM*. Technology Networks - Analysis & Separations. https://www.technologynetworks.com/analysis/articles/sem-vs-tem-331262

Government of Canada. (2021, June 16). *Coal tars*. Canada.ca. https://www.canada.ca/en/health-canada/services/chemicals-product-safety/coal-tars.html

Hansen, A. T. (1987). *Effects of wood shrinkage in buildings*. https://doi.org/10.4224/20325670

Jayamon, J., Charney, F., & Line, P. (2016). EVALUATION OF DAMPING IN WOOD-FRAME SHEAR WALL BUILDINGS. *World Conference on Timber Engineering*, Austria.

https://www.researchgate.net/publication/316283504_EVALUATION_OF_DAMPING_IN_WOOD-FRAME_SHEAR_WALL_BUILDINGS

Lemaire-Paul, M., Beuthe, C. A., Riahinezhad, M., & Foruzanmehr, M. (2022). The impact of vacuum pressure on the effectiveness of SiO_2 impregnation of Spruce Wood. *Wood Science and Technology*, *57*(1), 147–171. https://doi.org/10.1007/s00226-022-01448-0

Li, X., Tabil, L. G., & Panigrahi, S. (2007). Chemical Treatments of Natural Fiber for Use in Natural Fiber-Reinforced Composites: A Review. *Journal of Polymers and the Environment*, 15(1), 25–33. https://doi.org/10.1007/s10924-006-0042-3

Machová, D., Baar, J., Paschová, Z., Pařil, P., Křenková, J., & Kúdela, J. (2019). Color changes and accelerated ageing in oak wood treated with ammonia gas and iron nanoparticles. European Journal of Wood and Wood Products, 77(4), 705–716. https://doi.org/10.1007/s00107-019-01406-x

Mohomane, S. M., Motloung, S. V., Koao, L. F., & Motaung, T. E. (2021). Effect of silica on alkaline bagasse cellulose and softwood cellulose. Wood Research, 66(1), 85–94. https://doi.org/10.37763/wr.1336-4561/66.1.8594

Reeb, J. E. (2009). *Wood and Moisture Relationships, EM8600*. Oregon State University Extension Service. https://catalog.extension.oregonstate.edu/sites/catalog/files/project/pdf/em8600.pdf

Reiniati, I., Osman, N. B., Mc Donald, A. G., & Laborie, M.-P. (2015). Linear viscoelasticity of hot-pressed hybrid poplar relates to densification and to the in situ molecular parameters of cellulose. *Annals of Forest Science,* 72(6), 693–703. https://doi.org/10.1007/s13595-014-0421-1

Reinprecht, L. (2016). Wood Deterioration, Protection and Maintenance (1st ed.). *Wiley*. https://doi.org/10.1002/9781119106500

Safarik, D., Elbrecht, J., & Miranda, W. (2022). State of Tall Timber 2022. CTBUH Journal, (2022 Issue I), 22–31. https://www.ctbuh.org/mass-timber-data

Shier, R. (2004). Statistics: 1.1 *Paired t-tests*. Mathematics Learning Support Centre. https://www.statstutor.ac.uk/resources/uploaded/paired-t-test.pdf.

Sigma-Aldrich. (2023a). *LUDOX® AS-40 colloidal silica*. https://www.sigmaaldrich.com/CA/en/product/aldrich/420840

Sigma-Aldrich. (2023b). *LUDOX® HS-40 colloidal silica*. https://www.sigmaaldrich.com/CA/en/product/aldrich/420816

Simpson, W. T. & Rosen, H. N. (1981). Equilibrium Moisture Content of Wood At High Temperatures. U.S. Dept. of Agriculture, Forest Service, Forest Products Laboratory. *Wood and Fiber*, 13(3), 150–158. https://wfs.swst.org/index.php/wfs/article/view/953.

Stangroom, J. (2018). *P Value from T Score Calculator*. https://www.socscistatistics.com/pvalues/tdistribution.aspx

StatsDirect Limited. (2016). *Unpaired (two sample) T test*. https://www.statsdirect.co.uk/help/parametric_methods/utt.htm

Tarmian, A., & Mastouri, A. (2019). Changes in moisture exclusion efficiency and crystallinity of thermally modified wood with aging. *iForest - Biogeosciences and Forestry*, 12(1), 92–97. https://doi.org/10.3832/ifor2723-011

Toba, K., Yamamoto, H., & Yoshida, M. (2013). Crystallization of cellulose microfibrils in wood cell wall by repeated dry-and-wet treatment, using X-ray diffraction technique. Cellulose, 20(2), 633–643. https://doi.org/10.1007/s10570-012-9853-7

Van Loon, L. R., & Glaus, M. A. (1997). Review of the kinetics of alkaline degradation of cellulose in view of its relevance for safety assessment of radioactive waste repositories. *Journal of Environmental Polymer Degradation*, 5(2), 97–109. https://doi.org/10.1007/BF02763593

Walker, J. C. F., Butterfield, B. G., Harris, J. M., Langrish, T. A. G., & Uprichard, J. M. (1993). Primary Wood Processing: Principles and practice. *Springer Netherlands*. https://doi.org/10.1007/978-94-015-8110-3

Welch, B. L. (1947). The generalization of 'student's' problem when several different population varlances are involved. *Biometrika*, 34(1–2), 28–35. https://doi.org/10.1093/biomet/34.1-2.28

WorldData.info. (2023). Climate: Ontario in Canada. https://www.worlddata.info/america/canada/climate-ontario.php

Yamamoto, H., Sakagami, H., Kijidani, Y., & Matsumura, J. (2013). Dependence of Microcrack Behavior in Wood on Moisture Content during Drying. *Advances in Materials Science and Engineering*, 2013, 1–7. https://doi.org/10.1155/2013/802639

Yona, A. M. C., Žigon, J., Matjaž, P., & Petrič, M. (2021). Potentials of silicate-based formulations for wood protection and improvement of mechanical properties: A review. *Wood Science and Technology*, 55(4), 887–918. https://doi.org/10.1007/s00226-021-01290-w

Yu, Y., & Wu, H. (2010). Significant Differences in the Hydrolysis Behavior of Amorphous and Crystalline Portions within Microcrystalline Cellulose in Hot-Compressed Water. *Industrial & Engineering Chemistry Research*, 49(8), 3902–3909. https://doi.org/10.1021/ie901925g

Zeniya, N., Obataya, E., Endo-Ujiie, K., & Matsuo-Ueda, M. (2019). Application of time–temperature–humidity superposition to the mass loss of wood through hygrothermally accelerated ageing at 95–140 °C and different relative humidity levels. *SN Applied Sciences*, 1(1), 3. https://doi.org/10.1007/s42452-018-0009-8

Zhan, T., Jiang, J., Lu, J., Zhang, Y., & Chang, J. (2018). Influence of hygrothermal condition on dynamic viscoelasticity of Chinese fir (Cunninghamia lanceolata). Part 2: Moisture desorption. Holzforschung, 72(7), 579–588. https://doi.org/10.1515/hf-2017-0130

Zou, X., Gurnagul, N., Uesaka, T., & Bouchard, J. (1994). Accelerated aging of papers of pure cellulose: Mechanism of cellulose degradation and paper embrittlement. *Polymer Degradation and Stability*, 43(3), 393–402. https://doi.org/10.1016/0141-3910(94)90011-6

Žlahtič, M., & Humar, M. (2016). Influence of Artificial and Natural Weathering on the Hydrophobicity and Surface Properties of Wood. *BioResources*, 11(2), 4964–4989. https://doi.org/10.15376/biores.11.2.4964-4989

Chapter 4

4.0 Effects of freeze-thaw cycling on the performance of nanosilica (SiO_2)-treated spruce wood

4.1 Abstract

This research builds upon previous research into the behaviour of spruce wood samples impregnated with a nanoparticle colloid when subjected to accelerated aging. For this study, white spruce wood samples were impregnated with a nano-SiO_2 colloid at a gauge pressure of -90 kPa. Both the SiO_2-treated samples and a set of non-treated samples were placed in a freeze-thaw cycling chamber that performed 6 cycles per day from 25°C to -18°C and back. The samples were taken out of the chamber for characterization every 100 cycles, and the test series was ended at 300 cycles. The characterization methods used for this project included powder X-Ray diffraction, dynamic mechanical analysis, tensiometry, and thermogravimetric analysis. The results of this analysis demonstrated that despite the well-known detrimental effects of the treatment process on the wood cell structure, the SiO_2-treated samples demonstrated a reduction in water uptake, an increase and stabilization in crystallinity at 0 cycles and after 100 cycles respectively, and an increase in cellulose degradation temperature.

Keywords: Spruce Wood, Wood Treatment, Accelerated Aging, Freeze-Thaw Aging, Silica Nanoparticles, Vacuum Impregnation, Viscoelastic Properties, Water Uptake, Thermal Degradation, True Density, Modulus of Rupture, XRD.

4.2 Introduction

Wood remains an attractive option for applications such as cladding and siding, and requires regular upkeep in the form of preservative application to prevent biological attack and maintain a visually appealing appearance (Wiedehopf Building Façade Systems, 2022). However, the colder climate of Canada also poses an additional risk to wood structures. When considering the use of wood as a construction material for elements such as siding and cladding in Canada, wood preservation methods must not only be considered for common risk factors such as decay and flammability, but also the effects of freezing during the winter and of frequent freezing and thawing periods during the transitional period from fall to winter and from winter to spring. Extensive studies have been conducted to determine the effects of freeze-thaw cycling on

the properties of wood. These studies have proven that the freeze-thaw cycling process can be detrimental to wood properties such as the ultimate bearing capacity (He *et al.*, 2020), mechanical properties (Szmutku *et al.*, 2013), and hardness (Campean *et al.*, 2008).

Due to the hydrophilic nature of the material, wood typically requires treatment to prevent swelling, decay, and other detrimental effects when used for exterior applications. Traditional wood treatment methods include coatings and varnishes. However, because the vast majority of these preservative coatings are hydrophobic, an interfacial incompatibility between the coating and wood arises (Li *et al.*, 2007) and in the long term, water will be able to infiltrate the spaces between the wood and the coating. The use of nanoparticle impregnation as a treatment method has risen to prominence as an alternative method of wood treatment. Nanoparticle impregnation can provide considerable benefits over traditional treatment methods since the vacuum pressure applied during the impregnation process allows the chosen solution or colloid to infiltrate the vascular system of wood. In particular, the impregnation of a nano-SiO_2 colloid can simultaneously improve the mechanical properties and reduce the water uptake capacity of wood (Lemaire-Paul *et al.*, 2022).

As highlighted by Blanchet & Pepin (2021), the lack of research on the effects of freeze-thaw cycling on wood treated with both traditional methods and nanoparticle impregnation represents a knowledge gap that has yet to be addressed. One study of note was performed by Zhao *et al.* (2022) on the effects of freeze-thaw cycling on wood coated with a superhydrophobic coating synthesized from perfluorinated chained silica nanoparticles and polystyrene microspheres in distilled water. Zhao *et al.* (2022) found that samples coated with this solution retained excellent hydrophobicity and self-healing properties.

In the previous study presented in Chapter 3, it was determined that the impregnation of SiO_2 nanoparticles had a beneficial effect on the properties of spruce wood under high temperature and high humidity conditions. This chapter aims to bridge a gap in the knowledge by investigating the effects of freeze-thaw cycling on the properties of spruce wood vacuum-treated with a nano-SiO_2 colloid to determine whether this treatment method remains just as effective under a temperature cycle ranging from low to ambient conditions.

4.3 Materials and Methods

4.3.1 Sample Preparation

Picea glauca (white spruce) wood samples were cut along the longitudinal axis to expose the tangential-radial plane of the wood structure and sanded with 150 grit sandpaper to obtain a consistently smooth and level surface for all samples. The samples were dried at the conventional drying temperature of 103°C for 24 hours (Curling, 2017) before beginning the vacuum-induced impregnation process.

The samples were placed into a Buehler Cast N' Vac 1000 vacuum chamber and a pressure of -90 kPa was applied and maintained for ten minutes to remove as much air as possible from the vascular system of the wood. This pressure was found to be the optimal impregnation pressure by Lemaire-Paul *et al.* (2022). The samples were then submerged in a nano-SiO_2 colloid while under vacuum, and the chamber was subsequently pressurized to atmospheric pressure to allow the colloid to infiltrate and agglomerate within the vascular system of the wood. The Sigma-Aldrich LUDOX AS-40 colloid was used for this experiment. This colloid consists of a 40 wt. % suspension of silica in H_2O with a particle size of 20-24 nm, an aqueous density of 1.3 g/cm^3 at 25°C, and a pH of 9.1 (Sigma-Aldrich, 2023). The samples were then placed in an oven for one hour at 50°C, followed by 103°C for ten minutes to promote the continued agglomeration of the colloid within the wood cell structure. However, as shown by the micrographs in Section 3.4.1 and the results of the ATR-FTIR tests in Appendix C, the colloid was unable to infiltrate the lumens of the wood and instead agglomerated to form a protective layer on the longitudinal and tangential-radial planes of the samples.

Due to the presence of hydroxyl groups in the chemical structure of wood, the material is highly susceptible to cellulose hydrolysis under exposure to water and alkaline conditions. In order to combat the detrimental effects of alkaline attack on the samples, a repeated secondary vacuum cycle using distilled water was implemented after the preliminary drying cycle had been completed. For this procedure, the samples were again placed into the vacuum chamber under -90 kPa for ten minutes. The samples were then submerged in the distilled water and subjected to three 10-minute pressurizations cycles from -90 kPa to atmospheric pressure to "flush" the wood vascular system and mitigate the detrimental effects of the colloid alkalinity on the wood. After the three-cycle washing process was completed, the samples were once again dried at 103°C for 24 hours. This washing procedure was introduced after a 1-month preliminary testing process determined that the peak cellulose degradation temperatures of unwashed samples were significantly lower than those found for washed samples. The results of these tests are presented in Appendix A.

4.3.2 Accelerated Aging Conditions

Bound water in wood does not freeze even when subjected to a maximum of -70°C (Engelund *et al.*, 2012). However, free water does freeze and is known to be dependent on the moisture content (MC) of wood. This was demonstrated by Klement *et al.* (2021), who found that wood with an average MC of 35% froze fully at -13.2°C, whereas wood with an average MC of 81% froze at -20°C.

For the experiment performed in the current study, a Tenney C-EVO C30 temperature humidity chamber was set to cycle from 25°C to -18°C and back at a rate of 6 cycles per day. These conditions were chosen based on the literature to ensure that all of the free water absorbed by the wood during the thawing portion of the cycle would also freeze during the freezing portion of the cycle. The RH within the chamber was uncontrolled and fluctuated between 55% RH at -18°C and 10% RH at 25°C. This property remained uncontrolled in order to reflect typical outdoor conditions.

Samples were subjected to a total of 300 cycles and removed for testing after every 100 cycles. A non-treated (NT) set of spruce wood samples was aged and tested alongside the SiO_2-treated samples to establish a baseline and determine the effects of the SiO_2 treatment by comparing the results. Samples used for non-destructive characterization tests were returned to the chamber for further aging after each testing interval.

4.3.3 Characterization

To reduce the potential effects that variations in moisture content may have on the readings, the samples were dried before and after each test at 103°C for 24 hours. The characterization methods used for this study include dynamic mechanical analysis (DMA), tensiometry, thermogravimetric analysis (TGA), and powder X-Ray Diffraction (XRD). Statistical analysis was applied to the data obtained from each characterization method.

4.3.3.1 Dynamic Mechanical Analysis

Dynamic Mechanical Analysis (DMA) was performed on NT and SiO_2-treated samples with dimensions of 25 × 10 × 1.8 mm using a TA Instruments Q800 DMA. The sample dimensions were measured at each testing interval before performing any tests. A temperature ramp of 5-40°C at a rate of 5°C/min and a frequency of 1 Hz was applied to measure the storage modulus, loss modulus, and damping of each sample using a 3-point bending clamp.

4.3.3.2 Tensiometry

Tensiometry was performed on SiO_2-treated and NT samples with dimensions of (7 × 2 × 1 mm). Tests were performed using an Attension Sigma 701 Force Tensiometer. The Washburn method for porous materials (Auvinen, 2020) was used to measure the water uptake of the samples. The samples were weighed and measured immediately after drying and before performing any tests. Samples were suspended by a sample holder clip and brought into contact with a small beaker of distilled water. The water was allowed to infiltrate the sample via the tangential-radial plane for ten minutes, during which mass uptake readings were taken by the apparatus at a rate of 0.2-0.4 seconds. These readings were manually converted to Weight % using:

$$Weight\ \% = 100 \times \frac{M_{test}}{M_{dry}} \quad (1)$$

Where M_{test} is the mass recorded by the apparatus throughout the test (in g), and M_{dry} is the mass of the sample after drying for 24 hours (in g).

This equation differs from the standard equation used to calculate Weight %:

$$Weight\ \% = 100 \times \frac{(M_{wet} - M_{dry})}{M_{dry}} \quad (2)$$

Where M_{wet} is the mass of the sample (in g) after the absorption of water.

Equation (1) was used in this study as the tensiometer zeroes the balance the moment a sample comes into contact with the water. Therefore, the mass recorded by the instrument represents only the mass uptake of the samples, and the standard procedure of subtracting the dry mass from the wet mass in the numerator of Equation (2) was not required.

In order to mitigate the effect that small variations in sample length can have on the readings, these Weight % values were plotted as a function of $\sqrt{t}/L$, where t is the time elapsed and L is the length of the sample, as shown in Figure 25. Weight % readings at $\sqrt{t}/L = 3$ were taken when forming an average to easily compare the weight uptake of different samples.

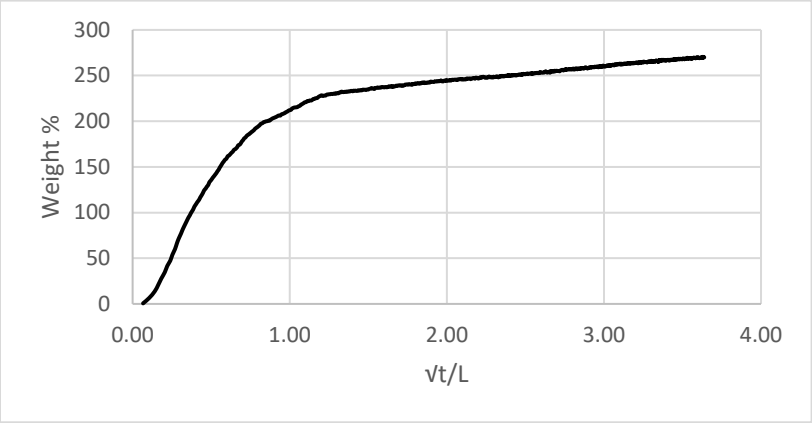

Figure 25. A typical water uptake graph

4.3.3.3 Thermogravimetric Analysis

Changes in weight were recorded over time in the form of derivative weight readings, expressed as the first derivative of Weight % with respect to temperature. Due to the high temperatures employed by this method, these tests could be performed immediately after removing the samples from the chamber and did not first require a 24-hour drying cycle.

Thermogravimetric analysis was performed on SiO_2-treated and NT samples with dimensions of 7 × 2 × 1 mm. Tests were performed using a TA Instruments Q600 SDT. Samples were subjected to a temperature ramp of 20-500°C at a rate of 10°C/min, while changes in weight were recorded over time in the form of derivative weight readings. These readings are expressed as the first derivative of Weight % with respect to temperature.

4.3.3.4 X-Ray Diffraction

The crystallinity index of NT and SiO_2-treated samples was determined using powder X-Ray Diffraction (XRD). A Bruker D8 Endeavor with a LinxEye XE-T 1-D silicon strip detector were used to take these measurements. A copper K-alpha beam frequency was used to create diffractograms such as the one pictured in Figure 26, with intensity plotted as a function of 2θ (the exit angle of the beam). Since intensity is a factor that can vary depending on the properties of the sample tested, the intensity of different samples cannot be compared if a control graph is unable to be established. In these situations, the crystallinity index is primarily used to compare the crystallinity of different samples.

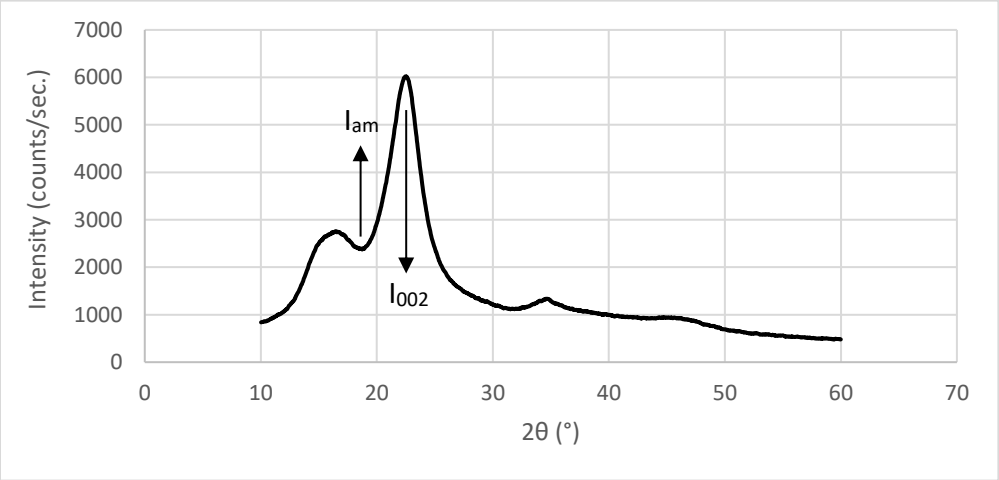

Figure 26. A typical XRD diffractogram

The crystallinity index of each sample was determined using the following equation (Segal *et al.*, 1959):

$$CrI = \left(1 - \left(\frac{I_{am}}{I_{002}}\right)\right) \times 100 \qquad (10)$$

Where CrI is the crystallinity index, I_{am} is the intensity of the amorphous valley, and I_{002} is the intensity of the crystalline peak. An example of the points on an XRD diffractogram where these variables can be identified is shown in Figure 26.

4.3.3.5 Statistical Analysis

Two different types of statistical analysis were applied to the results of this study: Welch's T-test and the paired Student's T-test. All samples were considered to be independent for both types of analysis.

Welch's T-test (Welch, 1947) was applied for both destructive and non-destructive characterization tests to determine the significance of the experimental results when comparing the SiO_2-treated samples to the NT samples at each testing interval. It was also used to compare individual differences in both types of samples at each testing interval exclusively for destructive tests, since the samples tested were not the same throughout the process. This test was chosen to account for the possibility of unequal variances. Welch's T-test is defined using the following equations (StatsDirect Limited, 2016).

The T-score was calculated using:

$$t = \frac{\bar{x}_1 - \bar{x}_2}{\sqrt{\frac{s_1^2}{n_1} + \frac{s_2^2}{n_2}}} \tag{11}$$

where *t* is the T-score, $\bar{x}_1$ and $\bar{x}_2$ are the sample means, s_1 and s_2 are sample standard deviations, and n_1 and n_2 are the sample sizes.

The sample standard deviations were calculated using:

$$s_j^2 = \frac{\sum_{i=1}^{n_j}(x_i - \bar{x}_j)^2}{n_j - 1} \tag{12}$$

where *j* represents either the number 1 or 2 depending on the sample.

The number of degrees of freedom, *df*, was calculated using:

$$df = \frac{\left[\frac{s_1^2}{n_1} + \frac{s_2^2}{n_2}\right]^2}{\frac{\left(\frac{s_1^2}{n_1}\right)^2}{n_1 - 1} + \frac{\left(\frac{s_2^2}{n_2}\right)^2}{n_2 - 2}} \tag{13}$$

The paired Student's T-test was applied to determine the significance of the differences in both NT and SiO_2-treated sample results from one testing interval to the next, but only for non-destructive tests where the samples remained the same throughout the testing period. This test was chosen since it applies exclusively to the same set of samples compared before and after testing (Shier, 2004). The paired Student's T-test is defined using the following equations (Shier, 2004).

The T-score was calculated using:

$$t = \frac{\bar{d}}{SE(\bar{d})} \tag{14}$$

Where *t* is the T-score, $\bar{d}$ is the mean difference, and $SE(\bar{d})$ is the standard error of the mean difference.

The standard error of the mean differences was calculated using:

$$SE(\bar{d}) = \frac{s_d}{\sqrt{n}} \tag{15}$$

Where s_d is the sample standard deviation of the differences and *n* is the number of samples.

The number of degrees of freedom, *df*, was calculated using:

$$df = n - 1 \tag{16}$$

For both types of tests, the corresponding P-value was calculated using the *P Value from T Score Calculator* provided online by Stangroom (2023). A significance level of 0.05, or 95% confidence interval was used. Thus, if the P-value was found to be smaller than 0.05, the result was considered to be significant.

4.4 Results and Discussion

Characterization tests for samples subjected to freeze-thaw cycling in an environmental chamber were performed at 0 cycles (control) and after 100 cycles, 200 cycles, and 300 cycles. DMA and tensiometry tests are considered to be non-destructive and the same samples were returned to the chamber after each testing interval. STA is a destructive test and different sets of samples were used at each interval. XRD is a non-destructive test and was performed on different samples picked from each testing interval after the aging process had been completed.

4.4.1 X-Ray Diffraction

The crystallinity index of four sets of samples was determined by performing powder XRD. Each set corresponded to a different testing interval (0/100/200/300 cycles) and was composed of an average of 10 NT and 10 SiO_2-treated samples. As shown in Figure 27 and Table 13, the SiO_2 treatment process increased the crystallinity of the unaged spruce wood samples, as shown by the statistically significant difference between the two types of samples at 0 cycles. This increase in crystallinity was caused by the degradation of the amorphous phase of the cellulose due to alkaline hydrolysis during the treatment process, as described by Van Loon & Glaus (1997) and elaborated upon in Section 3.4.2. At 100 cycles and beyond, the crystallinity index values of both the NT and SiO_2-treated samples remained relatively similar throughout the freeze-thaw cycling process, as the differences between the two types of samples at all aging intervals were found to be statistically insignificant as demonstrated in Table 13.

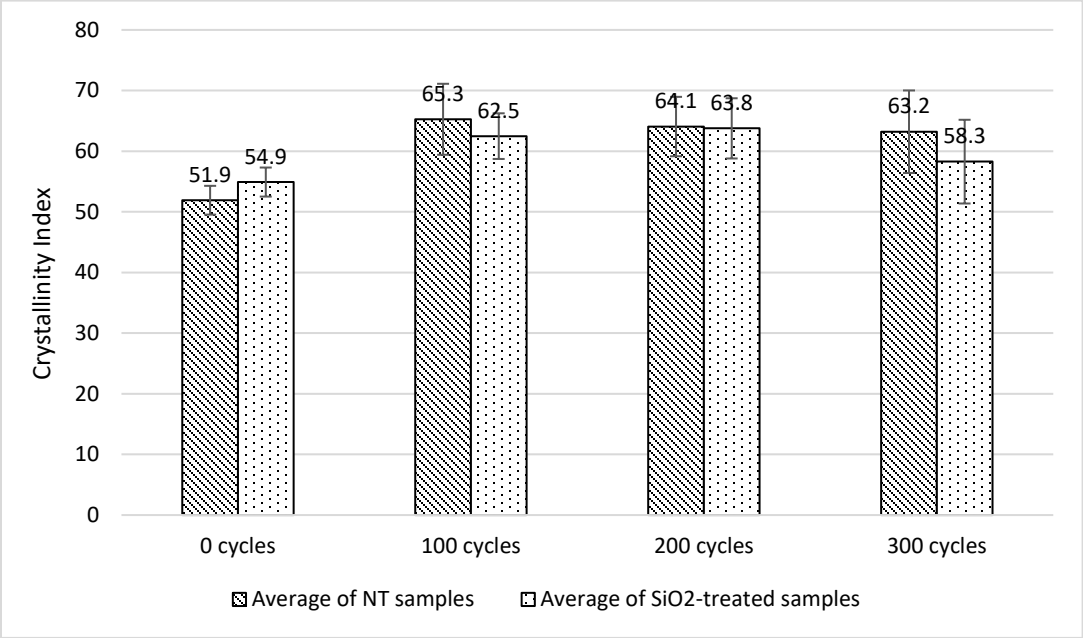

Figure 27. Crystallinity index of NT and SiO_2-treated samples at different freeze-thaw cycling intervals

As shown in Table 13, increases in crystallinity demonstrated by both the SiO_2-treated samples and the NT samples when aging from 0 cycles to 100 cycles were found to be statistically significant. This increase in crystallinity was likely caused by drying the samples at 103°C after they were removed from the chamber, since drying at high temperatures can trigger an increase in crystallinity (Tarmian & Mastouri, 2019). The crystallinity of both types of samples appeared to stabilize after 100 cycles as the differences between the crystallinity index values at 100-200 and 200-300 cycles were all found to be statistically insignificant. The data shown in Table 14 indicates an increase in the intensity of the crystalline and amorphous regions for both types of samples. The intensity of these regions appears to decrease again for both types of samples at 300 cycles. However, these apparent fluctuations were found to be statistically insignificant as shown in Table 15, likely due to the large standard deviation values shown in Figure 27. Additional testing with a larger sample size would be required to determine whether this behaviour may be an indicator of an underlying mechanism related to the freeze-thaw aging conditions.

It is possible that the 55% RH value detected during the freezing portions of the freeze-thaw cycling process may have also contributed to the initial increase in crystallinity at 100 cycles. Bhuiyan *et al.* (2000) found that the crystallinity of wood may also increase under high-humidity conditions, however this study was performed in conjunction with high-temperature conditions and the effects of high RH values on wood subjected to low-temperature conditions have yet to be studied. Therefore, examining the effects of high-

humidity, low-temperature aging represents a potential avenue of research for future studies on the behaviour of both NT and nanoparticle-treated spruce wood.

Table 12. Statistical analysis for crystallinity index values of NT and SiO_2-treated samples at different freeze-thaw cycling intervals

Comparison Type	Aging Period	T-score	P-value	Result
NT samples	0 to 100 cycles	-6.250	<< .05	Significant
	0 to 200 cycles	-6.557	<< .05	Significant
	0 to 300 cycles	-4.656	<< .05	Significant
	100 to 200 cycles	0.474	> .05	Not Significant
	200 to 300 cycles	0.306	> .05	Not Significant
SiO_2-treated samples	0 to 100 cycles	-4.624	<< .05	Significant
	0 to 200 cycles	-4.440	<< .05	Significant
	0 to 300 cycles	-1.291	> .05	Not Significant
	100 to 200 cycles	-0.584	> .05	Not Significant
	200 to 300 cycles	1.836	> .05	Not Significant
NT vs SiO_2-treated samples	0 cycles	-2.279	<< .05	Significant
	100 cycles	1.182	> .05	Not Significant
	200 cycles	0.125	> .05	Not Significant
	300 cycles	1.489	> .05	Not Significant

Table 13. Average crystalline and amorphous peak values of NT and SiO_2-treated samples at different freeze-thaw cycling intervals

Sample Type	Peak	0 cycles	100 cycles	200 cycles	300 cycles
NT samples	I_{am}	4690.61	4088.71	4508.00	3494.07
	I_{002}	9428.74	11860.93	13558.92	10002.81
SiO_2-treated samples	I_{am}	1732.35	1504.64	2099.84	1692.94
	I_{002}	3846.015	4190.60	6033.26	4226.50

Table 14. Statistical analysis for crystalline and amorphous peak values of NT and SiO_2-treated samples at different freeze-thaw cycling intervals

		I_{am}			I_{002}		
Comparison Type	**Aging Period**	**T-score**	**P-value**	**Result**	**T-score**	**P-value**	**Result**
NT samples	0 to 100 cycles	2.241	<< .05	Significant	-2.296	<< .05	Significant
	0 to 200 cycles	0.622	> .05	Not Sig.	-3.495	<< .05	Significant
	0 to 300 cycles	2.479	<< .05	Significant	-0.339	> .05	Not Sig.
	100 to 200 cycles	-1.219	> .05	Not Sig.	-1.254	> .05	Not Sig.
	200 to 300 cycles	1.919	> .05	Not Sig.	1.879	> .05	Not Sig.
SiO_2-treated samples	0 to 100 cycles	1.376	> .05	Not Sig.	-0.611	> .05	Not Sig.
	0 to 200 cycles	-1.252	> .05	Not Sig.	-2.548	<< .05	Significant
	0 to 300 cycles	0.262	> .05	Not Sig.	-0.780	> .05	Not Sig.
	100 to 200 cycles	-1.849	> .05	Not Sig.	-1.884	> .05	Not Sig.
	200 to 300 cycles	1.294	> .05	Not Sig.	1.929	> .05	Not Sig.

4.4.2 Tensiometry

Water uptake measurements were performed on 10 SiO_2-treated samples and 10 NT samples. These measurements were taken at regular intervals during the freeze-thaw cycling process. The tensiometry results of the freeze-thaw cycled samples shown in Figure 28 demonstrate that the SiO_2-treated samples showed a higher degree of stabilization than the NT samples, since the standard deviation values of the NT samples were higher. The statistical analysis shown in Table 15 indicates that the differences from 0 to 100/200/300 cycles for the NT samples were statistically significant, whereas they were found to be insignificant for the SiO_2-treated samples. This is reflected by the large fluctuations in water uptake for the NT samples and the stability of the SiO_2-treated samples exhibited in Figure 28. Additionally, the differences between NT and SiO_2-treated water uptake readings at 100 cycles and 300 cycles were found to be statistically insignificant.

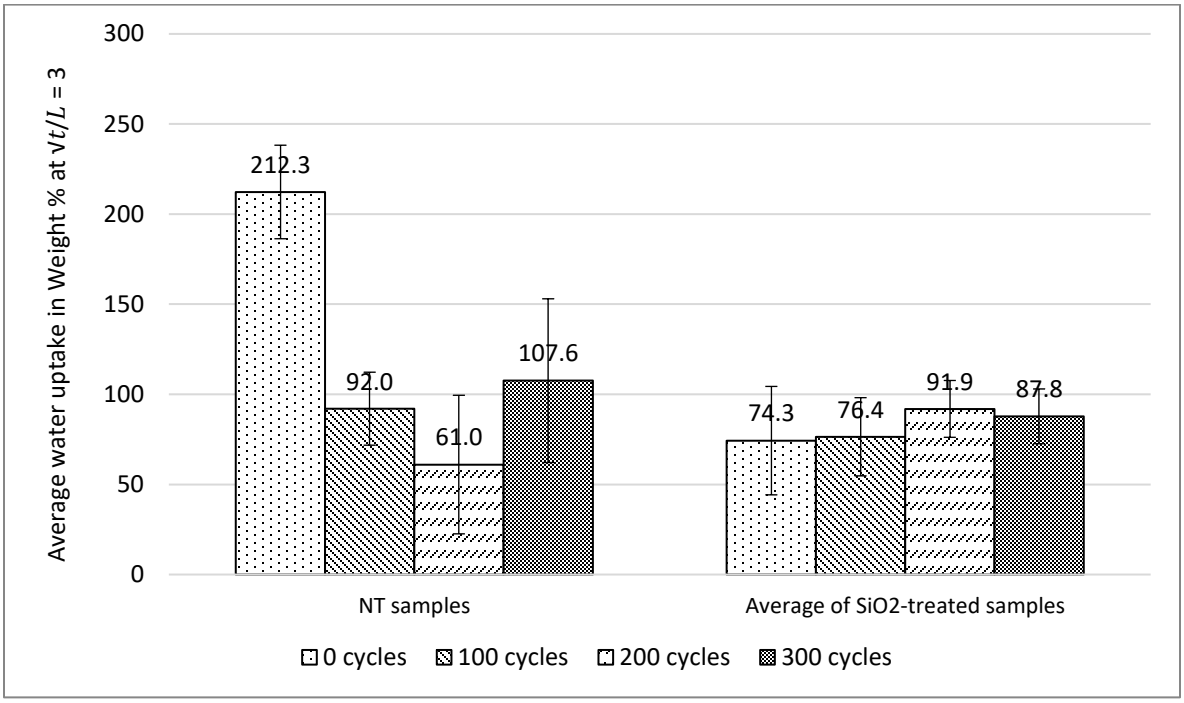

Figure 28. Average water uptake of freeze-thaw cycled NT and SiO_2-treated samples

The fluctuation of the RH from 55% to 10% and back during the freeze-thaw cycling process may have caused the wood to shrink and swell over the course of each cycle, resulting in the formation of a hysteresis loop (Walker *et al.*, 1993) while the samples remained in the chamber. However, unlike the phenomenon exhibited by the hydrolytically aged samples in Section 3.4.3, the freeze-thaw aged samples did not experience an increase in water uptake at the first testing interval (100 cycles). Because the samples were removed from the freeze-thaw chamber at an RH of 10% (during the thaw portion of the cycle), they likely experienced less shrinkage than the hydrolytically aged samples when dried at 103°C. Therefore, it is possible that microcracks did not develop to the same extent in the freeze-thaw aged samples. However, this drying process still caused the samples to undergo compaction due to shrinkage, resulting in lower water uptake values for the NT samples at 100 cycles and 200 cycles. From 200 to 300 cycles, the NT samples exhibited a statistically significant increase in their water uptake capacity. The wood may have reached a point of fatigue and started degrading due to continuous freeze-thaw cycling and shrinkage/swelling. More testing would be required to determine whether this increase continues past 300 cycles.

The water uptake values of the SiO_2-treated samples remained stable throughout the aging process, likely due to the agglomeration of the colloid on the surface of the samples. The reduction of open lumens may have prevented the SiO_2-treated samples from adsorbing water when the RH inside the chamber increased to 55%, resulting in little to no change in water uptake values throughout the freeze-thaw cycling process.

Therefore, it can be concluded that the SiO_2 vacuum-treatment process represents an effective means of reducing and stabilizing the water uptake readings of wood over time when subjected to freeze-thaw cycling.

Table 15. Statistical analysis of the water uptake readings of freeze-thaw cycled NT and SiO_2-treated samples

Comparison Type	Aging Period	T-score	P-value	Result
NT samples	0 to 100 cycles	9.759	<< .05	Significant
	0 to 200 cycles	9.420	<< .05	Significant
	0 to 300 cycles	5.338	<< .05	Significant
	100 to 200 cycles	3.843	<< .05	Significant
	200 to 300 cycles	-3.851	<< .05	Significant
SiO_2-treated samples	0 to 100 cycles	-0.202	> .05	Not Significant
	0 to 200 cycles	-1.511	> .05	Not Significant
	0 to 300 cycles	-1.349	> .05	Not Significant
	100 to 200 cycles	-2.413	<< .05	Significant
	200 to 300 cycles	0.807	> .05	Not Significant
NT vs SiO_2-treated samples	0 cycles	10.418	<< .05	Significant
	100 cycles	1.577	> .05	Not Significant
	200 cycles	-2.230	<< .05	Significant
	300 cycles	1.241	> .05	Not Significant

4.4.3 Dynamic Mechanical Analysis

DMA tests were performed on sets of 10 SiO_2-treated samples and 10 NT samples. Each sample was subjected to a temperature sweep of 5-40°C at a constant frequency of 1 Hz at regular intervals during the freeze-thaw cycling process to study the effects of this aging method on the viscoelastic properties of each sample. In this study, the average storage modulus, loss modulus, and damping (tanδ) values recorded at a temperature of 25°C (ambient) were used to compare the two sets of samples. Values at 10°C (below ambient) and 35°C (above ambient) were also examined and yielded similar results to the ones described below for 25°C. The numerical results of this further analysis are listed in Appendix B.

Figures 29-31 show the results of the DMA testing performed on freeze-thaw cycled samples at regular intervals. The storage and loss moduli values of the SiO_2-treated samples were consistently lower than the NT samples, demonstrating that the alkaline attack that occurred during the SiO_2 treatment process had a detrimental effect on the viscoelastic properties of the samples (see Section 3.4.4). When comparing the

viscoelastic properties of the NT and SiO_2-treated samples, all differences were found to be statistically insignificant as shown in Table 17. However, the results found at 0 cycles for these samples do not reflect those found in Section 3.4.3, where the storage modulus values of the NT and SiO_2-treated samples were found to be significantly different at 0 months. This discrepancy can be attributed to the inherent variability in wood properties and the small sample size chosen for this experiment. This is demonstrated by the large standard deviation values found for both sample types at all aging conditions, as shown in Figures 29-31 and Table 18.

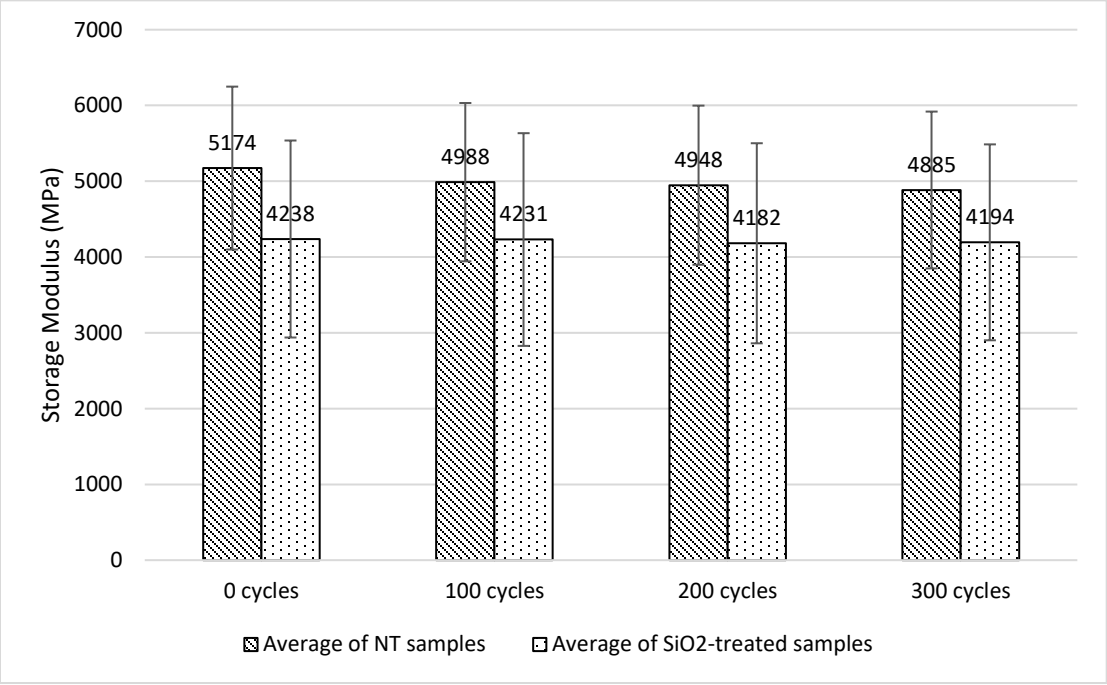

Figure 29. Average storage modulus of freeze-thaw cycled NT and SiO_2-treated samples at 25°C over time

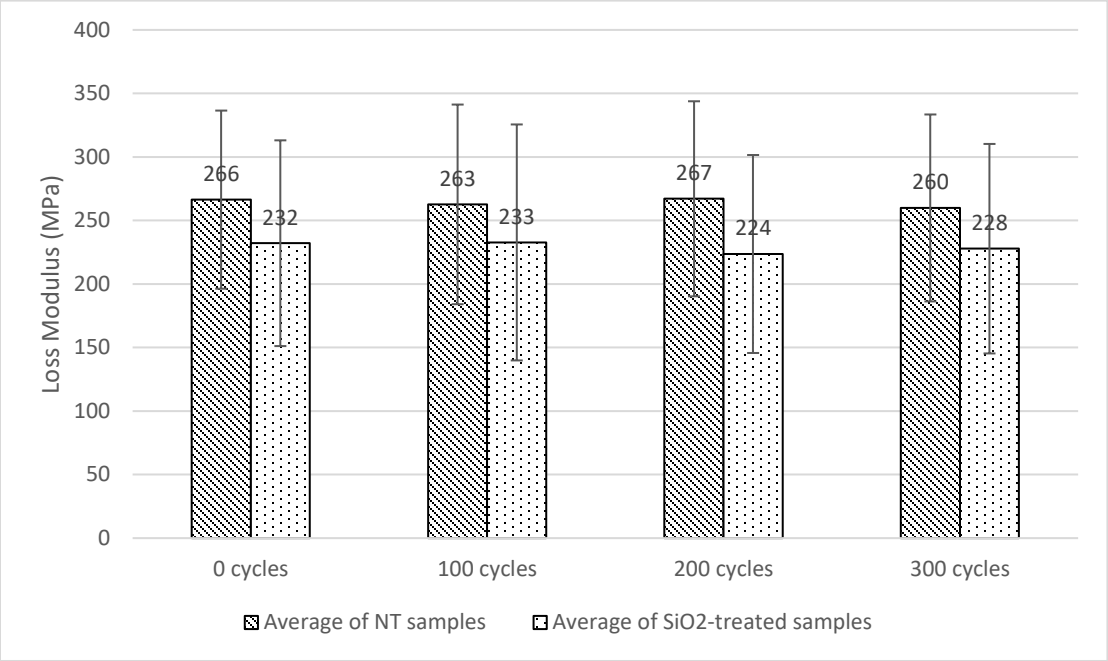

Figure 30. Average loss modulus of freeze-thaw cycled NT and SiO_2-treated samples at 25°C over time

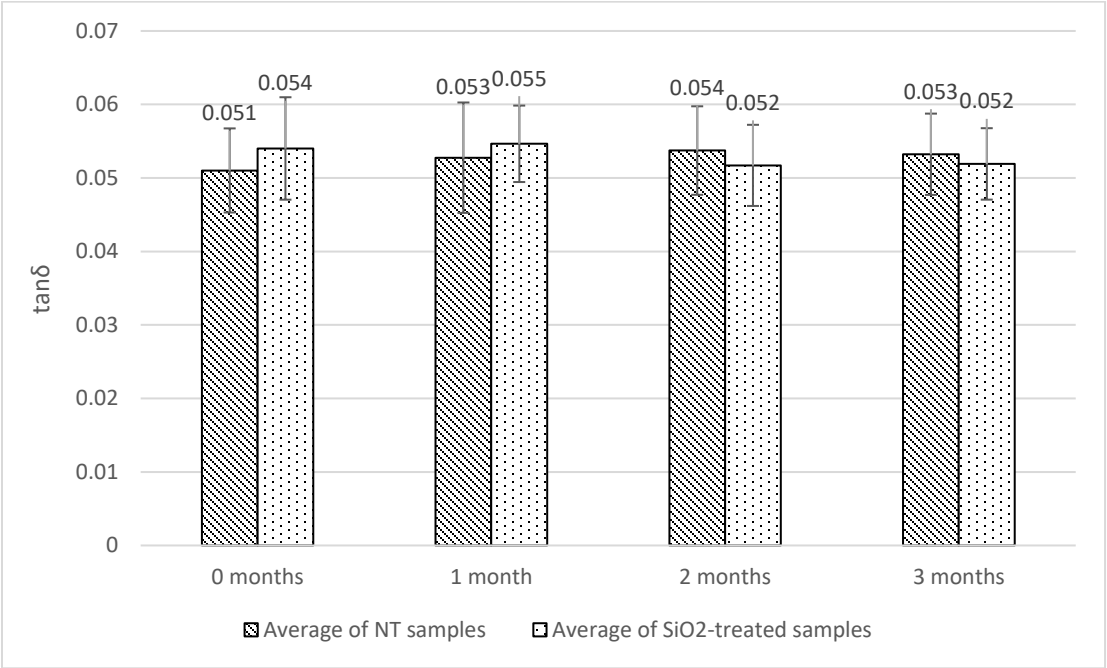

Figure 31. Average tanδ values of freeze-thaw cycled NT and SiO_2-treated samples at 25°C over time

Table 16 shows that when examining the behaviour of both sample types at each time interval, all results were found to be statistically insignificant with the exception of the storage modulus between 0 cycles and 100/200/300 cycles for the NT samples. It is possible that this significant decrease in storage modulus exhibited by the NT samples past 0 cycles may be attributed to a phenomenon described by Campean *et al.* (2008) that occurs exclusively when wood freezes. Free water within the lumens freezes and expands, compacting the wood cell walls and allowing the still-liquid bound water to pass into the lumens due to a pressure differential between the air vapour pressure and the bound water. The bound water will then act as free water and crystallize in the lumens. When the temperature rises above 0°C, both the free and bound water within the lumens will thaw and evaporate through capillary movement. This process would have led to the formation of microcracks (Campean *et al.*, 2008) and thus a decrease in the storage modulus of the NT samples. This effect may have been less pronounced for the SiO_2-treated samples since the agglomerated colloid formed a layer on the surface of the treated samples. This layer may have prevented the majority of the bound water from evaporating, causing a stabilization in the storage modulus of the SiO_2-treated samples since very little water entered or left the vascular system of the wood when compared to the NT samples.

However, the level of confidence for this hypothesis is not very high due to the high standard deviation values exhibited by the samples. For future experiments, increasing the number of samples tested would be necessary to reach a definitive conclusion on the viscoelastic behaviour of spruce wood samples under freeze-thaw cycling.

Table 16. Statistical analysis of the viscoelastic properties of freeze-thaw cycled NT and SiO_2-treated samples at 25°C

	NT Samples			SiO_2-treated samples		
Comparison Interval	**Statistical analysis of average values at 25°C**			**Statistical analysis of average values at 25°C**		
Storage Modulus	**T- score**	**P-value**	**Result**	**T- score**	**P-value**	**Result**
0 cycles vs 100 cycles	-2.798	<< .05	Sig.	-0.083	> .05	Not Sig.
0 cycles vs 200 cycles	-2.406	<< .05	Sig.	-0.524	> .05	Not Sig.
0 cycles vs 300 cycles	-4.313	<< .05	Sig.	-1.150	> .05	Not Sig.
100 cycles vs 200 cycles	-0.385	> .05	Not Sig.	-0.538	> .05	Not Sig.
200 cycles vs 300 cycles	-1.029	> .05	Not Sig.	0.745	> .05	Not Sig.
Loss Modulus	**T- score**	**P-value**	**Result**	**T- score**	**P-value**	**Result**
0 cycles vs 100 cycles	-0.725	> .05	Not Sig.	0.048	> .05	Not Sig.
0 cycles vs 200 cycles	0.147	> .05	Not Sig.	-0.732	> .05	Not Sig.
0 cycles vs 300 cycles	-1.128	> .05	Not Sig.	-0.959	> .05	Not Sig.
100 cycles vs 200 cycles	0.895	> .05	Not Sig.	-0.831	> .05	Not Sig.
200 cycles vs 300 cycles	-1.170	> .05	Not Sig.	1.892	> .05	Not Sig.
Tan delta	**T- score**	**P-value**	**Result**	**T- score**	**P-value**	**Result**
0 cycles vs 100 cycles	1.166	> .05	Not Sig.	-0.112	> .05	Not Sig.
0 cycles vs 200 cycles	2.798	<< .05	Sig.	-0.623	> .05	Not Sig.
0 cycles vs 300 cycles	1.513	> .05	Not Sig.	-0.357	> .05	Not Sig.
100 cycles vs 200 cycles	1.658	> .05	Not Sig.	-0.578	> .05	Not Sig.
200 cycles vs 300 cycles	-0.597	> .05	Not Sig.	1.174	> .05	Not Sig.

Table 17. Statistical analysis of the viscoelastic properties of NT samples when compared to SiO_2-treated samples at 25°C (freeze-thaw cycled)

Comparison Interval	Statistical analysis of average values at 25°C		
Storage Modulus	**T-score**	**P-value**	**Result**
0 cycles	1.754	> .05	Not Sig.
100 cycles	1.369	> .05	Not Sig.
200 cycles	1.438	> .05	Not Sig.
300 cycles	1.049	> .05	Not Sig.
Loss Modulus	**T-score**	**P-value**	**Result**
0 cycles	1.012	> .05	Not Sig.
100 cycles	0.779	> .05	Not Sig.
200 cycles	1.256	> .05	Not Sig.
300 cycles	0.632	> .05	Not Sig.
Tan delta	**T-score**	**P-value**	**Result**
0 cycles	-1.049	> .05	Not Sig.
100 cycles	-0.653	> .05	Not Sig.
200 cycles	0.782	> .05	Not Sig.
300 cycles	0.551	> .05	Not Sig.

Table 18. Average storage modulus, loss modulus, and tanδ values of freeze-thaw cycled NT and SiO_2-treated samples at 25°C

	NT Samples		SiO_2-treated samples	
Aging Intervals	**Average Storage Modulus at 25°C (MPa)**	**Standard Deviation**	**Average Storage Modulus at 25°C (MPa)**	**Standard Deviation**
0 cycles	5173.60	1075.08	4237.90	1299.76
100 cycles	4988.10	1044.64	4230.90	1403.54
% change	-3.59		-0.17	
0 cycles	5173.60	1075.08	4237.90	1299.76
200 cycles	4948.20	1049.86	4181.50	1320.01
% change	-4.36		-1.33	
0 cycles	5173.60	1075.08	4237.90	1299.76
300 cycles	4884.80	1034.43	4194.00	1292.48
% change	-5.58		-1.04	
Aging Intervals	**Average Loss Modulus at 25°C (MPa)**	**Standard Deviation**	**Average Loss Modulus at 25°C (MPa)**	**Standard Deviation**
0 cycles	266.41	70.10	232.13	80.96
100 cycles	262.69	78.57	232.73	92.87
% change	-1.40		0.26	
0 cycles	266.41	70.10	232.13	80.96
200 cycles	267.09	76.76	223.64	77.91
% change	0.26		-3.66	
0 cycles	266.41	70.10	232.13	80.96
300 cycles	259.88	73.57	227.81	82.44
% change	-2.45		-1.86	
Aging Intervals	**Average tanδ at 25°C (MPa)**	**Standard Deviation**	**Average tanδ at 25°C (MPa)**	**Standard Deviation**
0 cycles	0.05102	0.00572	0.05401	0.00697
100 cycles	0.05276	0.00751	0.05465	0.00520
% change	3.41		1.18	
0 cycles	0.05102	0.00572	0.05401	0.00697
200 cycles	0.05373	0.00602	0.05171	0.00552
% change	5.31		-4.26	
0 cycles	0.05102	0.00572	0.05401	0.00697
300 cycles	0.05323	0.00553	0.05191	0.00486
% change	4.33		-3.89	

4.4.4 Thermogravimetric Analysis

An average of 2-5 SiO_2-treated samples and 2-5 NT samples were subjected to TGA at each testing interval during the freeze-thaw cycling process. Like the samples that were subjected to accelerated aging, the peak cellulose degradation temperatures of both types of samples were found to be between 350-370°C as shown in Figure 32. TGA results for the freeze-thaw cycled samples show the peak cellulose degradation temperature of the SiO_2-treated samples remained significantly lower than that of the NT samples over a period of 300 freeze-thaw cycles, as shown in Figure 33 and Table 19. This reflects the trend described in Section 3.4.3 and shows the negative effects the vacuum-induced impregnation process had on the thermal stability of the SiO_2-treated samples.

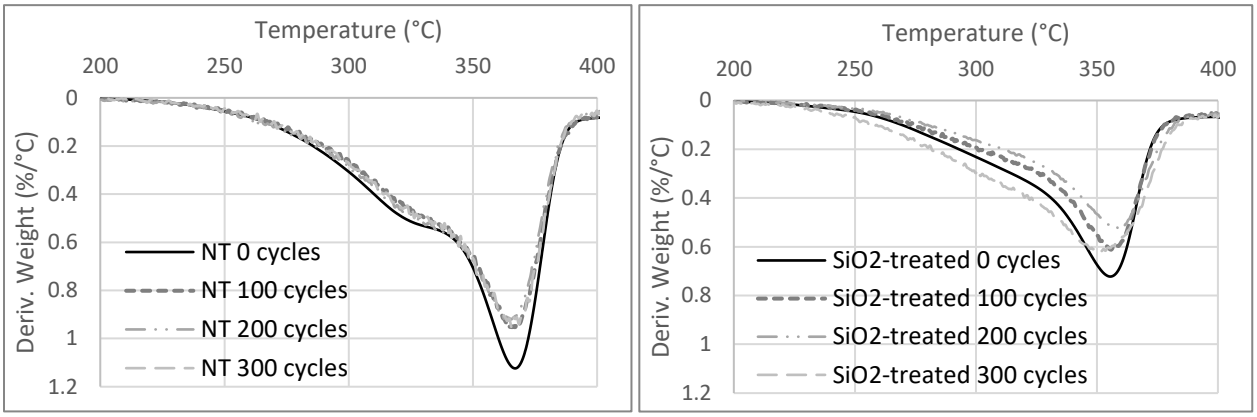

Figure 32. DTG curves of freeze-thaw cycled NT and SiO_2-treated samples at different aging intervals

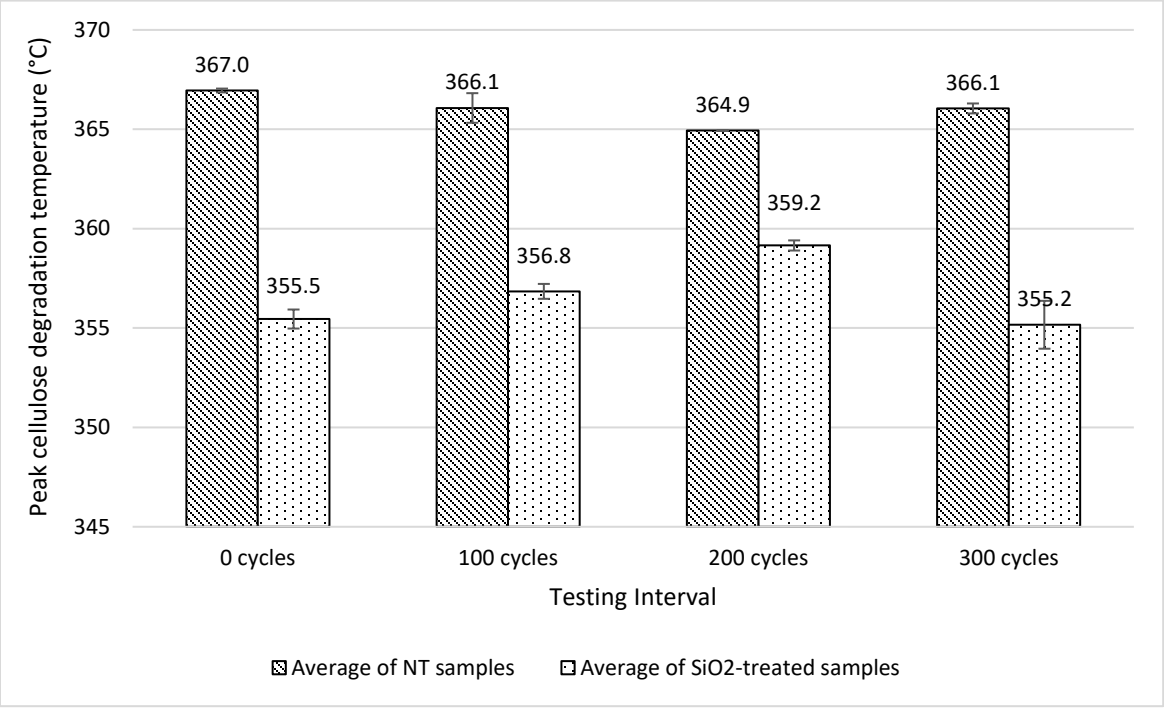

Figure 33. Peak cellulose degradation temperature for NT and SiO_2-treated samples at different freeze-thaw cycling intervals

The SiO_2-treated samples demonstrated a significant increase in peak cellulose degradation temperature while the NT samples appeared to remain stable between 0-200 cycles. This may be due to the increase and stabilization of the crystallinity exhibited by the SiO_2-treated samples between 100-200 cycles, since an increase in crystallinity will result in an increase in the thermal stability of cellulose (Halpern & Patai, 1969). Results at 200 cycles were found to be statistically significant for both types of samples when compared to results at 0 cycles, as shown in Table 19. However, they were found to be statistically insignificant at 100 cycles for the NT samples when compared to 0 cycles, which shows that the freeze-thaw cycling process had no effect on the NT samples after 100 cycles.

Results were also found to be statistically insignificant from 0 to 300 cycles and from 200 to 300 cycles for the SiO_2-treated samples. This is further reinforced by the large standard deviation found at 300 cycles for the SiO_2-treated samples as demonstrated in Figure 33. Therefore, further testing would be required in order to reach a definitive conclusion on the effects of the cycling process on the SiO_2-treated samples at 300 cycles. The compaction effect described in Section 4.4.2 may have contributed to the significant decrease in cellulose degradation temperature from 200 to 300 cycles for the NT samples, as the loss of bound water over the freeze-thaw cycling period would help accelerate the pyrolysis of the samples (Winandy *et al*.,

2022). This effect would not have been as pronounced for the SiO_2-treated samples due to the agglomeration of the nano-SiO_2 colloid on the surface of the wood preventing the evaporation of bound water.

Table 19. Statistical analysis for differences in peak cellulose degradation temperature of freeze-thaw cycled TGA samples

Comparison Type	Aging Period	T-score	P-value	Result
NT samples	0 to 100 cycles	1.995	> .05	Not Significant
	0 to 200 cycles	20.642	<< .05	Significant
	0 to 300 cycles	3.365	<< .05	Significant
	100 to 200 cycles	2.643	> .05	Not Significant
	200 to 300 cycles	-4.452	<< .05	Significant
SiO_2-treated samples	0 to 100 cycles	-8.823	<< .05	Significant
	0 to 200 cycles	3.287	<< .05	Significant
	0 to 300 cycles	-4.315	> .05	Not Significant
	100 to 200 cycles	-13.182	<< .05	Significant
	200 to 300 cycles	0.235	> .05	Not Significant
NT vs SiO_2-treated samples	0 cycles	44.587	<< .05	Significant
	100 cycles	19.164	<< .05	Significant
	200 cycles	39.058	<< .05	Significant
	300 cycles	8.845	<< .05	Significant

4.5 Conclusions

For the samples subjected to freeze-thaw cycling from 25°C to -18°C, the XRD results indicate that the SiO_2-treated samples experienced a significant increase in crystallinity between 0 cycles and 100 cycles. A stabilization in the crystallinity index of both types of samples was detected from 100-200 cycles when subjected to freeze-thaw cycling. Alkaline attack caused by the treatment process had a detrimental effect on the storage and loss moduli of the SiO_2-treated samples. Additionally, the freeze-thaw cycling process likely caused the formation of microcracks in the NT samples due to the dissipation of bound water, resulting in a decrease in storage modulus values, while the SiO_2-treated samples remained unaffected due to the protective layer formed by the SiO_2 colloid on the wood surface. More testing would be required to reduce the standard deviation of the storage modulus, loss modulus, and damping behaviour of the sample averages and confirm these hypotheses.

The NT samples demonstrated a comparable degree of water uptake to the SiO_2-treated samples, and it was found that the difference in water uptake between the SiO_2-treated samples and the NT samples was statistically insignificant after 300 cycles. This effect may have been caused by the shrinkage caused during the freeze-thaw cycling process and the drying process, which could result in a reduction of open pores in the NT samples. However, it was also found that the water uptake values of the SiO_2-treated samples had a higher degree of stability than the NT samples over a period of 300 cycles due to the clogging of sample extremities by the SiO_2 colloid, further demonstrating the benefits of this treatment process.

The compaction effect perpetuated by the freeze-thaw cycling process may have also contributed to the gradual decrease in cellulose degradation temperature for the NT samples over 300 freeze-thaw cycles, since a reduction in bound water may cause an increase in flammability. This phenomenon is expected to have less of an effect on the SiO_2-treated samples due to the colloid agglomeration within the samples. This may be the reason for the increase in peak cellulose degradation temperature witnessed in the SiO_2-treated samples over 300 cycles. Additionally, the increase and stabilization in the crystallinity index of the SiO_2-treated samples between 100-200 cycles may also have increased the thermal stability of the wood cellulose.

The effects of cellulose hydrolysis were likely less pronounced during the freeze-thaw cycling process when compared to the high temperature and relative humidity conditions tested in Chapter 3. Ultimately, the results of this research provide insight into the behaviour of spruce wood when subjected to freeze-thaw cycling and emphasize the benefits of the nano-SiO_2 vacuum impregnation process when used to treat wood intended for use in cold climates.

4.6 References

Auvinen, H. (2020, July 7). *Powder Wettability - how to measure wettability of powders?*, Biolin Scientific https://www.biolinscientific.com/blog/powder-wettability-how-to-measure-wettability-of-powders

Bhuiyan, Md. T. R., Hirai, N., & Sobue, N. (2000). Changes of crystallinity in wood cellulose by heat treatment under dried and moist conditions. *Journal of Wood Science*, 46(6), 431–436. https://doi.org/10.1007/BF00765800

Blanchet, P., & Pepin, S. (2021). Trends in Chemical Wood Surface Improvements and Modifications: A Review of the Last Five Years. *Coatings*, 11(12), 1514. https://doi.org/10.3390/coatings11121514

Campean, M., Ispas, M., & Porojan, M. (2008). Considerations on Drying Frozen Spruce Wood and Effects upon Its Properties. *Drying Technology*, 26(5), 596–601. https://doi.org/10.1080/07373930801946411

Curling, S. (2017). Test methods for bio-based building materials. In Jones, D. and Brischke, C. (Eds.), *Performance of bio-based Building Materials* (pp. 385–481). essay, Elsevier Science & Technology. https://doi.org/10.1016/C2015-0-04364-7

Engelund, E. T., Thygesen, L. G., Svensson, S., & Hill, C. A. (2012). A critical discussion of the physics of wood–water interactions. *Wood Science and Technology*, 47(1), 141–161. https://doi.org/10.1007/s00226-012-0514-7

Halpern, Y., & Patai, S. (1969). Pyrolytic Reactions of Carbohydrates. Part V. Isothermal Decomposition of Cellulose in Vacuo. *Israel Journal of Chemistry*, 7(5), 673–683. https://doi.org/10.1002/ijch.196900088

He, K., Chen, Y., & Wang, J. (2020). Axial Mechanical Properties of Timber Columns Subjected to Freeze-Thaw Cycles. *Journal of Renewable Materials*, 8(8), 969–992. https://doi.org/10.32604/jrm.2020.09573

Klement, I., Vilkovský, P., & Vilkovská, T. (2021). The influence of wood moisture content on the processes of freezing and heating. *Applied Sciences*, 11(13), 6099. https://doi.org/10.3390/app11136099

Lemaire-Paul, M., Beuthe, C. A., Riahinezhad, M., & Foruzanmehr, M. (2022). The impact of vacuum pressure on the effectiveness of SiO_2 impregnation of Spruce Wood. *Wood Science and Technology*, *57*(1), 147–171. https://doi.org/10.1007/s00226-022-01448-0

Li, X., Tabil, L. G., & Panigrahi, S. (2007). Chemical Treatments of Natural Fiber for Use in Natural Fiber-Reinforced Composites: A Review. *Journal of Polymers and the Environment*, 15(1), 25–33. https://doi.org/10.1007/s10924-006-0042-3

Sigma-Aldrich. (2023). *LUDOX® AS-40 colloidal silica*. https://www.sigmaaldrich.com/CA/en/product/aldrich/420840

Shier, R. (2004). Statistics: 1.1 *Paired t-tests*. Mathematics Learning Support Centre. https://www.statstutor.ac.uk/resources/uploaded/paired-t-test.pdf.

Stangroom, J. (2018). *P Value from T Score Calculator*. https://www.socscistatistics.com/pvalues/tdistribution.aspx

StatsDirect Limited. (2016). *Unpaired (two sample) T test*. https://www.statsdirect.co.uk/help/parametric_methods/utt.htm

Szmutku, M.B., Popa, V., & Câmpean, M. (2013). Experimental study regarding the freezing and thawing dynamics of spruce wood. *Pro Ligno*, 9(1). Retrieved from http://www.proligno.ro/en/articles/2013/201301.htm.

Tarmian, A., & Mastouri, A. (2019). Changes in moisture exclusion efficiency and crystallinity of thermally modified wood with aging. *iForest - Biogeosciences and Forestry*, 12(1), 92–97. https://doi.org/10.3832/ifor2723-011

Walker, J. C. F., Butterfield, B. G., Harris, J. M., Langrish, T. A. G., & Uprichard, J. M. (1993). Primary Wood Processing: Principles and practice. *Springer Netherlands*. https://doi.org/10.1007/978-94-015-8110-3

Welch, B. L. (1947). The generalization of 'student's' problem when several different population varlances are involved. *Biometrika*, 34(1–2), 28–35. https://doi.org/10.1093/biomet/34.1-2.28

Wiedehopf Building Façade Systems. (2022, May 3). *Wood Siding: Goods and Bads of an age-old method*. https://wiedehopf.ca/blog/wood-siding-goods-and-bads-of-an-age-old-method/

Winandy, J. E., Wiesner, F., Hassan, B., & Morrell, J. J. (2022). Fire performance of timber: Review for use in wildland-urban interfaces. *Holzforschung*, 76(8), 679–698. https://doi.org/10.1515/hf-2022-0038

Zhao, Y., Wang, Z., Lv, Y., Li, S., Ge, W., He, C., Yang, L., & Ge, D. (2022). Conformal fabrication of thick superhydrophobic coatings via reduction of sorption barrier against multiple damages. *Surface and Coatings Technology*, 444, 128658. https://doi.org/10.1016/j.surfcoat.2022.128658

Chapter 5

5.1 Conclusions

Initial hypotheses for this project assumed that the colloid would permeate into the lumens and infiltrate the wood cell walls, as shown in the study by Lemaire-Paul *et al.* (2022). However, the SEM results shown in Section 3.4.1 and the ATR-FTIR results shown in Appendix C demonstrate that the colloid was only able to agglomerate on the surface and extremities of the wood samples due a strong acid-base reaction between the alkaline colloid and the acidic wood. One potential reason for this behaviour is the properties of the colloid chosen for this experiment. The LUDOX HS-40 colloid used by Lemaire-Paul *et al.* (2022) had a nanoparticle size of approximately 12 nm, while the nanoparticles in the LUDOX AS-40 colloid used for this experiment were double the size at 20-24 nm. Therefore, it is likely that the nanoparticles were too large to permeate the wood cell walls. The treatment process was also found to have a detrimental effect on the initial storage modulus, loss modulus and degradation temperature values of the SiO_2-treated samples. The increase to atmospheric pressure from -90 kPa after 1 hour likely allowed the liquid phase of the colloid to enter the vascular system of the wood and allow for an alkaline hydrolysis reaction to occur.

The XRD results showed an increase in crystallinity after the initial unaged (0 month/0 cycle) test for both sample types. Under hydrolytic aging conditions, the SiO_2-treated samples exhibited significant decreases in storage modulus values. More research is required to determine the exact cause of this behaviour, although it may be related to the intensification of shrinkage at 1 month due to an increase in crystallinity. Under freeze-thaw cycling, the NT samples experienced a decrease in storage modulus, likely due to the formation of microcracks during the shrinkage/swelling process in the aging chamber as well as the oven-drying step performed before and after each test was performed. The viscoelastic properties of the SiO_2-treated samples appeared to be unaffected by the freeze-thaw aging conditions, likely due to a lack of swelling under high-humidity conditions caused by the protective SiO_2 layer on the surface of the samples.

The tensiometry results showed that for the hydrolytic aging conditions, the water uptake values of the SiO_2-treated samples were significantly lower than the NT samples, and under freeze-thaw cycling conditions, the water uptake values of the SiO_2-treated samples maintained a higher degree of stability than the NT samples. Finally, for the TGA results, it was found that the peak cellulose degradation temperature values of SiO_2-treated samples had a lower rate of decrease than the NT samples under hydrolytic aging conditions and demonstrated an increase under freeze-thaw cycling conditions.

The results shown in this study indicate the potential of the nano-SiO_2 impregnation process as a viable alternative to traditional treatment methods. Despite the detrimental effects of the treatment process, samples

treated with a nano-SiO_2 colloid under vacuum demonstrate not only an improvement of various properties over NT samples, but also show a higher resistance to two different types of accelerated aging: hydrolytic aging and freeze-thaw cycling. However, it is necessary to keep in mind that these artificial aging conditions do not represent conditions that can be found in nature. Accelerated aging is most commonly used to predict the long-term behaviour of materials by subjecting them to an exaggeration of real-world conditions (Frigione & Rodríguez-Prieto, 2021). Therefore, it can be said that the level of degradation caused by different temperature and humidity conditions on SiO_2-treated wood samples will vary and will likely be less pronounced in real-world conditions.

Damage caused by the infiltration of water in the vascular system of wood is a primary point of concern for real-world applications. Wood exhibits a naturally high water uptake capacity, and prolonged exposure to water may not only promote a hydrolysis reaction, but will also result in an increase in the FSP of wood. This increase in FSP will lead to a high higher degree of swelling and shrinkage, causing the continuous formation of microcracks that will compromise the integrity of the wood cell structure. Therefore, the most notable discovery made in this study is likely the significant maintained reduction and stabilization in the water uptake of the SiO_2-treated samples when subjected to both hydrolytic aging and freeze-thaw cycling. Given the excellent performance of these samples under accelerated aging conditions, it can be expected that this treatment method will be even more effective when wood is subjected to natural aging through exposure to rain or snow.

5.2 Future Work

The focus of future studies will shift to the impregnation of wood with acidic colloids instead of the alkaline ones to prevent an acid-base reaction from occurring on the surface of the samples. Moreover, this study has opened doors for the accelerated aging conditions to serve as pre-treatments capable of modifying fundamental properties, such as the crystallinity and FSP of wood. Future work will attempt to optimize these pre-treatments. Additionally, the number of samples tested for each characterization method will be increased to better manage the high level of variability in wood properties.

Appendices

Appendix A: Results of Preliminary Testing

The washing process described in Sections 3.3.1 and 4.3.1 was introduced to the treatment process due to trends exhibited by the TGA results obtained from a preliminary 1-month hydrolytic aging and testing period. SiO_2-treated samples used for the preliminary test were prepared using the same process described in Sections 3.3.1 and 4.3.1, with the exception of the secondary vacuum cycling/washing process. This section details the results obtained during the preliminary testing period and compares them to the results shown in Section 3.4.5. Samples that have been subjected to the secondary washing process are referred to as "washed" in this section, and samples that have not are referred to as "unwashed".

During this preliminary testing period, TGA was performed on two sets of unwashed spruce wood samples composed of 2-5 SiO_2-treated samples per set. The first set was tested at 0 months (unaged), and other set were tested after 1 month of accelerated aging at a temperature of 90°C and a RH of 80%. Figures 34 and 35 demonstrate the differences in peak cellulose degradation temperature between the washed SiO_2-treated samples and NT samples described in Section 3.4.5, and the unwashed SiO_2-treated samples used during the preliminary testing period.

The peak degradation temperature of the NT samples ranged from and was higher than both the washed and unwashed SiO_2-treated samples due to the effects of alkaline hydrolysis on the treated samples. However, the unwashed SiO_2-treated samples exhibited significantly lower peak cellulose degradation temperatures when compared to the washed SiO_2-treated samples after 1 month. The peak degradation temperature of the unwashed SiO_2-treated samples ranged from 330-336°C, while the peak degradation temperature of the washed samples ranged from 350-355°C. Additionally, the unwashed SiO_2-treated samples demonstrated a 1.82% decrease in peak cellulose degradation temperature after 1 month, while the NT samples and washed SiO_2-treated samples exhibited a decrease of only 0.85% and 0.57%, respectively. These results prove the ability of the secondary vacuum cycling/washing process to mitigate of the damage caused by alkaline hydrolysis during vacuum impregnation.

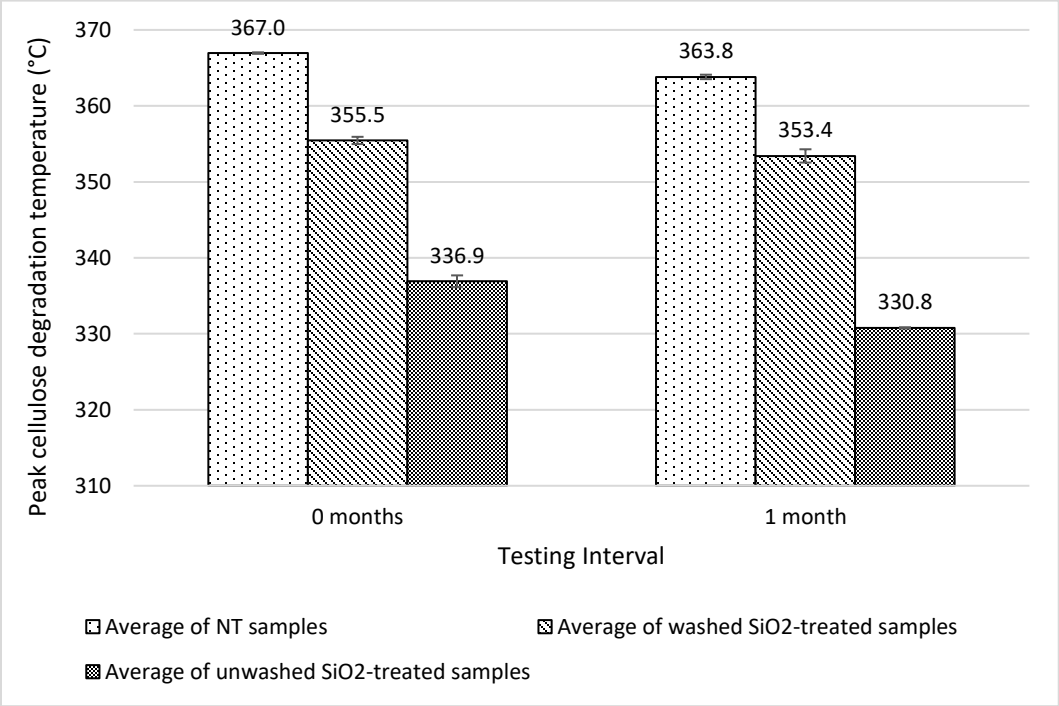

Figure 34. Peak cellulose degradation temperature for NT and washed/unwashed SiO_2-treated samples after 1 month of hydrolytic aging

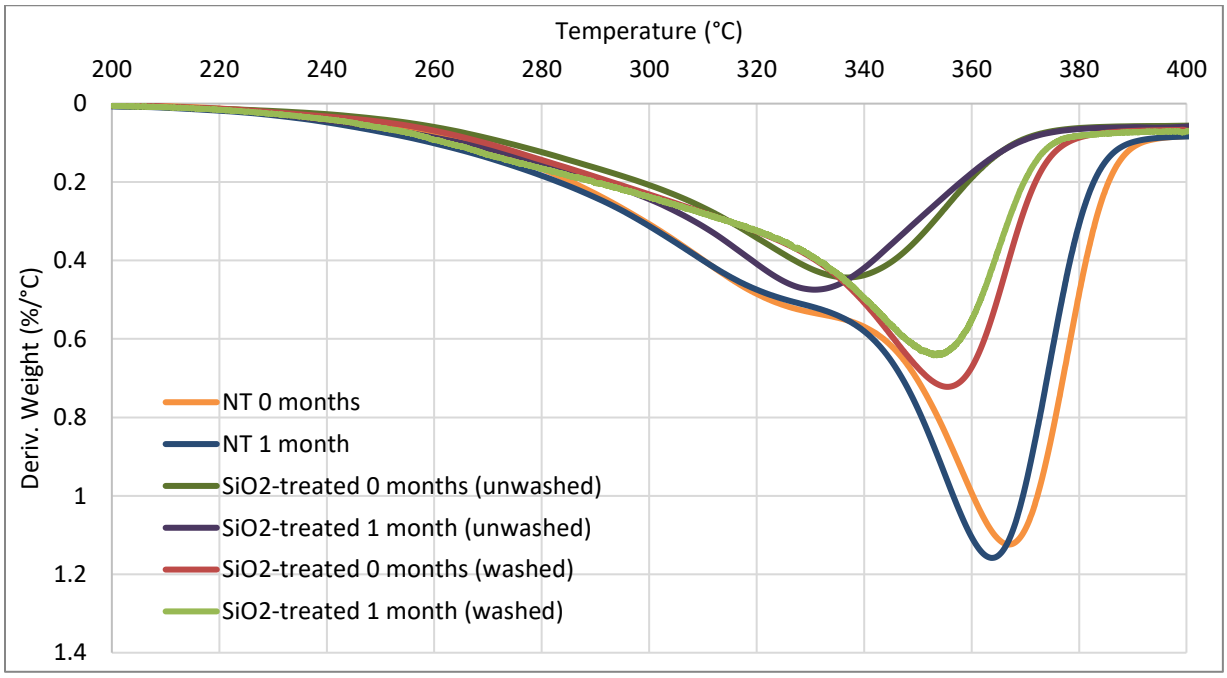

Figure 35. Comparison of DTG curves of spruce wood samples at different aging intervals and treatment conditions

Appendix B: Additional Dynamic Mechanical Analysis Results

This section summarizes the numerical results of DMA measurements taken at below ambient (10°C) and above ambient (35°C) temperatures for both NT and SiO_2-treated samples subjected to hydrolytic aging and freeze-thaw cycling.

B.1 Hydrolytic Aging

Table 20. Statistical analysis of the viscoelastic properties of hydrolytically aged NT samples at 10°C and 35°C

Comparison Interval	Statistical analysis of average values at 10°C			Statistical analysis of average values at 35°C		
Storage Modulus	**T- score**	**P-value**	**Result**	**T- score**	**P-value**	**Result**
0 months vs 1 month	-5.010	<< .05	Sig.	-5.299	<< .05	Sig.
0 months vs 2 months	-5.185	<< .05	Sig.	-5.005	<< .05	Sig.
0 months vs 3 months	-3.626	<< .05	Sig.	-3.819	<< .05	Sig.
1 month vs 2 months	-3.249	<< .05	Sig.	-2.689	> .05	Not Sig.
2 months vs 3 months	-2.379	> .05	Not Sig.	-2.717	> .05	Not Sig.
Loss Modulus	**T- score**	**P-value**	**Result**	**T- score**	**P-value**	**Result**
0 months vs 1 month	-5.970	<< .05	Sig.	-4.395	<< .05	Sig.
0 months vs 2 months	-7.278	<< .05	Sig.	-5.352	<< .05	Sig.
0 months vs 3 months	-5.011	<< .05	Sig.	-4.194	<< .05	Sig.
1 month vs 2 months	-2.410	> .05	Not Sig.	-2.399	> .05	Not Sig.
2 months vs 3 months	-0.610	> .05	Not Sig.	-0.227	> .05	Not Sig.
Tan delta	**T- score**	**P-value**	**Result**	**T- score**	**P-value**	**Result**
0 months vs 1 month	-0.100	> .05	Not Sig.	-1.348	> .05	Not Sig.
0 months vs 2 months	-0.521	> .05	Not Sig.	-1.822	> .05	Not Sig.
0 months vs 3 months	0.232	> .05	Not Sig.	-0.684	> .05	Not Sig.
1 month vs 2 months	-2.667	<< .05	Sig.	-2.772	<< .05	Sig.
2 months vs 3 months	-0.524	> .05	Not Sig.	0.348	> .05	Not Sig.

Table 21. Statistical analysis of the viscoelastic properties of hydrolytically aged SiO_2-treated samples at 10°C and 35°C

Comparison Interval	Statistical analysis of average values at 10°C			Statistical analysis of average values at 35°C		
Storage Modulus	**T- score**	**P-value**	**Result**	**T- score**	**P-value**	**Result**
0 months vs 1 month	-2.767	<< .05	Sig.	-2.375	> .05	Not Sig.
0 months vs 2 months	-4.008	<< .05	Sig.	-3.672	<< .05	Sig.
0 months vs 3 months	-2.904	<< .05	Sig.	-2.324	> .05	Not Sig.
1 month vs 2 months	-5.001	<< .05	Sig.	-1.754	> .05	Not Sig.
2 months vs 3 months	-1.453	> .05	Not Sig.	-1.464	> .05	Not Sig.
Loss Modulus	**T- score**	**P-value**	**Result**	**T- score**	**P-value**	**Result**
0 months vs 1 month	-2.477	> .05	Not Sig.	-3.167	<< .05	Sig.
0 months vs 2 months	-4.522	<< .05	Sig.	-5.958	<< .05	Sig.
0 months vs 3 months	-1.978	> .05	Not Sig.	-2.152	> .05	Not Sig.
1 month vs 2 months	-3.289	<< .05	Sig.	-2.706	> .05	Not Sig.
2 months vs 3 months	-0.601	> .05	Not Sig.	-0.362	> .05	Not Sig.
Tan delta	**T- score**	**P-value**	**Result**	**T- score**	**P-value**	**Result**
0 months vs 1 month	-0.112	> .05	Not Sig.	-1.652	> .05	Not Sig.
0 months vs 2 months	-0.335	> .05	Not Sig.	-3.912	<< .05	Sig.
0 months vs 3 months	-1.111	> .05	Not Sig.	-2.760	<< .05	Sig.
1 month vs 2 months	3.078	<< .05	Sig.	3.240	<< .05	Sig.
2 months vs 3 months	0.548	> .05	Not Sig.	0.968	> .05	Not Sig.

Table 22. Statistical analysis of the viscoelastic properties of NT samples when compared to SiO_2-treated samples at 10°C and 35°C (hydrolytically aged)

Comparison Interval	Statistical analysis of average values at 10°C			Statistical analysis of average values at 35°C		
Storage Modulus	**T-score**	**P-value**	**Result**	**T-score**	**P-value**	**Result**
0 months	2.826	<< .05	Significant	2.491	<< .05	Significant
1 month	2.649	<< .05	Significant	2.442	<< .05	Significant
2 months	2.409	<< .05	Significant	2.121	>.05	Not Sig.
3 months	2.882	<< .05	Significant	2.544	<< .05	Significant
Loss Modulus	**T-score**	**P-value**	**Result**	**T-score**	**P-value**	**Result**
0 months	0.813	>.05	Not Sig.	0.411	>.05	Not Sig.
1 month	0.619	>.05	Not Sig.	0.349	>.05	Not Sig.
2 months	0.626	>.05	Not Sig.	0.323	>.05	Not Sig.
3 months	1.035	>.05	Not Sig.	0.818	>.05	Not Sig.
Tan delta	**T-score**	**P-value**	**Result**	**T-score**	**P-value**	**Result**
0 months	-4.583	<< .05	Significant	-5.498	<< .05	Significant
1 month	-3.253	<< .05	Significant	-3.759	<< .05	Significant
2 months	-3.457	<< .05	Significant	-3.929	<< .05	Significant
3 months	-3.512	<< .05	Significant	-3.903	<< .05	Significant

Table 23. Average storage modulus, loss modulus, and tanδ values of hydrolytically aged NT samples at 10°C and 35°C

Aging Intervals	Average Storage Modulus at 10°C (MPa)	Standard Deviation	Average Storage Modulus at 35°C (MPa)	Standard Deviation
0 months	4762.70	1213.55	4468.00	1157.42
1 month	4436.78	1090.51	4211.89	1059.82
% change	-6.84		-5.73	
0 months	4762.70	1213.55	4468.00	1157.42
2 months	4266.38	1174.58	4080.38	1139.51
% change	-10.42		-8.68	
0 months	4762.70	1213.55	4468.00	1157.42
3 months	4420.25	966.99	4188.88	961.42
% change	-7.19		-6.25	
Aging Intervals	**Average Loss Modulus at 10°C (MPa)**	**Standard Deviation**	**Average Loss Modulus at 35°C (MPa)**	**Standard Deviation**
0 months	205.25	61.14	209.99	64.80
1 month	199.01	56.71	197.86	59.36
% change	-3.04		-5.78	
0 months	205.25	61.14	209.99	64.80
2 months	173.53	58.74	171.01	61.04
% change	-15.45		-18.56	
0 months	205.25	61.14	209.99	64.80
3 months	193.62	54.61	195.49	57.92
% change	-5.67		-6.91	
Aging Intervals	**Average tanδ at 10°C (MPa)**	**Standard Deviation**	**Average tanδ at 35°C (MPa)**	**Standard Deviation**
0 months	0.04274	0.00477	0.04652	0.00488
1 month	0.04348	0.00358	0.04562	0.00430
% change	-1.73		-1.93	
0 months	0.04274	0.00477	0.04652	0.00488
2 months	0.04244	0.00461	0.04393	0.00474
% change	-0.70		-5.57	
0 months	0.04274	0.00477	0.04652	0.00488
3 months	0.04294	0.00382	0.04567	0.00371
% change	0.47		-1.83	

Table 24. Average storage modulus, loss modulus, and tanδ values of hydrolytically aged SiO_2-treated samples at 10°C and 35°C

Aging Intervals	Average Storage Modulus at 10°C (MPa)	Standard Deviation	Average Storage Modulus at 35°C (MPa)	Standard Deviation
0 months	3485.50	892.70	3379.80	884.06
1 month	3104.29	974.06	3003.57	968.43
% change	-10.94		-11.13	
0 months	3485.50	892.70	3379.80	884.06
2 months	3065.43	892.63	3026.57	924.93
% change	-12.05		-10.45	
0 months	3485.50	892.70	3379.80	884.06
3 months	3122.40	792.51	3052.00	785.22
% change	-10.42		-9.70	
Aging Intervals	**Average Loss Modulus at 10°C (MPa)**	**Standard Deviation**	**Average Loss Modulus at 35°C (MPa)**	**Standard Deviation**
0 months	184.90	56.67	199.01	61.01
1 month	179.49	68.13	186.29	71.70
% change	-2.93		-6.39	
0 months	184.90	56.67	199.01	61.01
2 months	156.60	54.13	161.90	56.72
% change	-15.31		-18.65	
0 months	184.90	56.67	199.01	61.01
3 months	162.84	62.37	170.07	64.47
% change	-11.93		-14.54	
Aging Intervals	**Average tanδ at 10°C (MPa)**	**Standard Deviation**	**Average tanδ at 35°C (MPa)**	**Standard Deviation**
0 months	0.05241	0.00517	0.05820	0.00513
1 month	0.05215	0.00683	0.05549	0.00631
% change	-0.50		-4.66	
0 months	0.05241	0.00517	0.05820	0.00513
2 months	0.05118	0.00660	0.05348	0.00612
% change	-2.35		-8.11	
0 months	0.05241	0.00517	0.05820	0.00513
3 months	0.05104	0.00605	0.05396	0.00547
% change	-2.61		-7.29	

B.2 Freeze-thaw Cycling

Table 25. Statistical analysis of the viscoelastic properties of freeze-thaw cycled NT samples at 10°C and 35°C

Comparison Interval	Statistical analysis of average values at 10°C			Statistical analysis of average values at 35°C		
Storage Modulus	**T- score**	**P-value**	**Result**	**T- score**	**P-value**	**Result**
0 cycles vs 100 cycles	-2.385	<< .05	Sig.	-3.358	> .05	Not Sig.
0 cycles vs 200 cycles	-2.244	> .05	Not Sig.	-2.779	<< .05	Sig.
0 cycles vs 300 cycles	-4.082	<< .05	Sig.	-4.796	<< .05	Sig.
100 cycles vs 200 cycles	-0.520	> .05	Not Sig.	-0.251	> .05	Not Sig.
200 cycles vs 300 cycles	-1.124	> .05	Not Sig.	-0.722	> .05	Not Sig.
Loss Modulus	**T- score**	**P-value**	**Result**	**T- score**	**P-value**	**Result**
0 cycles vs 100 cycles	-0.566	> .05	Not Sig.	-1.512	> .05	Not Sig.
0 cycles vs 200 cycles	-0.026	> .05	Not Sig.	-0.447	> .05	Not Sig.
0 cycles vs 300 cycles	-1.637	> .05	Not Sig.	-1.375	> .05	Not Sig.
100 cycles vs 200 cycles	0.506	> .05	Not Sig.	1.216	> .05	Not Sig.
200 cycles vs 300 cycles	-1.665	> .05	Not Sig.	-0.902	> .05	Not Sig.
Tan delta	**T- score**	**P-value**	**Result**	**T- score**	**P-value**	**Result**
0 cycles vs 100 cycles	1.663	> .05	Not Sig.	0.489	> .05	Not Sig.
0 cycles vs 200 cycles	3.191	<< .05	Sig.	2.111	> .05	Not Sig.
0 cycles vs 300 cycles	1.551	> .05	Not Sig.	1.229	> .05	Not Sig.
100 cycles vs 200 cycles	1.701	> .05	Not Sig.	1.812	> .05	Not Sig.
200 cycles vs 300 cycles	-0.889	> .05	Not Sig.	-0.538	> .05	Not Sig.

Table 26. Statistical analysis of the viscoelastic properties of freeze-thaw cycled SiO_2-treated samples at 10°C and 35°C

Comparison Interval	Statistical analysis of average values at 10°C			Statistical analysis of average values at 35°C		
Storage Modulus	**T- score**	**P-value**	**Result**	**T- score**	**P-value**	**Result**
0 cycles vs 100 cycles	-0.084	> .05	Not Sig.	-0.396	> .05	Not Sig.
0 cycles vs 200 cycles	-0.642	> .05	Not Sig.	-0.538	> .05	Not Sig.
0 cycles vs 300 cycles	-1.245	> .05	Not Sig.	-1.176	> .05	Not Sig.
100 cycles vs 200 cycles	-0.703	> .05	Not Sig.	-0.319	> .05	Not Sig.
200 cycles vs 300 cycles	0.767	> .05	Not Sig.	0.666	> .05	Not Sig.
Loss Modulus	**T- score**	**P-value**	**Result**	**T- score**	**P-value**	**Result**
0 cycles vs 100 cycles	0.137	> .05	Not Sig.	-0.064	> .05	Not Sig.
0 cycles vs 200 cycles	-0.641	> .05	Not Sig.	-0.846	> .05	Not Sig.
0 cycles vs 300 cycles	-1.026	> .05	Not Sig.	-1.101	> .05	Not Sig.
100 cycles vs 200 cycles	-0.858	> .05	Not Sig.	-0.821	> .05	Not Sig.
200 cycles vs 300 cycles	1.365	> .05	Not Sig.	2.038	> .05	Not Sig.
Tan delta	**T- score**	**P-value**	**Result**	**T- score**	**P-value**	**Result**
0 cycles vs 100 cycles	0.034	> .05	Not Sig.	-0.142	> .05	Not Sig.
0 cycles vs 200 cycles	-0.301	> .05	Not Sig.	-0.833	> .05	Not Sig.
0 cycles vs 300 cycles	-0.140	> .05	Not Sig.	-0.634	> .05	Not Sig.
100 cycles vs 200 cycles	-0.390	> .05	Not Sig.	-0.756	> .05	Not Sig.
200 cycles vs 300 cycles	0.886	> .05	Not Sig.	1.101	> .05	Not Sig.

Table 27. Statistical analysis of the viscoelastic properties of NT samples when compared to SiO_2-treated samples at 10°C and 35°C (freeze-thaw cycled)

Comparison Interval	Statistical analysis of average values at 10°C			Statistical analysis of average values at 35°C		
Storage Modulus	**T-score**	**P-value**	**Result**	**T-score**	**P-value**	**Result**
0 months	1.853	> .05	Not Sig.	1.680	> .05	Not Sig.
1 month	1.461	> .05	Not Sig.	1.320	> .05	Not Sig.
2 months	1.547	> .05	Not Sig.	1.359	> .05	Not Sig.
3 months	1.365	> .05	Not Sig.	1.244	> .05	Not Sig.
Loss Modulus	**T-score**	**P-value**	**Result**	**T-score**	**P-value**	**Result**
0 months	1.161	> .05	Not Sig.	-0.377	> .05	Not Sig.
1 month	0.879	> .05	Not Sig.	-0.434	> .05	Not Sig.
2 months	1.331	> .05	Not Sig.	-0.113	> .05	Not Sig.
3 months	0.946	> .05	Not Sig.	-0.215	> .05	Not Sig.
Tan delta	**T-score**	**P-value**	**Result**	**T-score**	**P-value**	**Result**
0 months	-0.944	> .05	Not Sig.	-1.251	> .05	Not Sig.
1 month	-0.555	> .05	Not Sig.	-1.028	> .05	Not Sig.
2 months	0.672	> .05	Not Sig.	0.460	> .05	Not Sig.
3 months	0.380	> .05	Not Sig.	0.195	> .05	Not Sig.

Table 28. Average storage modulus, loss modulus, and tanδ values of freeze-thaw cycled NT samples at 10°C and 35°C

Aging Intervals	Average Storage Modulus at 10°C (MPa)	Standard Deviation	Average Storage Modulus at 35°C (MPa)	Standard Deviation
0 cycles	5309.80	1116.13	5104.40	1065.10
100 cycles	5121.60	1091.08	4895.60	1021.18
% change	-3.54		-4.09	
0 cycles	5309.80	1116.13	5104.40	1065.10
200 cycles	5061.60	1060.97	4871.40	1046.50
% change	-4.67		-4.56	
0 cycles	5309.80	1116.13	5104.40	1065.10
300 cycles	4985.30	1050.60	4827.00	1033.56
% change	-6.11		-5.43	
Aging Intervals	**Average Loss Modulus at 10°C (MPa)**	**Standard Deviation**	**Average Loss Modulus at 35°C (MPa)**	**Standard Deviation**
0 cycles	262.94	71.16	267.05	69.77
100 cycles	260.18	79.21	259.47	77.05
% change	-1.05		-2.84	
0 cycles	262.94	71.16	267.05	69.77
200 cycles	262.82	76.14	265.01	76.68
% change	-0.046		-0.76	
0 cycles	262.94	71.16	267.05	69.77
300 cycles	253.92	72.61	259.55	74.71
% change	-3.43		-2.81	
Aging Intervals	**Average tanδ at 10°C (MPa)**	**Standard Deviation**	**Average tanδ at 35°C (MPa)**	**Standard Deviation**
0 months	0.04902	0.00520	0.05184	0.00567
1 month	0.05077	0.00684	0.05297	0.00739
% change	3.57		2.18	
0 months	0.04902	0.00520	0.05184	0.00567
2 months	0.05161	0.00534	0.05411	0.00600
% change	5.28		4.38	
0 months	0.04902	0.00520	0.05184	0.00567
3 months	0.05091	0.00530	0.05369	0.00563
% change	3.86		3.57	

Table 29. Average storage modulus, loss modulus, and tanδ values of freeze-thaw cycled SiO_2-treated samples at 10°C and 35°C

Aging Intervals	Average Storage Modulus at 10°C (MPa)	Standard Deviation	Average Storage Modulus at 35°C (MPa)	Standard Deviation
0 cycles	4306.40	1298.99	4204.30	1317.26
100 cycles	4298.60	1408.65	4174.60	1393.86
% change	-0.18		-0.71	
0 cycles	4306.40	1298.99	4204.30	1317.26
200 cycles	4235.30	1314.12	4144.80	1327.57
% change	-1.65		-1.42	
0 cycles	4306.40	1298.99	4204.30	1317.26
300 cycles	4246.50	1281.87	4150.86	1302.13
% change	-1.39		-1.27	
Aging Intervals	**Average Loss Modulus at 10°C (MPa)**	**Standard Deviation**	**Average Loss Modulus at 35°C (MPa)**	**Standard Deviation**
0 cycles	225.23	74.13	236.33	83.45
100 cycles	227.06	88.94	235.55	94.72
% change	-0.81		-0.33	
0 cycles	225.23	74.13	236.33	83.45
200 cycles	218.29	73.41	226.56	80.88
% change	-3.08		-4.13	
0 cycles	225.23	74.13	236.33	83.45
300 cycles	221.13	77.89	230.75	84.20
% change	-1.82		-2.36	
Aging Intervals	**Average tanδ at 10°C (MPa)**	**Standard Deviation**	**Average tanδ at 35°C (MPa)**	**Standard Deviation**
0 months	0.05161	0.00695	0.05545	0.00714
1 month	0.05230	0.00540	0.05600	0.00566
% change	1.34		0.99	
0 months	0.05161	0.00695	0.05545	0.00714
2 months	0.05006	0.00493	0.05292	0.00560
% change	-3.00		-4.56	
0 months	0.05161	0.00695	0.05545	0.00714
3 months	0.05005	0.00457	0.05321	0.00515
% change	-3.02		-4.04	

Appendix C: Fourier Transform Infrared Spectroscopy

This section discusses the results obtained by performing FTIR spectroscopy measurements on unaged NT and SiO_2-treated spruce wood samples.

C.1 Materials and Methods

FTIR spectroscopy measurements using attenuated total reflectance (ATR) were performed on SiO_2-treated and NT spruce wood samples. These measurements were taken using a Thermo Fisher Nicolet iS50R FTIR Spectrometer with an ATR accessory. The sample absorbance according to the wavelength was measured using a single-bounce diamond crystal set at an incidence angle of 45°. The spectra were read at a wavelength range of 4000-400 cm^{-1}, taken as the average of 32 scans at a resolution of 4 cm^{-1}.

NT sample readings were performed on a (127 x 12.7 x 7 mm) sample both on a slice taken of the surface of the sample and a slice taken from the interior of the sample at a depth of 1 mm below the surface. SiO_2-treated sample measurements were performed on a (25 x 10 x 1.8 mm) SiO_2-treated sample, comparable in size to the DMA samples used in this study. Figure 36 demonstrates how the SiO_2-treated sample was cut and where readings were taken.

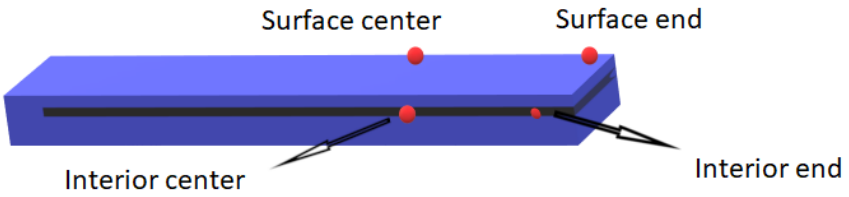

Figure 36. SiO_2-treated sample cutting diagram (courtesy of Esmizadeh, 2023)

C.2 Sample Characterization

Figure 37 shows the absorbance spectra of the NT and SiO_2-treated samples. Absorbance readings taken near the interior center of the SiO_2-treated sample were comparable to those found in the NT sample. This signifies that the nano-SiO_2 particles were not able to fully permeate the wood sample.

The peak at 3300 cm^{-1} represents O-H stretching in hydroxyl groups, and the peaks between 2800 cm^{-1} and 2900 cm^{-1} represent CH stretching of the cellulose molecule and methyl/methylene groups, respectively (Sharma *et al.*, 2020). The flattening of these peaks at the surface and interior end of the SiO_2-treated sample indicate a reduction in hydroxyl groups and carbohydrates. This was likely caused by the formation of strong

bonds between the wood and the SiO_2 nanoparticles (Sun *et al.*, 2011). For the NT sample, the peak at 1048 cm^{-1} is attributed to C-O stretching in lignin and cellulose (Leto *et al.*, 2018; Sharma *et al.*, 2020). For the SiO_2-treated sample, the lower absorbance peak at 1048 cm^{-1} can be related to a characteristic SiO_2 peak representing asymmetric stretching vibrations of Si-O-Si. The pronounced peaks at 792 cm^{-1} and 463 cm^{-1} can be related to characteristic SiO_2 peaks representing the symmetric stretching vibration and bending vibration of Si-O-Si bonds (Wang *et al.*, 2011; Dong *et al.*, 2019; Gu *et al.*, 2020). The flattening of the bands between 1260-1730 cm^{-1} for the SiO_2-treated sample may be related to the degradation of cellulose, hemicellulose, and lignin due to cellulose hydrolysis and alkaline attack during the vacuum treatment process.

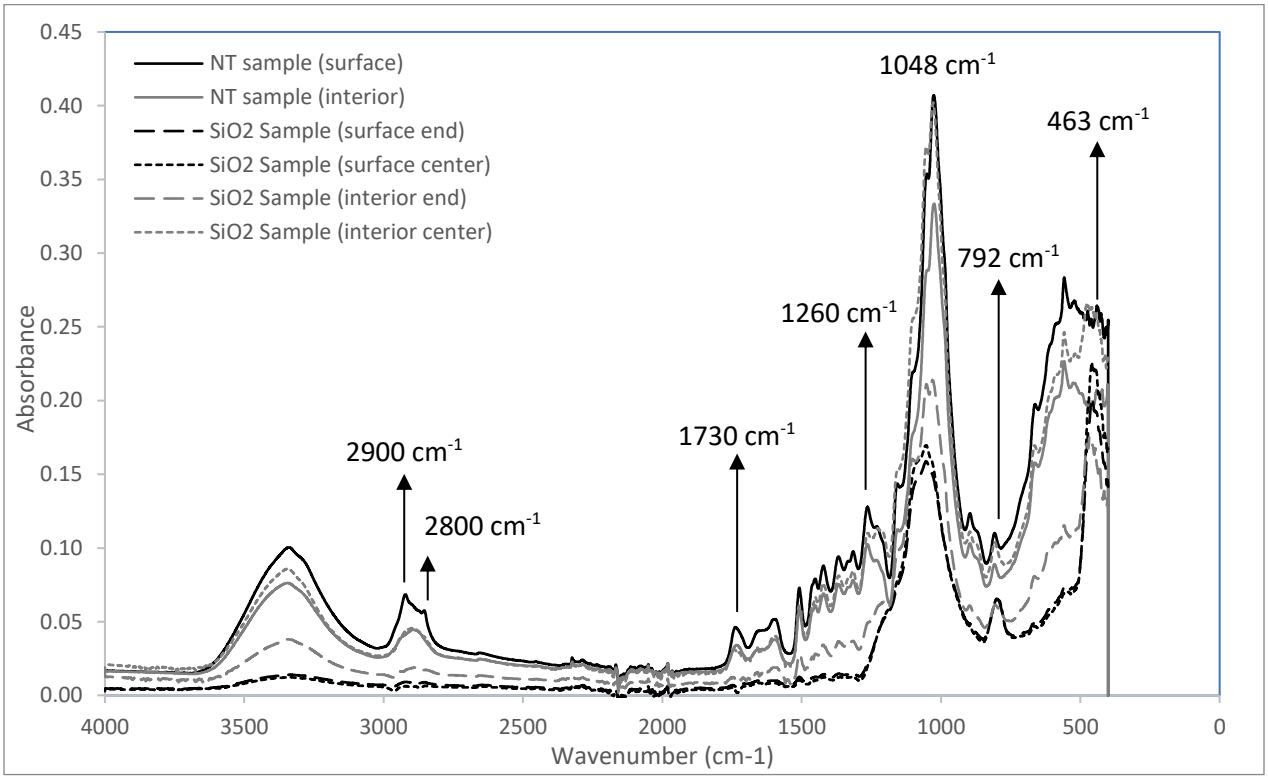

Figure 37. ATR-FTIR spectra of the NT and SiO_2-treated samples

C.3 References

Esmizadeh, E. (2022). *Cutting diagram of a small spruce wood sample*. Unpublished.

Dong, R., Wang, L., Zhu, J., Liu, L., & Qian, Y. (2019). A novel SiO2–GO/acrylic resin nanocomposite: Fabrication, characterization and properties. *Applied Physics A*, 125(8), 551. https://doi.org/10.1007/s00339-019-2847-7

Gu, N., Zhang, H., Ge, H., Wang, F., & Liu, B. (2021). In-situ polymerization of graphene/SiO2 hybrids modified phenolic resin for improved thermal stability at an ultralow filler loading. *Polymer Bulletin*, 78(10), 5963–5976. https://doi.org/10.1007/s00289-020-03409-8

Lehto, J., Louhelainen, J., Kłosińska, T., Drożdżek, M., & Alén, R. (2018). Characterization of alkali-extracted wood by FTIR-ATR spectroscopy. *Biomass Conversion and Biorefinery*. https://doi.org/10.1007/s13399-018-0327-5

Sharma, V., Yadav, J., Kumar, R., Tesarova, D., Ekielski, A., & Mishra, P. K. (2020). On the rapid and non-destructive approach for wood identification using ATR-FTIR spectroscopy and Chemometric methods. *Vibrational Spectroscopy*, 103097. https://doi.org/10.1016/j.vibspec.2020.103097

Sun, Q., Lu, Y., & Liu, Y. (2011). Growth of hydrophobic TiO2 on wood surface using a hydrothermal method. *Journal of Materials Science*, 46(24), 7706–7712. https://doi.org/10.1007/s10853-011-5750-y

Wang, S., Liu, C., Liu, G., Zhang, M., Li, J., & Wang, C. (2011). Fabrication of superhydrophobic wood surface by a sol–gel process. *Applied Surface Science*, 258(2), 806–810. https://doi.org/10.1016/j.apsusc.2011.08.100